ELECTRIC CHARGING IN LIQUID HYDROCARBON FILTRATION

by

PETER W. HUBER

B.S., Massachusetts Institute of Technology
(1974)

S.M., Massachusetts Institute of Technology
(1974)

SUBMITTED IN PARTIAL FULFILLMENT
OF THE REQUIREMENTS FOR THE
DEGREE OF

DOCTOR OF PHILOSOPHY

at the

MASSACHUSETTS INSTITUTE OF TECHNOLOGY

MAY 1976

Signature of Author .....
Department of Mechanical Engineering, May 6, 1976

Certified by .....
Thesis Supervisor

Accepted by .....
Chairman, Department Committee on Graduate Students

MASS. INST. TECH.
JUL 9 1976
LIBRARIES

ELECTRIC CHARGING IN LIQUID HYDROCARBON FILTRATION

by

PETER W. HUBER

Submitted to the Department of Mechanical Engineering on May 6, 1976 in partial fulfillment of the requirements for the Degree of Doctor of Philosophy.

ABSTRACT

A theory is presented for the electric charging process which occurs when low-conductivity fluids are passed through a filter. It is shown that the process can be characterized by a charging emf which depends on filter and fluid properties and flow conditions. Explicit analytic expressions are derived for the charging emf for a wide range of flow conditions and filter and fuel properties.

Experiments in which doped n-heptane was passed through Millipore and Velcon filters support the model and theoretical predictions. Filter tortuosities and ionic mobilities are determined from the charging data.

A detailed criticism of a previous experimental study by Gavis and Wagner is presented.

Thesis Supervisor: Ain A. Sonin
Title: Professor of Mechanical Engineering

FOREWORD AND ACKNOWLEDGMENTS

This thesis consists of three chapters written for separate publication in the open literature. Chapter I describes our model and theory (to be submitted to the Journal of Colloid and Interface Science, 1976), Chapter II presents the results of a series of experiments that we conducted to test the theory (to be submitted to the Journal of Colloid and Interface Science, 1976), and Chapter III is a detailed analysis and discussion of some previous experimental work by independent investigators (to be submitted to Chemical Engineering Science, 1976).

The substance of this thesis evolved in the period 1972-1976 as a result of exchange and interaction between Professor Sonin and me, with professorial and student contributions in about the usual proportions. Chapter I and the first part of Chapter II have undergone extensive revision and rewriting by Professor Sonin in preparation for journal publication (co-authors P.W. Huber and A.A. Sonin) - I discovered with only mild chagrin that as a student I was not, at all times, as articulate or scientifically skillful as the persons endeavoring to instruct and assist me. The fact that the final pages have not undergone such exhaustive transformation can be attributed only to the departmental deadline which put a premature stop even to necessary changes.

This research was motivated, supervised, and sustained by Professor Sonin with inexhaustible patience throughout. An acknowledgment is inadequate

recognition of his contribution to this work.

The other two members of my thesis committee - Professor Melcher and Professor Probstein - have also been very helpful. Both have been understanding and patient, even in our most chaotic committee meetings and during the final hectic days in which these pages were assembled. Professor Probstein was the first to draw our attention to the interesting boundary layer behavior that emerges from Eq. (54), Chapter I.

I have been fortunate to receive the able assistance of Mr. Dick Fenner, who built the experimental apparatus described in Chapter II.

Miss Cindy Polansky typed the manuscript, enduring my tortured handwriting and incessant textual alterations with manifest perseverance for which I am most grateful.

A former apartment-mate and mathematician, Mr. Leonardo Rub, spent a productive evening with me deriving Eq. (17), Chapter I, from Eq. (76), Chapter I.

Others who have had no direct input into the thesis have made contributions which have been of more than slight importance to me in the last four years: Roger, office-mate and hockey team-mate; Sadeq and Giorgio, apartment-mates past and present; and Hopie and Susie, neighbors and psychiatric counsellors. Members of my family, dispersed in Switzerland, Canada, Tanzania, and Britain have been a constant source of support and encouragement.

This research was sponsored by the National Science Foundation under Grant Number ENG 74-20951 A01 of the Division of Engineering, Fluid Mechanics Section.

TABLE OF CONTENTS

ACKNOWLEDGMENTS 3

CHAPTER I: Theory for the Electric Charging Process in Liquid Hydrocarbon Filtration

1. Introduction 9

2. Model and Summary of Main Results 11

3. The Basic Equations 25

4. Solutions for the Charging Emf 33

5. Discussion 48

Appendix A. Bulk-Averaged Form of Poisson's Equation 55

Appendix B. Order of Magnitude of the Dimensionless Current 57

References 59

CHAPTER II. Electric Charging in Filtration: A Comparison of Theory and Experiments

Introduction 61

SECTION A. Apparatus, Filters, and Fluid 63

SECTION B. Millipore Filter Experiments 76

1. Low θ Experiments 76

2. High θ Experiments 85

3. Tortuosities and Mobilities Inferred from the Data 92

4. Summary of Results 94

5. Discussion of Millipore Filter Experiments 94

SECTION C. Velcon Filter Experiments 102

Concluding Remarks 110

Appendix A. Test Conditions and the Theoretical Assumptions 112

References 118

CHAPTER III. A New Look at Some Old Data on Electric Charging in Fuel Filtration

Introduction 121

SECTION A. Summary of Gavis and Wagner's Work 122

SECTION B. Correlation of Gavis and Wagner's Data 134

1. Fluid Conductivity, $I \propto \sigma_0^{\frac{1}{4}}$ 134

2. Filter Structure 142

3. Filter Fixed Charge and Reaction Kinetics 147

SECTION C. Summary and Analysis of Gavis and Wagner's Data in Terms of Our Theory 149

Conclusions 156

Appendix 158

References 160

CHAPTER I

THEORY FOR THE ELECTRIC CHARGING PROCESS IN LIQUID HYDROCARBON FILTRATION

1. INTRODUCTION

Electric charging is a well-known hazard in operations involving gasolines and other hydrocarbon liquids with very low electrical conductivity.[1] Net electric charge appears in liquids near solid bounding surfaces or near interfaces between the liquid and air. In liquids which have extremely low electrical conductivity, this charge can be convected downstream and distributed over large distances if flow occurs. Very large potential differences can be induced.

Charging is known to be particularly severe in filtration, because a filter presents a very large interior surface to, and can therefore cause a high total charge to be induced in, the liquid which penetrates it.[1,2] Several research and testing programs have been undertaken during the past decade to establish the charging phenomena in filtration.[3-5] Most of the work has been experimental, but some investigators have proposed qualitative models for the charging mechanism to explain their various observations.[3,5] No coherent theory has emerged, however, nor has any empirical correlation for predicting charging phenomena in filtration come to be widely accepted.

In a recent paper,[6] we proposed a relatively simple electrokinetic model for the charging mechanism in filtration, one which resembles those used for flows of aqueous saline solutions through charged membranes,[7,8] but which differs in several key respects from previously suggested models. We derived an explicit analytic solution for the charging effects as a function of filter and fluid properties and flow conditions, and showed that the model agreed well with a series of experiments. However, the

particular solution which was derived is applicable only under conditions of relatively low flow speed and/or high fluid conductivity, and many (if not most) filtration conditions of interest fall outside its range of validity.

In this chapter, we generalize our theory to a much broader range of flow conditions and fluid properties. The theory is extended to high flow speed and low fluid conductivity, and the previous assumption that positive and negative ions have equal mobilities is relaxed. Our model, assumptions, and main new results are summarized in Section 2. Sections 3 and 4 develop the underlying equations and derive mathematical solutions by the singular perturbation technique (the problem contains some novel boundary layer features which arise from the interaction of flow and space-charge phenomena). A discussion of how our theory relates to practical filtration conditions is given in Section 5.

Chapters 2 and 3[9] compare our theory with experimental data.

2. MODEL AND SUMMARY OF MAIN RESULTS

Model and Parameters

In our model the filter is viewed as a porous structure with fixed charge adsorbed on the surfaces of its solid matrix. [6] The fluid which flows through it is a very weak electrolyte. The ions (we shall call them ions, although our analysis is not basically altered if electrons are the negative species) arise either from the dissociation of the pure fluid itself, or from the dissociation of some dissolved additive or impurity. Upstream of the filter, the fluid is electrically neutral and the positive and negative ions have equal concentrations. As the fluid enters the pores in the filter, the ion concentrations are thrown into imbalance: a net charge develops in the fluid so as to tend to neutralize the fixed charge which lines the surrounding pore walls. Flow tends to convect the countercharge downstream, and this gives rise to a convection current through the filter and also to an electric field in the flow direction. The total current through the filter is the algebraic sum of the convection current and the current which results from the migration of the ions in the electric field (diffusion also plays a role in regions where high charge gradients are set up). The filter thus behaves somewhat as a flow-driven current generator with a parallel internal resistance. Its output is essentially an emf if the total resistance in the current loop, including that of the fluid outside the filter (see Figure 1) is large compared with the "internal" resistance of the filter region where the emf is developed.

In what follows, we shall be concerned with basically one-dimensional,

steady filtration (Figure 1). Fluid is forced through a plane filter at constant speed, and sufficient time has elapsed for all electrical effects to reach a steady state. The filter is bounded by two electrodes, shown in Figure 1 as grids, one upstream and the other downstream. A current passes through the filter from one electrode to the other. The electrodes are connected to an external circuit which completes the current loop.

As regards the electric charging caused by the filter, the central question is the following: for a given current, how much does the potential difference between the electrodes exceed the value it would have in the absence of flow through the filter? We shall call this flow-generated potential difference the charging emf, $\mathscr{E}$:

> $\mathscr{E}$, the charging emf (V), is defined as the amount by which the potential difference between the downstream and the upstream electrodes exceeds the value it would have in the absence of flow through the filter, given the current.

The charging emf represents the flow-generated potential difference in excess of the inevitable voltage drop which occurs whenever current passes between the electrodes. The total potential difference $\Delta\phi$ between the downstream and upstream electrodes is

$$\Delta\phi = \mathscr{E} - IR_0 \quad , \qquad [1]$$

where R_0 is the resistance of the fluid and fluid-impregnated filter between the electrodes, measured under no-flow conditions. Once the charging emf is known as a property of the filter and flow conditions, the entire current-voltage characteristic can be obtained from Eq. [1] for any given electrode placement and system geometry outside the filter.

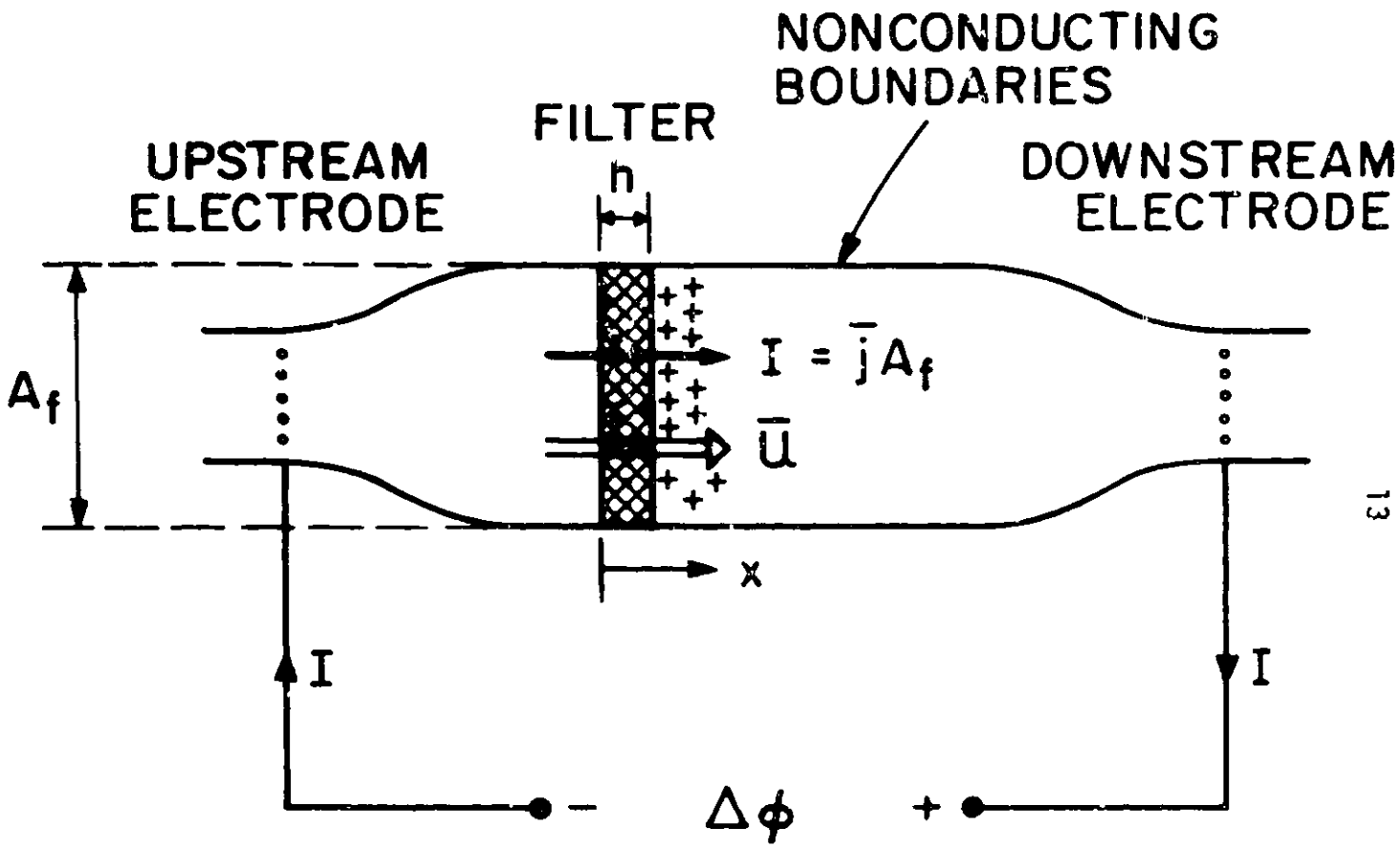


FIGURE 1. Filtration configuration.

In our model the charging emf will be related to the following filter properties, fluid properties, and operating variables:

Filter

h , filter thickness (m);

P , filter porosity, or ratio of the volume occupied by fluid to the total volume;

τ , tortuosity, or the average distance traveled by a fluid particle as it traverses the filter, divided by the filter thickness;

Z_f , sign of the fixed charge associated with the filter (+1 for positive fixed charge, -1 for negative fixed charge);

ρ_f , magnitude of the fixed charge density associated with the filter, expressed for convenience as the amount of fixed charge per unit volume of pore space ($C\ m^{-3}$). This quantity should actually be considered a property of the filter/fluid combination, since different fluids may induce different fixed charge densities on the same solid surface. Note that the symbol ρ was used for ρ_f in Reference 6;

ε_s , permittivity of the solid material of which the filter matrix is composed ($C^2\ N^{-1} m^{-2}$);

σ_s , electrical conductivity of the solid material of which the filter matrix is composed ($\Omega^{-1}\ m^{-1}$);

a , effective radius of a pore in the filter (m).

Fluid

σ_0 , electrical conductivity of the fluid in its neutral, undisturbed state (Ω^{-1} m^{-1});

κ_a , mobility of the fluid counterion, that is, the ion with charge sign opposite to that of the filter fixed charge (m^2 $sec^{-1}volt^{-1}$);

κ_b , mobility of the fluid co-ion, the ion having the same charge sign as the filter fixed charge (m^2 $sec^{-1}volt^{-1}$);

ε_0 , permittivity of the fluid ($C^2N^{-1}m^{-2}$)

Operating Conditions

$\bar{u}$, superficial flow speed through filter, that is, volume flow rate per unit total filter cross-section (m sec^{-1});

$\bar{j}$, superficial current density through filter, that is, charge transported across unit total filter cross-section per unit time (A m^{-2}).

The filter pore radius a and matrix conductivity σ_s do not actually appear in our present results for charging effects. However, they do figure in the criteria for when the results apply.

Simplifying Assumptions

The theoretical results which we derive in this paper are not totally general, but are based on some simplifying assumptions with the help of which we are able to obtain rigorous and reasonably tractable solutions of

the governing equations. Although the list of assumptions may seem rather long at first sight, it is actually not very restrictive. Our solutions do cover a range of practical filtration conditions. What is more, because they are rigorous and in explicit analytic form, they provide a good basis for laboratory studies of the charging characteristics of filter/fluid combinations.

The simplifying assumptions are the following:

(a) The filter pore radius a must be small compared with the Debye length,

$$a < \lambda_D \quad . \qquad [2]$$

Here,

$$\lambda_D = (\varepsilon_0 D_{av}/\sigma_0)^{\frac{1}{2}} \qquad [3]$$

is the Debye length, based on the average diffusion coefficient of the counter and co-ions,

$$D_{av} \equiv \frac{D_a + D_b}{2} \quad . \qquad [4]$$

(b) The electrical conductance of the filter's solid matrix must be negligible compared with the conductance of the fluid in the pores,

$$(1 - P)\sigma_s \ll P\sigma_0 \quad . \qquad [5]$$

(c) We consider a plane filter, and assume basically one-dimensional conditions in the region downstream of the filter where a net charge density is induced in the fluid. The thickness of the

latter region is of the order of the convective charge relaxation length $\varepsilon_0\bar{u}/\sigma_0$ (ε_0/σ_0 is the charge relaxation time in the undisturbed, that is, uncharged, fluid).

Conditions do not need to be one-dimensional outside the region of space charge for our theory to apply.

(d) The separation between the filter and the downstream electrode must be large compared with both the filter thickness and the convective charge relaxation length,

$$\ell_0 \gg h \quad , \quad \varepsilon_0\bar{u}/\sigma_0 \quad . \qquad [6]$$

Here,

$$\ell_0 \equiv \sigma_0 A_f R_0 \qquad [7]$$

is an equivalent electrode separation, A_f being the total area of the filter. ℓ_0 is the separation the electrodes would have to have, given the resistance, if the fluid between them were confined to a constant cross-sectional area equal to that of the filter. It is a property of the system geometry and independent of σ_0, since $R_0 \sim \sigma_0^{-1}$.

(e) The Péclet number based on the filter thickness must be large compared with unity,

$$\frac{\bar{u}\, h}{D_{av}} \gg 1 \quad . \qquad [8]$$

(This requirement is actually not necessary if $\varepsilon_0\bar{u}/\sigma_0 h \ll 1$, provided that $\lambda_D^2 \ll h^2$ instead.)

(f) The fluid is assumed to behave as a weak electrolyte in local thermodynamic equilibrium with singly charged positive and negative ions.

We shall see later that assumptions (a), (b), and (e) are usually met in practical filtration conditions. Assumptions (c) and (d) are easy to satisfy in laboratory tests of filters, but may be violated under some practical conditions where the fluid conductivity is very low and the filtration speed very high.

Summary of Solutions

When the assumptions listed above apply, it turns out that flows can be categorized as having either "low charge density" or "high charge density, depending on operating conditions and the filter fixed charge density, and explicit analytic solutions can be derived for the charging emf for each of these flow conditions. Thus, explicit analytic solutions are available for all operating conditions except those which lie in a transition corridor between the two regions. The criteria for when one or the other of the solutions applies are stated in terms of two dimensionless parameters. The first[†] is the ratio of the convective charge relaxation length in the fluid to the filter thickness,

$$\theta \equiv \frac{\varepsilon_0 \bar{u}}{\sigma_0 h} \quad . \qquad [9]$$

It can be viewed as a dimensionless speed. The second is a dimensionless filter fixed charge density,

$$\gamma_f = \frac{\rho_f \kappa_{av}}{\sigma_0} \qquad [10]$$

where

$$\kappa_{av} = \frac{\kappa_a + \kappa_b}{2} \qquad [11]$$

[†]Referred to in the electrohydrodynamic literature as the electric Reynolds number.

is the average mobility of the counter and co-ions.

The low charge density solution, which applies when either $\gamma_f << 1$ or $\gamma_f << \theta$ (see Figure 2), is given by

$$-Z_f \mathcal{E} = \frac{\tau^2}{P} \frac{\rho_f \bar{u} h}{\sigma_0} \left[1 - \left(1 - \frac{P^2}{\tau^2} \right) \frac{\varepsilon_f}{\varepsilon_0 P^2} \theta \left(1 - e^{-\frac{\varepsilon_0 P^2}{\varepsilon_f \theta}} \right) \right] . \quad [12]$$

Here,

$$\varepsilon_f = \varepsilon_0 P + \varepsilon_s (1 - P) \quad [13]$$

is a bulk-averaged permittivity of the filter as a whole, ε_0 being the permittivity of the fluid and ε_s that of the solid matrix. Note that

$$-Z_f \mathcal{E} = \frac{\tau^2}{P} \frac{\rho_f \bar{u} h}{\sigma_0} \quad \text{when} \quad \theta << 1$$
$$= \frac{P \rho_f \bar{u} h}{\sigma_0} \quad \text{when} \quad \theta >> 1 \quad . \quad [14]$$

The high charge density solution applies when both $\gamma_f >> 1$ and $\gamma_f >> \theta$ (again, see Figure 2). It is given by

$$-Z_f \mathcal{E} = \frac{\tau^2}{P} \frac{\bar{u} h}{\kappa_a} + F(t_a) \frac{\varepsilon_0 \bar{u}^2}{\kappa_a \sigma_0} \quad . \quad [15]$$

Here,

$$t_a = \frac{\kappa_a}{\kappa_a + \kappa_b} \quad [16]$$

is the transport number of the counterion in the undisturbed fluid, and

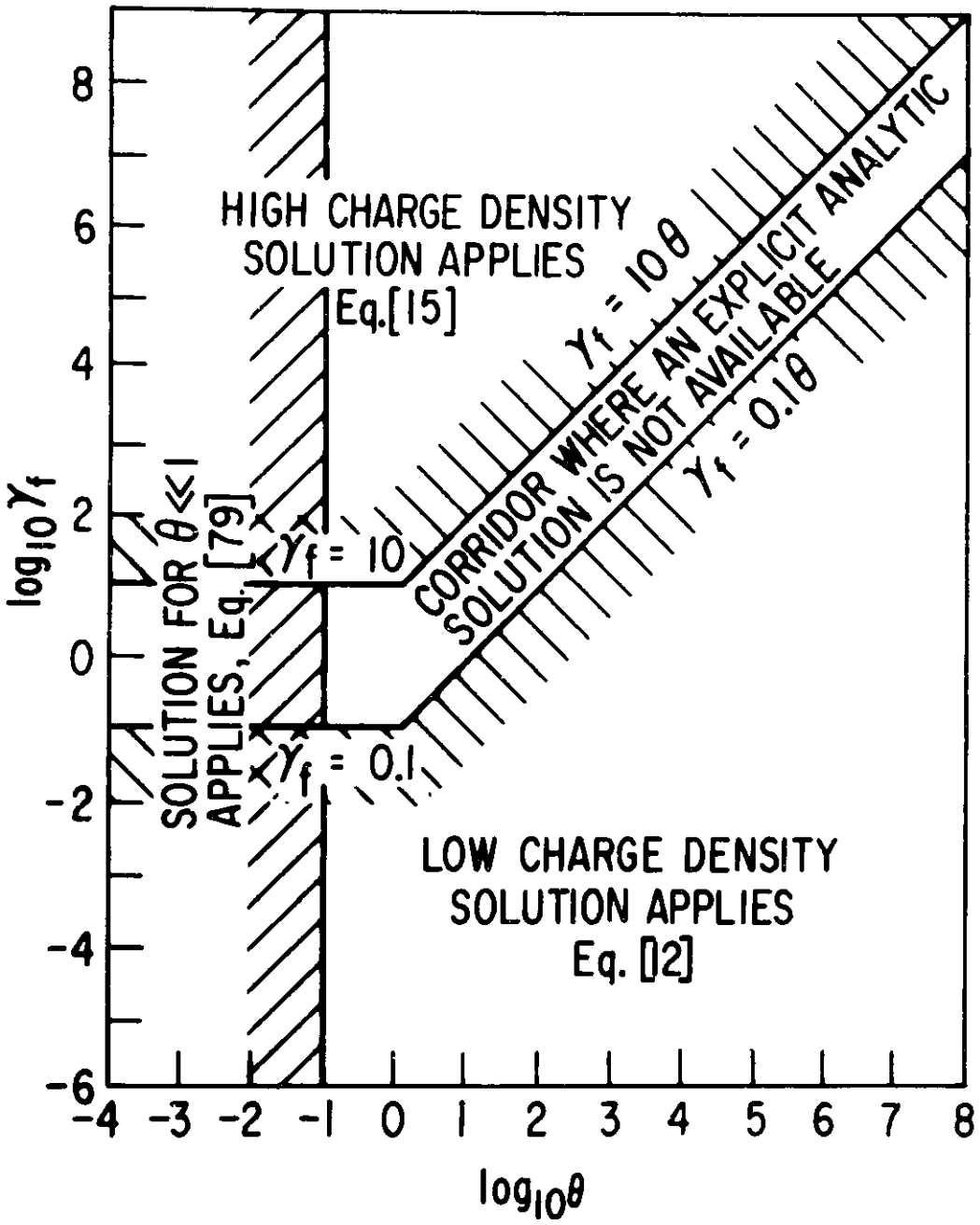


FIGURE 2. Operating conditions where low and high charge density solutions apply.

$$F(t_a) = \frac{1}{4}\left[\frac{2t_a - 1}{t_a - 1} + \frac{1}{(1 - t_a)^{3/2}\, t_a^{1/2}} \tan^{-1}\left(\frac{1 - t_a}{t_a}\right)^{1/2}\right] \quad [17]$$

Values of $F(t_a)$ are listed in Table 1. It should be noted that $F(t_a)$ is typically of order unity.

The regions of applicability of the two analytic solutions can be shown succinctly on a (γ_f , θ) plot, as in Figure 2. The boundaries shown in Figure 2 are approximate, since we have simply taken 0.1 as being small compared with unity and 10 as large. Inspection of the more detailed equations shows that these boundaries are reasonably conservative. In any case, in the context of all the possible conditions which might arise in practice, the corridor where neither Eq. [12] nor Eq. [15] applies is relatively narrow. For $\theta << 1$, we actually have an analytic solution which applies for all values of γ_f (see Section 4).

The sign of the charging emf is always opposite to that of the filter's fixed charge, Z_f . When the low charge density solution applies, the charging emf is always directly proportional to flow speed and filter thickness, and also proportional to the filter's fixed charge density. It is inversely proportional to the fluid conductivity if the filter's fixed charge is unaffected by the conductivity. One anticipates practical difficulties in applying Eq. [12]. For one thing, virtually nothing is known about the magnitudes of the fixed charge density associated with typical combinations of filter material and hydrocarbon liquid. For another, it is very possible that the fixed charge magnitude will be very sensitive to impurities in the

TABLE 1. Values for $F(t_a)$

t_a	$F(t_a)$	t_a	$F(t_a)$
0.05	1.861	0.55	0.7656
0.10	1.379	0.60	0.7485
0.15	1.172	0.65	0.7337
0.20	1.052	0.70	0.7207
0.25	0.9728	0.75	0.7092
0.30	0.9153	0.80	0.6989
0.35	0.8716	0.85	0.6896
0.40	0.8370	0.90	0.6813
0.45	0.8088	0.95	0.6736
0.50	0.7854	1.0	0.6667

liquid, particularly ionized impurities, and great care may have to be taken in ascribing a fixed charge density to a given filter/fluid combination. Finally, although the charging emf does not depend explicitly on the filter pore size, the amount of fixed charge associated with unit pore volume may depend on the pore size, so that an apparent dependence on pore size might be deduced in experiments where the pore size is varied without monitoring the fixed charge density.

There are no such difficulties if the high charge density solution applies. The charging emf is then independent not only of the pore size, but also of the fixed charge density, despite the fact that it is the fixed charge which induces the emf in the first place. Provided the fixed charge is high enough to satisfy both the criteria $\gamma_f >> 1$ and $\gamma_f >> \theta$, the magnitude of the charging emf for a given flow will be the same for all filters with the same sign, porosity, and tortuosity. Note that if the sign of the filter's fixed charge is changed, the co-ion is changed to the counterion and vice versa, so that the values of both κ_a and t_a change. Hence, the magnitude of $\mathcal{E}$ may be different for filters with opposite sign, even if the tortuosity, porosity, filter thickness, and flow conditions are the same. Note also that the dependence on flow speed changes from a linear one at low flow speeds and/or high conductivities where $\theta << 1$ (the ratio of the second and first terms on the right hand side of Eq. [15] is of the order of θ) to a $\overline{u^2}$ dependence at high flow speeds and/or low conductivities, where $\theta >> 1$. Furthermore, when $\theta << 1$, the charging potential is proportional to filter thickness, whereas at high speeds and/or low conductivities, where $\theta >> 1$, it becomes independent of filter thickness.

It is important to note that the high charge density solution represents an upper bound to the charging potential. First, the charging emf it predicts is always higher than that predicted by the low charge density expression when the latter applies (the ratio of Eq. [12] and Eq. [15] is of the order of γ_f when $\theta < 1$ and of the order of γ_f/θ when $\theta > 1$, that is, always small when the criteria for the low charge density solution apply). Secondly, the violation of any of our assumptions, except possibly (f), about which we know little, would tend to reduce the charging emf.

3. THE BASIC EQUATIONS

The principles which govern the charging process are charge conservation, which in our basically one-dimensional, steady case simply reduces to the statement that the superficial current density is the same everywhere between the electrodes, and Poisson's relation between the charge distribution and the potential field. Our problem is somewhat unconventional for two reasons. First, the convection and diffusion contributions to the current play significant roles, so that the simple ohmic relation does not apply. The current density depends strongly on the local charge density, through the convection and diffusion terms as well as through the charge density-sensitive conductivity in the ohmic term. Secondly, we need to derive bulk-averaged forms for both the current density and Poisson's equation for the interior of the filter, so that the filter can be treated as a continuous phase rather than as a complicated solid matrix traversed by a multitude of tortuous, fluid-filled pores.

The Equation for the Current Density

In a one-dimensional situation, the current density j_i carried by ions of species i in the fluid is given by

$$j_i = FZ_i \left(c_i u - D_i \frac{dc_i}{ds} - Z_i c_i \kappa_i \frac{d\phi}{ds} \right), \qquad [18]$$

where F is Faraday's constant, Z_i is the charge number of the species, c_i is the species concentration in moles per unit volume, u is the bulk

fluid flow speed, ϕ is the electric potential, D_i and κ_i are the diffusion coefficient and mobility, respectively, of the ions, and s is the coordinate measured in the direction of variation. On the right, the first term represents convection, the second diffusion, and the third migration in the electric field.

Equation [18] applies in fluid regions outside the filter (Figure 1), where conditions are truly one-dimensional and s is simply equal to the coordinate x perpendicular to the filter. If $a < \lambda_D$, it also applies in the fluid inside the pores of the filter, since the charge density in the fluid is then distributed essentially uniformly over a pore cross-section.[6] However, in that case, s has to be interpreted as the distance measured along the pore axis and j_i and u must be interpreted as the average species current density and average fluid flow speed over the cross-section of the pore.

The total current density j is the sum of the contributions of the counterions, for which $Z_i = -Z_f$, and the co-ions, for which $Z_i = +Z_f$ (we are assuming singly charged ions; recall that $Z_f = +1$ if the fixed charge is positive and $Z_f = -1$ if the fixed charge is negative). From Eq. [18] we obtain

$$j = -Z_f(j_a - j_b) = -Z_f\rho u - \sigma \frac{d\phi}{ds} + Z_f F \left(D_a \frac{dc_a}{ds} - D_b \frac{dc_b}{ds} \right) , \quad [19]$$

where the subscripts a and b refer to counterions and co-ions, respectively,

$$\rho = F(c_a - c_b) \quad [20]$$

is the magnitude of the local charge density in the fluid (its sign is opposite to that of the fixed charge), and

$$\sigma = F(c_a\kappa_a + c_b\kappa_b) \qquad [21]$$

is the local electrical conductivity of the fluid.

Now, if the fluid behaves as a very weak electrolyte with the ionic constituents in local thermodynamic equilibrium with the dissociating constituent, we can write

$$c_a c_b = c_0^2 \quad , \qquad [22]$$

where c_0 is the value of both c_a and c_b in the undisturbed liquid where there is no net charge density. Eq. [22] would apply regardless of whether the dissociating constituent is the hydrocarbon liquid itself or an impurity or additive. c_0 can be expressed in terms of the undisturbed fluid conductivity (see Eq. [21]) as

$$c_0 = \frac{\sigma_0}{F(\kappa_a + \kappa_b)} \quad . \qquad [23]$$

Using Eqs. [20]-[22], we can write c_a and c_b in terms of ρ and σ_0 and express the conductivity as

$$\sigma = \sigma_0 f(\gamma) \qquad [24]$$

where

$$f(\gamma) \equiv (1 + \gamma^2)^{\frac{1}{2}} + (2t_a - 1)\gamma \qquad [25]$$

expresses the dependence of σ on the charge density,

$$\gamma \equiv \frac{\rho\kappa_{av}}{\sigma_0} \qquad [26]$$

being a dimensionless local charge density which represents the ratio of the charge density to the charge density that would exist in the undisturbed fluid if both the co-ions and counterions had positive charge. Similarly, by writing c_a and c_b in terms of ρ and σ_0 in Eq. [19], we obtain the following equation for the current density in terms of the local charge density and the electric field:

$$j = -Z_f \rho u - \sigma_0 f(\gamma) \frac{d\phi}{ds} + Z_f D_{av} g(\gamma) \frac{d\rho}{ds} \quad . \qquad [27]$$

Here,

$$g(\gamma) = \frac{2D_a}{D_a + D_b} - \frac{D_a - D_b}{D_a + D_b}\left[1 - \gamma(1 + \gamma^2)^{-\frac{1}{2}}\right] \qquad [28]$$

is a dimensionless quantity which expresses the dependence of the effective diffusion coefficient on the charge density. D_{av} is the average diffusion coefficient $(D_a + D_b)/2$. Note that

$$\begin{aligned} g &\simeq 1 \quad \text{when} \quad \gamma << 1 \\ &\simeq D_a/D_{av} \quad \text{when} \quad \gamma >> 1 \end{aligned} \qquad [29]$$

and that $g = 1$ when the counterions and co-ions have equal diffusion coefficients.

Eq. [27] applies inside a pore in the filter, if j is interpreted as the average axial current density over the pore cross-section, u as the average bulk flow speed in a pore, and s the distance along the pore axis. However, these quantities are not the ones that are measured in practice. The superficial current density $\bar{j}$ - that is, the charge crossing unit total filter cross-sectional area per unit time, which can be deduced fro the measured total current - is related to the average axial current density j in a pore by (6)

$$j = \frac{\tau}{P} \bar{j} \quad , \qquad [30]$$

and similarly, the superficial flow speed $\bar{u}$, or the volume flow rate per total filter cross-section, is related to the average axial flow speed u in a pore by

$$u = \frac{\tau}{P} \bar{u} \quad , \qquad [31]$$

where τ is the tortuosity of the pores and P is the porosity of the filter. Since furthermore $ds = \tau\, dx$, where x is measured transversely through the filter, Eq. [27] can be written as

$$\bar{j} = -Z_f \rho \bar{u} - \frac{P \sigma_0 f(\gamma)}{\tau^2} \frac{d\phi}{dx} + \frac{Z_f P D_{av} g(\gamma)}{\tau^2} \frac{d\rho}{dx} \qquad [32]$$

$$\text{for } 0 < x < h \ .$$

Charge and total mass conservation require that the superficial current density $\bar{j}$ and the superficial bulk flow speed $\bar{u}$ be constant everywhere between the electrodes. Outside the filter the situation is truly one-

dimensional and we can apply Eq. [27] directly, with $ds = dx$, $j = \bar{j}$, and $u = \bar{u}$:

$$\bar{j} = -Z_f \rho \bar{u} - \sigma_0 f(\gamma) \frac{d\phi}{dx} + Z_f D_{av} g(\gamma) \frac{d\rho}{dx} \qquad [33]$$

$$\text{for} \quad x < 0 \quad \text{and} \quad x > h \ .$$

Poisson's Equation

To complete the specification of the interior problem, Poisson's equation must be written in terms of the transverse coordinate x . The form we seek must be averaged over distances large compared with a pore diameter, but small compared with the filter thickness. To derive such an averaged form of Poisson's equation for a porous medium in general is not a trivial matter. However, proceeding in the same spirit as we did with the equation for the current density, we argue in Appendix A that for our present case, where $a < \lambda_D$, the equation we seek has the form

$$\frac{1}{\tau^2} \frac{d^2\phi}{dx^2} = \frac{-Z_f P(\rho_f - \rho)}{\varepsilon_f} \qquad [34]$$

where ε_f is the bulk-averaged permittivity of the filter as a whole, defined in Eq. [13]. Note that $Z_f P(\rho_f - \rho)$ is the net charge per unit total filter volume, since $Z_f \rho_f$ is by definition the fixed charge per unit pore volume and $-Z_f \rho$ is the free charge per unit volume of fluid, that is, also per unit pore volume. Thus, the quantity ε_f/τ^2 is an effective permittivity for the filter viewed as a continuous medium.

Outside the filter, Poisson's equation has the usual one-dimensional form

$$\frac{d^2\phi}{dx^2} = \frac{Z_f \rho}{\epsilon_0} \quad . \qquad [35]$$

Fixed charge exists only in the interior of the filter.

We shall see that the form of Poisson's equation inside the filter will affect the low charge density solution (Eq. [14]), but not the high charge density solution (Eq. [17]).

The Boundary Conditions

When the potential gradient is eliminated between Eqs. [32] and [34] and between Eqs. [33] and [35], one obtains second order differential equations for the charge density ρ in the filter and in the fluid outside the filter. Three different regions are involved (see Figure 1): the fluid region upstream of the filter, where $x < 0$; the interior of the filter, where $0 < x < h$; and the fluid region downstream of the filter, where $x > h$. Two boundary conditions are required for each of these regions, making a total of six. These are the following: first, since the electrodes are assumed to lie outside the region of space charge, charge density must approach zero far from the filter,

$$\rho \to 0 \quad \text{as} \quad x \to \pm\infty \quad . \qquad [36]$$

Second, ρ must be continuous across the two interfaces between the fluid and the filter, that is,

$$\rho_1 = \rho_2 \quad , \qquad [37]$$

where the subscript 1 refers to a point just outside the filter and the subscript 2 to a point just inside the filter at the same interface. This condition applies because we assume that the transition distance between the flow just inside a pore and the flow just outside the filter is small compared with the characteristic length of charge variation. Thus, fluid with a given charge per unit volume will maintain that charge per unit volume as it enters a pore or exits from it (continuity of j, u, and ϕ). Finally, no infinitely thin layers of charge can exist at the fluid-filter interfaces, since the filter fixed charges are already accounted for, and since in the fluid the characteristic charge relaxation length is not assumed to be zero. The conditions for this are that

$$\varepsilon \left(\frac{d\phi}{dx}\right)_1 = \frac{\varepsilon_f}{\tau^2} \left(\frac{d\phi}{dx}\right)_2 . \qquad [38]$$

Eq. [38] expresses the familiar condition that the product of the permittivity and the normal component of the electric field must be invariant across the interface between two phases if there is no surface charge. The quantity ε_f/τ^2 is essentially the effective permittivity of the filter. (see Eq. [34] and the discussion following). By using Eqs. [35] and [34] and integrating from $-\infty$ through the filter to $+\infty$, it is easy to show that the interfacial condition given by Eq. [38] automatically ensures that the total charge distributed in the fluid is equal in magnitude to the total fixed charge in the filter, as is required.

4. SOLUTIONS FOR THE CHARGING EMF

The Charging Emf

We define a local charging potential ϕ' which is the difference between the actual potential ϕ and the potential $\bar{\phi}$ which would exist at the same point in the absence of flow through the filter, everything else (including the current) being invariant:

$$\phi'(\vec{r}) \equiv \phi(\vec{r}) - \bar{\phi}(\vec{r}) \quad . \qquad [39]$$

The charging emf $\mathcal{E}$ is the total flow-generated potential difference between the downstream and the upstream electrodes (see Figure 1),

$$\mathcal{E} \equiv \phi'_{II} - \phi'_{I} = \int_{I}^{II} \nabla\phi'(\vec{r}) \cdot d\vec{r} \quad . \qquad [40]$$

Note that if the current-voltage relation of the filter and fluid between the electrodes is ohmic in the absence of flow, then

$$\bar{\phi}_{I} - \bar{\phi}_{II} = IR_0 \qquad [41]$$

where I is the total current and R_0 the zero-flow resistance. Eq. [1] follows immediately.

Now, the flow-induced field $\vec{E}' = -\nabla\phi'$ will be non-zero only in the region where the flow has perturbed the charge density distribution and where the charge has been convected downstream. Hence, if conditions are one-dimensional where the space charge is distributed, and if the electrode lie outside the space charge region [see our assumption (d)], then we can

write

$$\mathcal{E} = \int_{-\infty}^{+\infty} \frac{d\phi'}{dx}\, dx \quad . \qquad [42]$$

From Eqs. [32] and [33] we can deduce that

$$\frac{d\phi'}{dx} = -\frac{k_1 \bar{j}}{\sigma_0}\left[\frac{1}{f(\gamma)} - \frac{1}{f(\bar{\gamma})}\right] - \frac{k_1 Z_f \bar{u}}{\kappa_{av}} \frac{\gamma}{f(\gamma)} + \frac{Z_f D_a}{\kappa_{av}}\left[\frac{g(\gamma)}{f(\gamma)}\frac{d\gamma}{dx} - \frac{g(\bar{\gamma})}{f(\bar{\gamma})}\frac{d\bar{\gamma}}{dx}\right] \qquad [43]$$

where γ is the dimensionless charge density defined in Eq. [26], $\bar{\gamma}$ is the value which γ would have if there were no flow, and

$$k_1 \equiv 1 \quad \text{for} \quad x < 0 \quad \text{and} \quad x > h$$
$$\equiv \frac{\tau^2}{p} \quad \text{for} \quad 0 < x < h \; . \qquad [44]$$

The last term on the right hand side of Eq. [43] contributes nothing to the integral in Eq. [42], since both γ and $\bar{\gamma}$ are zero at upstream and downstream infinity. The contribution of the first term is small compared with that of the second if

$$\frac{\bar{j}\,\kappa_{av}}{\sigma_0\,\bar{u}} \ll 1 \quad . \qquad [45]$$

It is shown in Appendix B that Eq. [45] is always satisfied if assumption (d) applies. Thus, we have

$$-Z_f \mathcal{E} = \frac{\bar{u}\, h}{\kappa_{av}} \int_{-\infty}^{+\infty} \frac{k_1 \gamma}{f(\gamma)}\, dz \qquad [46]$$

where

$$z \equiv \frac{x}{h} \quad . \qquad [47]$$

What remains is to establish the dimensionless charge distribution in the fluid and to evaluate the integral

Dimensionless Equations and Parameters

We define the dimensionless potential and current density

$$\psi = Z_f \varepsilon_0 \kappa_{av} \phi / \sigma_0 h^2 \qquad [48]$$

and

$$J = Z_f \kappa_{av} \bar{j} / \sigma_0 \bar{u} \quad , \qquad [49]$$

and combine our expressions for the electric field, Eqs. [32] and [33] into the form

$$\frac{d\psi}{dz} = - k_1 \theta \frac{J + \gamma}{f(\gamma)} + \frac{\theta}{Pe} \frac{g(\gamma)}{f(\gamma)} \frac{d\gamma}{dz} \quad . \qquad [50]$$

Here, θ is the ratio of the convective relaxation length to the filter thickness, defined in Eq. [9], and Pe is the Péclet number based on the filter thickness, as defined in Eq. [8]. Similarly, Poisson's equation (Eqs. [34] and [35]) becomes

$$\frac{d^2\psi}{dz^2} = - k_2 (k_3\gamma_f - \gamma) \qquad [51]$$

where

$$k_2 = 1 \quad \text{for} \quad z < 0 \ , \quad z > 1$$
$$= \varepsilon_0 P\tau^2/\varepsilon_f \quad \text{for} \quad 0 < z < 1 \qquad [52]$$

$$k_3 = 0 \quad \text{for} \quad z < 0 \ , \quad z > 1$$
$$= 1 \quad \text{for} \quad 0 < z < 1 \qquad [53]$$

An equation for the charge density distribution is obtained by eliminating the electric field between Eqs. [50] and [51]:

$$\frac{\theta}{Pe} \frac{d}{dz}\left(\frac{g}{f}\frac{d\gamma}{dz}\right) - \theta k_1 \left\{ \frac{1 - \left[\gamma + (2t_a - 1)(1 + \gamma^2)^{\frac{1}{2}}\right] J}{f^2(1 + \gamma^2)^{\frac{1}{2}}} \right\} \frac{d\gamma}{dz}$$
$$= k_2 (\gamma - k_3\gamma_f) \qquad [54]$$

This equation must be solved in three regions: the region upstream of the filter, $z < 0$; the region inside the filter, $0 < z < 1$; and the downstream region, $z > 1$. The boundary conditions are that $\gamma \to 0$ as $z \to -\infty$ and $z \to +\infty$, and that at both of the two filter-fluid interfaces,

$$\gamma_1 = \gamma_2 \qquad [55]$$

and

$$\left(\frac{d\gamma}{dz}\right)_1 - \frac{\varepsilon_f}{\varepsilon_0\tau^2}\left(\frac{d\gamma}{dz}\right)_2 = Pe\left(1 - \frac{\varepsilon_f}{\varepsilon_0 P}\right)\frac{\gamma_1}{g(\gamma_1)} \qquad [56]$$

where the subscript 1 denotes a point in the fluid just outside the filter and the subscript 2 a point just inside the filter at the same interface. γ_{12} represents the common value of γ at these two points. Eq. [56] is derived from Eq. [38], using Eq. [50] and the assumption that

$$J \ll \gamma \quad , \qquad [57]$$

which allows the term involving the current density to be neglected in the boundary condition. We show in Appendix B that Eq. [57] is consistent with our results if assumption (d) of Section 2 applies.

High Péclet Number Solution

When $Pe \gg 1$, it is clear from Eqs. [54] - [56] that the charge density distribution must contain thin transition regions, or boundary layers, at the two filter-fluid interfaces. In the bulk regions, upstream of the filter, inside it, and downstream of it, the first term on the left of Eq. [54] (the diffusion term) is negligible; however, the boundary conditions expressed by Eqs. [55] and [56] cannot be satisfied without diffusion, and hence transition layers of thickness Pe^{-1} compared with the filter thickness must exist near the two filter-fluid interfaces at $x = 0$ and $x = 1$.

An analytic solution for $\gamma(x)$ can be obtained by the singular perturbation technique (10). The outer solution $\gamma \equiv \gamma_0(x)$, which applies everywhere except very near the interfaces at $x \simeq 0$ and $x \simeq 1$, satisfies Eq. [54] with the first term on the left (the diffusion term) neglected,

$$\theta \frac{d\gamma_0}{dz} = -\frac{k_2}{k_1} \frac{(\gamma_0 - k_3\gamma_f)(1 + \gamma_0^2)^{\frac{1}{2}} f^2(\gamma_0)}{1 - \left[\gamma_0 + (2t_a - 1)(1 + \gamma_0^2)^{\frac{1}{2}}\right] J} \quad . \qquad [58]$$

For $z < 0$ the only solution of Eq. [58] which satisfies the boundary condition $\gamma_0 \to 0$ as $z \to -\infty$ is

$$\gamma_0 = 0 \quad \text{for } z < 0 \quad . \qquad [59]$$

At the interfaces at $z = 0$ and $z = 1$, the outer solution γ_0 is discontinuous. Thus the solutions for $0 < z < 1$ and $z > 0$ will each contain one integration constant, say $\gamma_0(0^+)$ and $\gamma_0(1^+)$, respectively. Eq. [58] automatically satisfies the boundary condition $\gamma_0 \to 0$ as $z \to +\infty$.

The values of the two integration constants are obtained by determining the inner solutions for the two interfacial transition regions and matching them to the local outer solutions. For the transition region in the neighborhood of $z = 0$, we define the stretched inner variable

$$y = Pe\, z \qquad [60]$$

and determine the inner solution $\gamma_i(y)$ from Eq. [54] with the right hand side neglected (the neglected term is of order Pe^{-1}). Separate solutions must be obtained for $y < 0$ and $y > 0$, and joined by applying the boundary conditions Eqs. [55] and [56] at the filter-fluid interface, $y = 0$. In addition, this inner solution must be matched to the local outer solution, that is, we must have

$$\gamma_i(-\infty) = 0$$
$$\gamma_i(+\infty) = \gamma_0(0^+) \; . \qquad [61]$$

There is one excess constraint on the inner solution. This determines the value of the first outer integration constant $\gamma_0(0^+)$.

The inner solution $\gamma_i(y)$ for the downstream transition region on either side of $z = 1$ is expressed in terms of the stretched variable

$$y = Pe\ (z - 1) \quad . \tag{62}$$

The procedure for obtaining this solution is the same as that described above, except that it must match its own local outer solutions, that is,

$$\gamma_i(-\infty) = \gamma_0(1^-)$$
$$\gamma_i(+\infty) = \gamma_0(1^+) \quad . \tag{63}$$

Again, there is one excess constraint, and hence the value of the second outer integration constant $\gamma_0(1^+)$ emerges from this inner solution, thereby closing the problem.

We shall derive explicit analytic solutions only for two limiting cases which, however, together cover most of the conditions which are of interest: the low charge density case, where $\gamma << 1$ everywhere, and the high charge density case, where $\gamma >> 1$ throughout most of the filter.

Low Charge Density Solution for $Pe >> 1$. Consider the case where $\gamma << 1$ everywhere, and assume that Eq. [57] applies. To lowest order in γ , the equation for the outer solution becomes

$$\theta \frac{d\gamma_0}{dz} = -\frac{k_2}{k_1}(\gamma_0 - k_3\gamma_f) \quad . \tag{64}$$

The solution is

$$\gamma_0 = 0 \quad \text{for} \quad z < 0$$

$$= \gamma_f + \left[\gamma_0(0^+) - \gamma_f\right] e^{-\frac{\varepsilon_0 p^2 z}{\varepsilon_f \theta}} \quad \text{for} \quad 0 < z < 1 \qquad [65]$$

$$= \gamma_0(1^+)\, e^{-(z-1)/\theta} \quad \text{for} \quad z > 1$$

where $\gamma_0(0^+)$ and $\gamma_0(1^+)$ are integration constants.

The equation for the inner solutions (see Eqs. [54] - [56]) becomes

$$\frac{d^2\gamma_i}{dy^2} - k_1 \frac{d\gamma_i}{dy} = 0 \quad . \qquad [66]$$

Eq. [66] must be solved separately in the regions $y > 0$ and $y < 0$, and the two solutions joined at $y = 0$ by applying Eqs. [55] and [56], which for the case at hand take the forms

$$(\gamma_i)_1 = (\gamma_i)_2 \qquad [67]$$

$$\left(\frac{d\gamma_i}{dy}\right)_1 - \frac{\varepsilon_f}{\varepsilon_0 \tau^2}\left(\frac{d\gamma_i}{dy}\right)_2 = \left(1 - \frac{\varepsilon_f}{\varepsilon_0 p}\right)(\gamma_i)_1 \qquad [68]$$

Here, 1 denotes a point in the fluid just outside the filter and 2 a point just inside the filter.

When we follow this procedure and solve for the inner solution for the transition region around $z = 0$, and then match it to the local outer solution by applying Eq. [61], we find that

$$\gamma_i = 0 \quad \text{for} \quad y < 0 \quad \text{and} \quad y > 0 \quad \text{near} \quad z = 0 \qquad [69]$$

and

$$\gamma_0(0^+) = 0 \quad . \qquad [70]$$

That is, no charge density is induced in the fluid as it first enters the filter. At the downstream transition region, however, the inner solution is non-trivial. When we solve Eqs. [66] - [68] for the inner solution near $z = 1$, where $y \equiv Pe(z - 1)$, and match with the local outer solutions by applying Eq. [63], we obtain

$$\gamma_i = \gamma_f \left(1 - e^{-\frac{\varepsilon_0 P^2}{\varepsilon_f \theta}}\right) + \gamma_f \left(\frac{\varepsilon_f}{\varepsilon_0 P} - 1\right)\left(1 - e^{-\frac{\varepsilon_0 P^2}{\varepsilon_f \theta}}\right) e^{\tau^2 y/P} \quad \text{for } y < 0$$

$$= \gamma_0(1^+) \quad \text{for} \quad y > 0 \qquad [71]$$

where

$$\gamma_0(1^+) = \frac{\gamma_f \varepsilon_f}{\varepsilon_0 P}\left(1 - e^{-\frac{\varepsilon_0 P^2}{\varepsilon_f \theta}}\right) \quad . \qquad [72]$$

Eqs. [70] and [72] determine the integration constants which appear in Eq. [65]. The outer solution for the charge density distribution, which applies everywhere except very near $z = 0$ and $z = 1$, is thus

$$\gamma_0 = 0 \quad \text{for} \quad z < 0$$

$$= \gamma_f \left(1 - e^{-\frac{\varepsilon_0 P^2}{\varepsilon_f \theta} z}\right) \quad \text{for} \quad 0 < z < 1 \qquad [73]$$

$$= \frac{\gamma_f \varepsilon_f}{\varepsilon_0 P}\left(1 - e^{-\frac{\varepsilon_0 P^2}{\varepsilon_f \theta}}\right) e^{-(z-1)/\theta} \quad \text{for} \quad z > 1 \quad .$$

Figures 3 and 4 show typical (low) charge density distributions in the fluid, the former for a case with small θ and the latter for a case with large θ. The charge density in the fluid extends a distance of the order of θ filter thicknesses downstream of the fluid, and thus stretches far downstream when $\theta >> 1$ but dies off quite close to the filter when $\theta << 1$. When $\theta << 1$, the fluid and fixed charge densities are virtually equal through most of the filter, and very little of the charge is convected downstream. When $\theta >> 1$, on the other hand, the maximum charge density in the fluid is much less than γ_f (it is of order γ_f/θ), but the charge distribution extends correspondingly further downstream; the total integrated charge in the fluid is equal to the total fixed charge in the filter. Regardless of the value of θ, the transition region at the downstream interface has a thickness of order Pe^{-1}, that is, it is very thin compared with the filter thickness. The charge density jumps by a factor $\varepsilon_f/\varepsilon_0 P$ across the interface (see Eq. [72]).

The charging emf can be evaluated from Eq. [46], setting $\gamma \simeq \gamma_0$, since the contributions of the transition regions to the integral are of order Pe^{-1} and can be neglected. We obtain Eq. [12] for the low charge density charging emf. It is clear from Eq. [73] that the low charge density assumption $\gamma << 1$ is satisfied everywhere if either $\gamma << 1$ or $\gamma_f << \theta$.

<u>High Charge Density Solution for Pe >> 1</u>. When $\gamma >> 1$ throughout most of the region $0 < z < 1$ inside the filter, then $f(\gamma) \simeq 2t_a\gamma$ and Eq. [46] yields

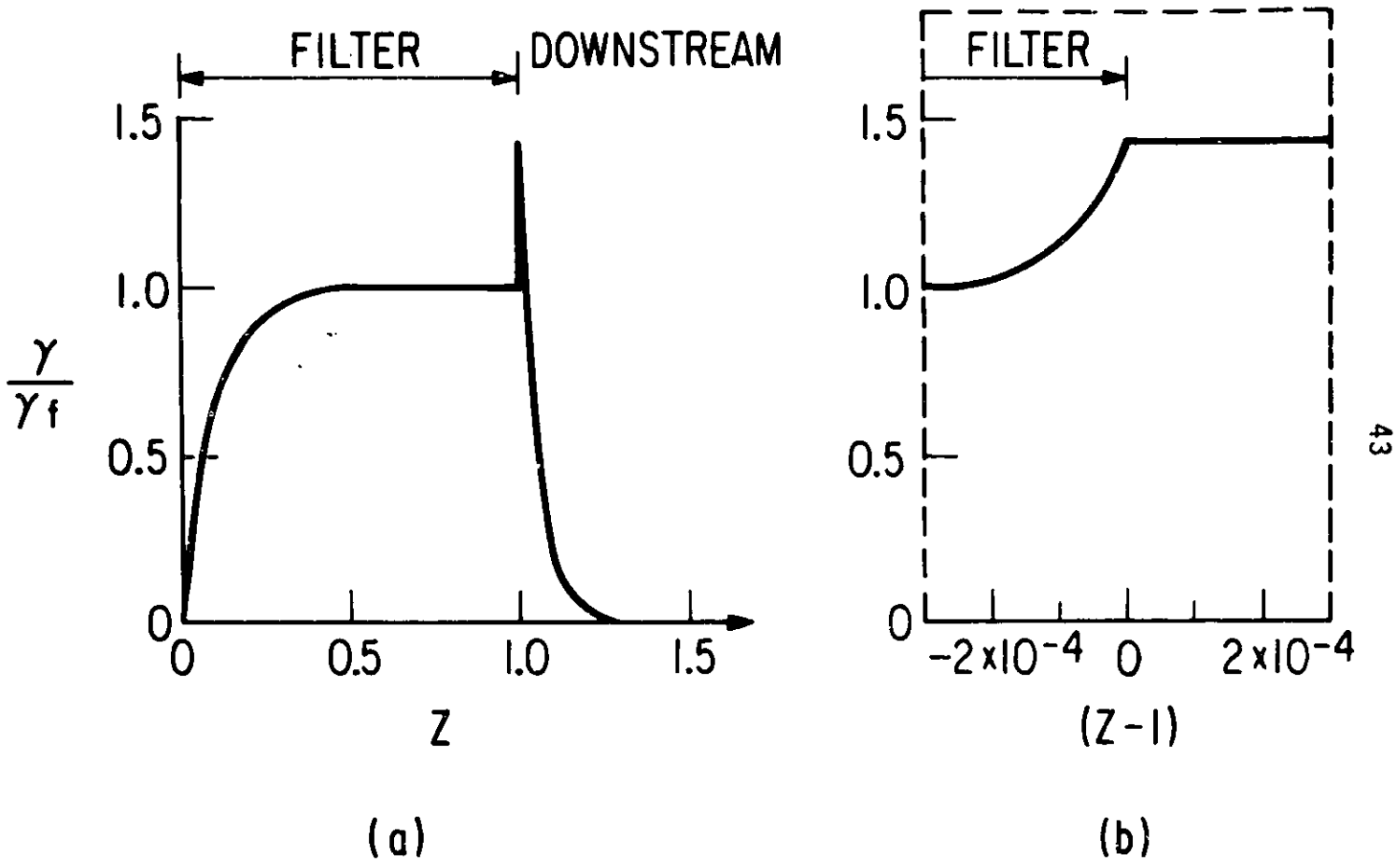


FIGURE 3. Charge density distribution in the fluid for a low flow speed case where $\theta = 0.05$. Other assumptions are $\gamma_f << 1$, $Pe = 10^4$, $P = 0.7$, $\tau = 1$, $\varepsilon_f = \varepsilon_0$.

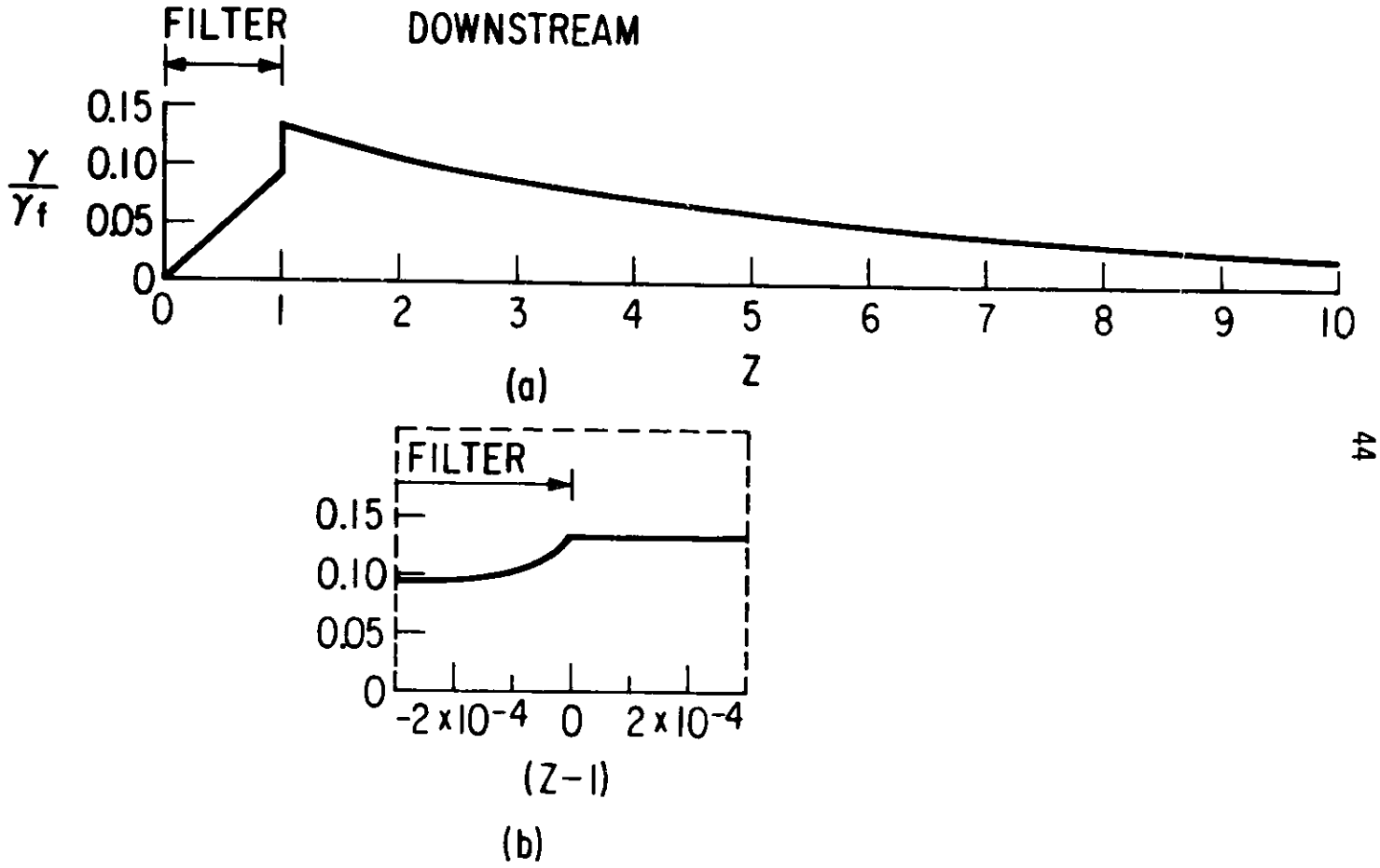


FIGURE 4. Charge density distribution in the fluid for a high flow speed case where $\theta = 5$. Other assumptions are $\gamma_f \ll \theta$, $Pe = 10^4$, $P = 0.7$, $\tau = 1$, $\varepsilon_f = \varepsilon_0$

$$-Z_f \, \& \simeq \frac{\bar{u}h}{\kappa_a} \left[\frac{\tau^2}{\bar{p}} + 2t_a \int_1^\infty \frac{\gamma}{f(\gamma)} \, dz \right] . \qquad [74]$$

In the region of integration that remains, γ is given by the outer solution γ_0. Substituting from Eq. [58], we can write the above equation as

$$-Z_f \, \& \simeq \frac{\bar{u}h}{\kappa_a} \left[\frac{\tau^2}{\bar{p}} + 2t_a \, \theta \int_0^{\gamma_0(1^+)} \frac{1 - \left[\gamma + (2t_a - 1)(1+\gamma^2)^{\frac{1}{2}} \right] J}{\gamma(1+\gamma^2)^{\frac{1}{2}} \, f^3(\gamma)} \, d\gamma \right] . \qquad [75]$$

Now, if $\gamma >> 1$ in the filter, then $\gamma_0(1^+) >> 1$. Furthermore, it is easy to demonstrate that virtually all of the contribution to the integral in Eq. [75] comes from the region where $\gamma < 3$, where the term involving J in the integrand is small (since $|J| << 1$; see Appendix B). Hence, Eq. [75] can to a very good approximation be written as Eq. [15], with

$$F(t_a) = 2t_a \int_0^\infty \frac{d\gamma}{\gamma^2(1+\gamma^2)^{\frac{1}{2}} \, f^3(\gamma)} . \qquad [76]$$

The integral in Eq. [76] can be evaluated explicitly in terms of the parameter t_a, $f(\gamma)$ being given by Eq. [25], and we obtain Eq. [17].

There remains the question of when the assumption that $\gamma >> 1$ throughout most of the filter is satisfied. Clearly, this can only be true if $\gamma_f >> 1$, since the free charge density in the filter approaches γ_f from below. However, there is a further requirement. We see from Eq. [58] that when $\gamma_f >> 1$, the charge density reaches a value large compared with unity in a dimensionless distance $\Delta z \sim \theta/\gamma_f$. Hence, the requirement $\gamma >> 1$

in most of the filter is satisfied only if $\theta/\gamma_f \ll 1$. There are thus two requirements, both of which must be satisfied: $\gamma_f \gg 1$ and $\gamma_f/\theta \gg 1$.

We note, finally, that the above derivation of the high charge density solution is independent of the precise form of Poisson's equation inside the filter. Only the equation for the electric field in the filter has been used directly.

Solution for $\theta \ll 1$, with Arbitrary Péclet Number

A simple analytic solution, again based on the singular perturbation technique, can be readily obtained for arbitrary values of Pe if $\theta \ll 1$ and if

$$\left(\frac{\lambda_D}{h}\right)^2 \ll 1 \qquad [77]$$

when Pe is not large. These two requirements ensure that the outer solution to Eq. [54] is simply $\gamma - k_3\gamma_f = 0$, that is, the outer solution is one of quasi-neutrality between the charge in the fluid and the fixed charge,

$$\begin{aligned} \gamma_0 &= \gamma_f \quad \text{for} \quad 0 < z < 1 \\ &= 0 \quad \text{for} \quad z < 0 \ , \quad z > 1 \end{aligned} \qquad [78]$$

Eq. [77] also ensures that the characteristic length for the transition regions at the two filter-fluid interfaces is very small compared with the filter thickness even if Pe is not large (the scale of the transition regions is then of order λ_D), so that we can regard the transition regions as discontinuities and obtain the charging emf from Eq. [46] using Eq. [78] directly:

$$-Z_f \mathfrak{E} = \frac{\tau^2}{P} \frac{\gamma_f}{f(\gamma_f)} \frac{\bar{u}h}{\kappa_{av}} \quad . \qquad [79]$$

Here $f(\gamma_f)$ is obtained from Eq. [25] with $\gamma = \gamma_f$. This is essentially the solution which we derived in our earlier paper (6), except that the present solution allows for a difference between the mobilities of the counterions and co-ions. Note that

$$-Z_f \mathfrak{E} \simeq \frac{\tau^2}{P} \frac{\gamma_f \bar{u}h}{\kappa_{av}} \qquad \text{when} \quad \gamma_f << 1$$

$$\simeq \frac{\tau^2}{P} \frac{\bar{u}h}{\kappa_a} \qquad \text{when} \quad \gamma_f >> 1 \quad . \qquad [80]$$

These forms match with the low and high charge density solutions, respectively, in the limit $\theta << 1$.

5. DISCUSSION

Our analysis is based on a set of assumptions [(a)-(f) in Section 2] about filtration conditions and filter and fluid properties. Some comments are in order on how well these assumptions are satisfied in typical fuel filtration situations.

Assumption (a) requires that the filter pore radius be smaller than the Debye length. The pore radii of fuel filters are usually in the range 0.5 - 10 μm .[11] Typical refinery products, including aircraft fuels, have conductivities [12] between 1 picomho/m , which corresponds to a Debye length of about 70 μm [based on a relative fluid permittivity of 2 and $D_{av} = 0.3 \times 10^{-9}$ m^2/sec [9]], and 10 picomho/m , which corresponds to a Debye length of about 20 μm . The criterion $a < \lambda_D$ is thus generally satisfied.

Some fuels are doped with antistatic additives to increase their conductivity and reduce general electrostatic hazards. Shell, for example, recommends [12] that the conductivity be increased to 50-300 picomho/m, which would put the Debye length in the range 10-4 μm . In this case our criterion $a < \lambda_D$ may not be satisfied in filters whose pore radii are at the higher end of the range 0.5 - 10 μm .

Assumption (b) requires that the solid matrix of the filter have an electrical conductivity small compared with that of the fluid which permeates the filter. Table 2 lists electrical conductivities of some materials which are typical of those used in filters. Most are well below the 1-10 picomho/m range of undoped fuels. Note that the criterion, as expressed

TABLE 2. Conductivities of Solid Filter Constituents

Material	$\sigma_s \times 10^{12}\ \Omega^{-1}m^{-1}$	Uses
Cellulose esters: [a]		
Cellulose acetate	1.4	paper filters
Cellulose triacetate	0.07	
Cellulose acetate butyrate	0.07	
Cellulose propionate	0.033	
Ethyl cellulose	0.1	
Teflon	0.0001	coating on monel separator elements[11]
Phenoxy resin [b] (Bakelite phenoxy, PRDA 8060, Union Carbide Corp.)	2	coating on paper and Fiberglass elements[4,11]
Silicone [c]	0.1 - 1	to treat filter separator cartridges[11]

a. Bikales, N.M. (ed.), "Encylopedia of Polymer Science and Technology," Vol. 5, p. 524, Wiley-Interscience, New York, 1964.

b. Ibid. Vol. 10, p. 115.

c. Ibid. Vol. 12, p. 529.

by Eq. [5], actually contains a factor with the filter porosity which serves to reduce the conductance of a filter below the value associated with a solid block of the filter material. In addition, Eq. [5] is a very conservative criterion when the high charge density solution applies, since the conductivity of the fluid in the filter pores is then a factor γ above the undisturbed fluid conductivity (see Eqs. [24] and [25]).

As regards assumption (c) about one-dimensionality in the region where charge exists in the fluid, it seems clear that some deviations will occur when the relaxation length is comparable with or larger than the filter pore diameter. The impact on the charging emf is difficult to assess without a complete analysis. It should be stressed, however, that we require one-dimensional conditions only in the region where there is space charge downstream of the filter, that is, some relaxation lengths downstream of the filter. The superficial flow speed in fuel filters is typically 1-5 cm/sec .[13] This places the charge relaxation length $\varepsilon_0\bar{u}/\sigma_0$ between about 2 and 100 cm in fuels with conductivity in the range 1-10 picomho/m. Not only does assumption (c) require one-dimensional conditions over this distance, but assumption (d) requires that the effective electrode separation (see Eq. [7]) be large compared with the charge relaxation length. The latter requirement is easy to satisfy in the laboratory, and can also be satisifed in practical situations (ℓ_0 can be very large if, for example, the walls of a collecting tank serve as the downstream electrode). However, it is also clear that the relaxation length can easily be larger than the separation between the filter and

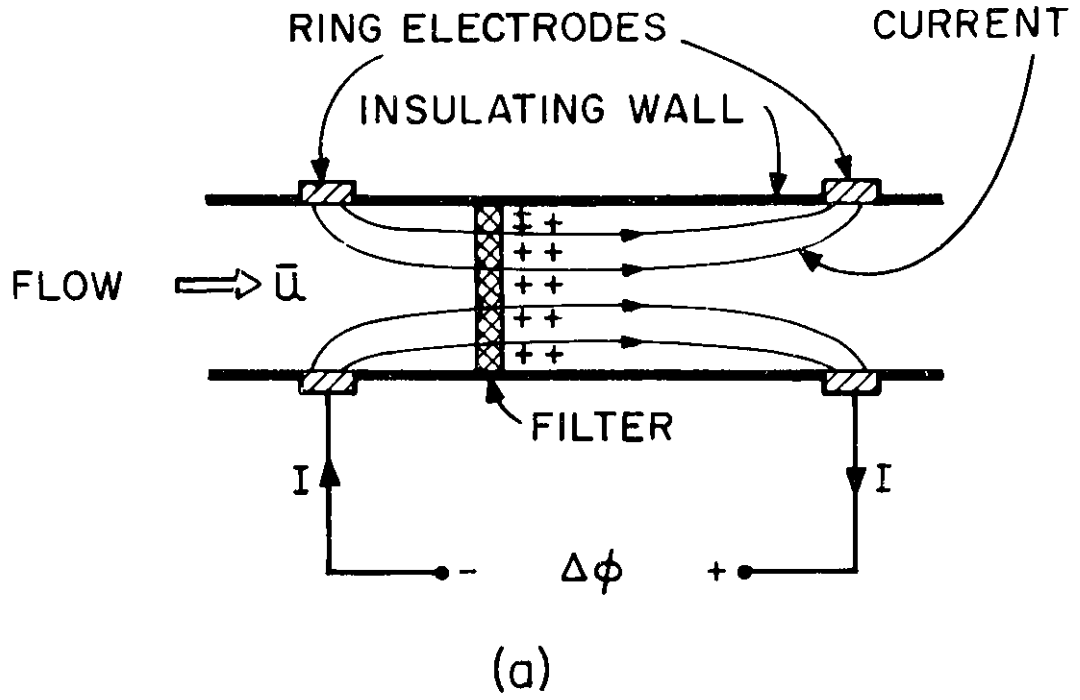
whatever serves as the downstream electrode, particularly if the latter is simply the walls of the pipe downstream of the filter.

Figure 5 emphasizes our point that one-dimensional conditions are necessary only in the region of space charge. Our analysis can be applied directly to the systems shown in Figure 5 if the electrodes are sufficiently far apart to ensure that the current density is approximately uniform over the filter and if one-dimensional conditions prevail in the region where the charge is distributed in the liquid. The charging emf can be deduced from the equations summarized in Section 2, and the actual current-voltage relations for the systems can be obtained from Eq. [1], where R_0 can be either computed or determined empirically (for example with the filter removed, since the filter region itself contributes very little to R_0 if Eq. [6] applies).

The high Péclet number assumption, Eq. [8], is satisfied in <u>all</u> fuel filtration situations of practical interest. Typical filter thicknesses are of the order of 1 mm, although Eq. [8] would be readily satisfied with much thinner filters.

Finally, little can be said about the assumption (f) regarding thermodynamic equilibrium between the ionized constituents and the fluid, since no data is available on the ionization and recombination rates of typical ions in hydrocarbon liquids. Some support for it, as well as for the companion assumption that the fluid behaves as a very weak electrolyte, may be deduced from our experiments, [9] which are in good agreement with our theory.

In conclusion, some qualitative comments might be in order on how



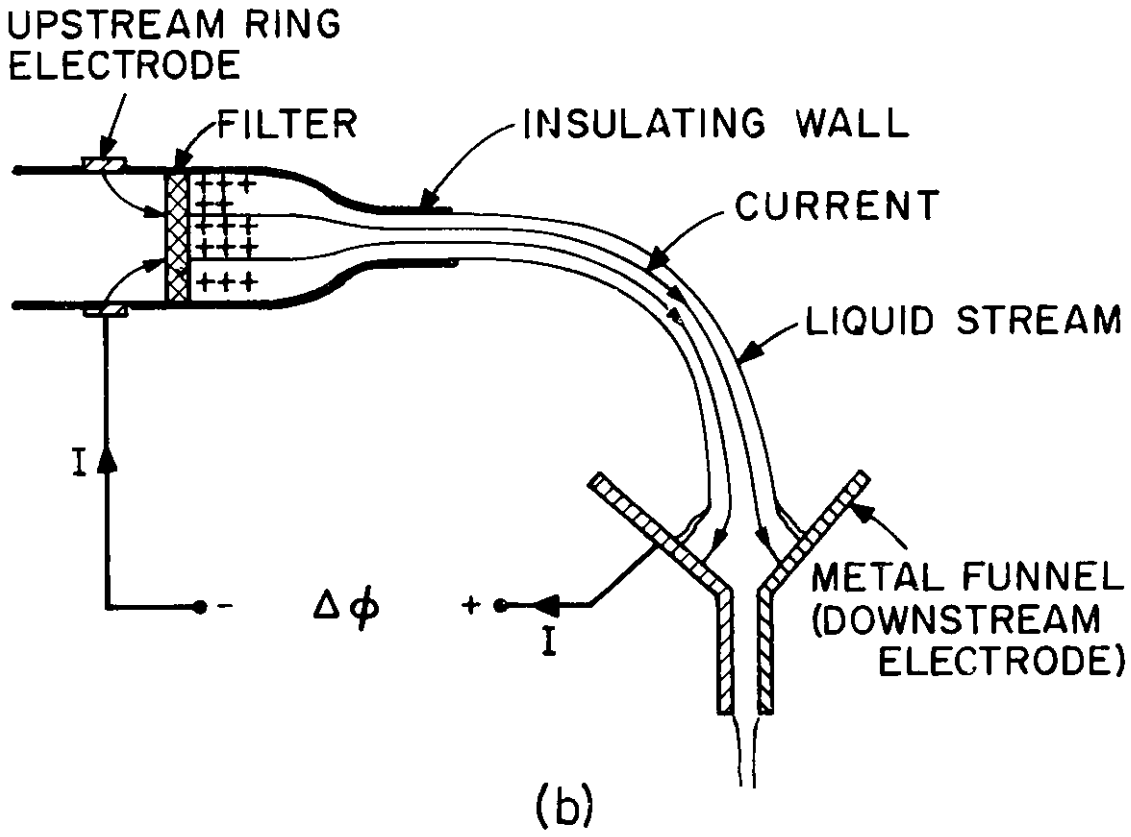


FIGURE 5. Some filtration configurations where conditions may be approximately one-dimensional in the charged regions of the fluid.

charging occurs in our model, and on how our model differs from some earlier hypotheses about the charging mechanism. In our model, the charging mechanism is the following. The fixed charge in the filter tends to induce a countercharge in the fluid which permeates the filter. A net charge arises locally in the fluid by dissociation of the ionizing constituent (see Eq. [22]); the solid matrix of the filter serves merely as an inert, non-conducting framework on which the fixed charge is distributed. Flow tends to convect the countercharge downstream. An electric field is set up, partly because the flow-induced convection current must be compensated by an opposite migration current if the total current is constrained, and partly because the flow-distorted charge distribution in the fluid (see Figures 3 and 4) gives rise to a new potential distribution via Poisson's equation. The flow thus induces a potential rise - the charging emf - across the region where the charge is distributed in the fluid. This charging emf drives the current (now by ionic migration) through the rest of the fluid regions between the electrodes, where there can be no convection current. The current path is from one electrode, through the filter, to the other electrode (see Figure 5).

Our model is thus quite different from for example Gavis and Wagner's (3) view of the charging mechanism. Gavis and Wagner thought that the solid matrix of the filter must serve as the upstream electrode, and that the current lines must originate from the surface of the solid matrix just inside the filter near its upstream face. In their view charging would be impossible if the filter matrix were non-conducting. This is contradicted by our own experimental results, [9] which are in very good

agreement with our own theory.

Finally, it should be emphasized that our model shows that the streaming current (the current measured with the electrodes externally shorted), which has been used in all previous studies as an empirical measure of a filter's charging properties under given flow conditions, is not in fact a property of the filter. The charging emf $\mathcal{E}$ is a property of the filtr (for given flow conditions), but the streaming current $I = \mathcal{E}/R_0$ (see Eq. [1]) depends on the total resistance of the fluid between the electrodes, and hence on the electrode separation and on the geometry of the particular system where the tests are carried out.

APPENDIX A

Bulk-Averaged Form of Poisson's Equation

Consider first a two-dimensional situation like the one shown in Figure A1. s is the distance measured parallel to the axis of a "pore." The shaded parts represent the solid matrix of the filter, which occupies a fraction $(1-P)$ of the cross section A, where P is the porosity. Take a control volume of cross-section A such that its sides lie at planes of symmetry where the electric field in the direction perpendicular to s is zero. The electric field E_s in the direction parallel to the solid-fluid interfaces is continuous at the interfaces, and is therefore the same in the fluid and the solid parts (there is little variation in the direction perpendicular to s since $a < \lambda_D$). In its general form Poisson's equation is

$$\int \varepsilon \vec{E} \cdot \vec{ds} = Q \quad , \qquad [A.1]$$

where ε is the local permittivity. When we apply this to the control volume in Figure A1, we obtain

$$\left[P\varepsilon_0 + (1 - P)\varepsilon_s\right]\frac{dE_s}{ds} A\, ds = Z_f\rho_f A\, ds - Z_f \rho A\, ds \quad . \qquad [A.2]$$

The first term on the right represents the fixed charge in the control volume. Whether this charge resides on the solid-fluid interface, or inside the solid, does not matter. $Z_f\rho_f$ is by definition the amount of fixed charge per unit volume of <u>pore</u> space. The second term on the right represents by definition the amount of charge in the fluid inside the

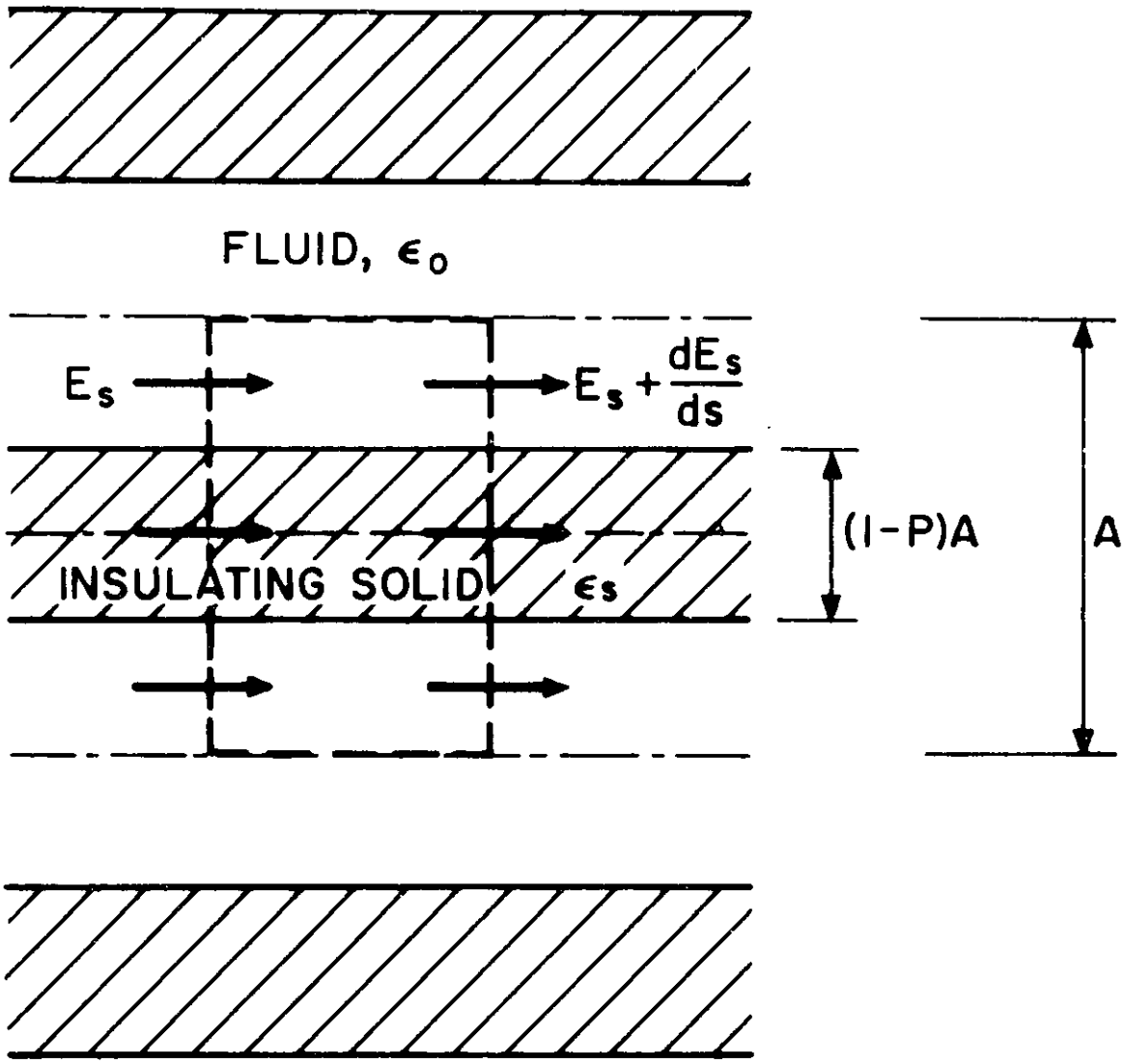


FIGURE A.1. Control volume inside filter for derivation of bulk-averaged Poisson's equation.

control volume.

When Eq. [A.2] is generalized in an ad hoc fashion to randomly porous media by setting $ds = \tau\, dx$ where x is defined in Figure 1, we obtain Eq. [34].

APPENDIX B

Order of Magnitude of the Dimensionless Current

The current density does not appear in our solutions for charging emf because we have made the assumptions that

$$J << 1 \qquad [B.1]$$

$$J << \gamma \qquad [B.2]$$

where $J \equiv Z_f \kappa_{av}\, \bar{j}/\sigma_0 \bar{u}$. We shall show that these assumptions are consistent with our results for charging emf if our basic assumption (d), as expressed in Eq. [6], applies.

The current density through the filter is maximum when the electrodes are externally shorted, that is, $\bar{j} \leq \mathcal{E}/R_0 A_f = \mathcal{E}\sigma_0/\ell_0$ (see Eqs. [1] and [7]) Hence,

$$J \leq \mathcal{E}\kappa_{av}/\ell_0 \bar{u} \qquad [B.3]$$

Consider first the case when either $\gamma_f << 1$ or $\gamma_f << \theta$, so that the low charge density solution for $\mathcal{E}$ applies. From Eq. [12] we have that

$\mathcal{E} \sim \rho_f \bar{u}h/\sigma_0 = \gamma_f \bar{u}h/\kappa_{av}$, and hence

$$J \leq \gamma_f(h/\ell_0) = (\gamma_f/\theta)\,(\varepsilon_0\bar{u}/\sigma_0\ell_0) \quad . \qquad [B.4]$$

This shows that if Eq. [6] is satisfied, Eq. [B.1] is also satisfied whenever the low charge density solution applies. As for Eq. [B.2], we note that in the low charge density solution $\gamma \sim \gamma_f$ when $\theta << 1$ and $\gamma \sim \gamma_f/\theta$ when $\theta >> 1$ (see Eq. [73]). Hence, Eq. [B.2] is also satisfied if the assumption Eq. [6] is satisfied.

The high charge density solution applies when both $\gamma_f >> 1$ and $\gamma_f >> \theta$. In this case, we have from Eq. [15] that $\mathcal{E} \sim (\bar{u}h/\kappa_a)(1 + \theta)$. Hence we find from Eq. [B.3] that

$$J \lesssim (h/\ell_0)(1 + \theta) \qquad [B.5]$$

That is, $J \lesssim h/\ell_0$ when $\theta < 1$ and $J \lesssim \varepsilon_0\bar{u}/\sigma_0\ell_0$ when $\theta >> 1$. Again, Eq. [B.1] is clearly satisfied whenever Eq. [6] applies. Since in this case $\gamma >> 1$ in the region of interest, Eq. [B.2] is automatically satisfied together with [B.1].

REFERENCES

1. Klinkenberg, A. and van der Minne, J.L. (Eds.), "Electrostatics in the Petroleum Industry," Elsevier, Amsterdam, 1958.
2. "Recommended Practice for Protection Against Ignitions Arising out of Static, Lightning and Stray Currents," API RP 2003, 2nd Ed., American Petroluem Institute, New York, 1967.
3. Gavis, J. and Wagner, J.P., Chem. Eng. Sci. 23, 381 (1968).
4. Leonard, J.T. and Carhart, H.W., J. Coll. Int. Sci. 32, 383 (1970).
5. Lauer, J.L. and Antal, P.G., J. Coll. Int. Sci. 32, 407 (1970).
6. Huber, P.W. and Sonin, A.A., J. Coll. Int. Sci. 52, 415 (1975).
7. Schlögl, R., Z. Physik, Chem. Neue Folge 3, 73 (1955).
8. Osterle, J.F., J. Appl. Mech. 31, 161 (1964); Morrison, F.A. Jr. and Osterle, J.F., J. Chem. Phys. 43, 2111 (1965); Gross, R.J. and Osterle, J.F., J. Chem. Phys. 49, 228 (1968).
9. Huber, P.W. and Sonin, A.A., submitted to J. Coll. Int. Sci. (1976)
10. Van Dyke, M., "Perturbation Methods in Fluid Mechanics," Parabolic Press, Stanford, 1975.
11. See for example Velcon Filters Inc., Sales Catalogue, San Jose, Calif.
12. "Shell Anti-Static Additive ASA-3," Shell Technical Bulletin ICSX:69:5, Revised, Charlmont Press, London, 1969.
13. "Electrostatic Discharges in Aircraft Fuel Systems - Phase II," Coordinating Research Council, New York, July 1961.

CHAPTER II

ELECTRIC CHARGING IN FILTRATION: A COMPARISON OF THEORY AND EXPERIMENTS

INTRODUCTION

This chapter describes a series of experiments whose purpose was to test our theory for electric charging in liquid hydrocarbon filtration (Chapter 1). The filters, fluid, and apparatus are described in Section A. Care was taken in the experiments to satisfy the assumptions on which our theory is based. Section B describes experiments with filters which turned out to have high fixed charge, in the sense that the dimensionless fixed charge density γ_f was large compared with unity, and Section C describes experiments with low fixed charge filters, where γ_f was small compared with unity.

The comparison between experiment and theory is, strictly speaking, not an absolute one. Independently measured values are not available for several of the quantities needed in the theory. In the experiments with high fixed charge filters (Section B), we lack independently determined values of the filter tortuosity τ and the mobilities κ_+ and κ of the positive and negative ions in the fluid. However, we shall see that our experimental data were structured so that it was possible to uniquely deduce the values of each of the three quantities κ_+, κ and τ by matching different properties of the data to the theory. The values which emerge are reasonable, in the sense that κ_+ and κ are close to the values expected for ions of the type involved here, and τ is near unity. With the values for κ_+, κ_-, and τ so obtained, the experimental data are in excellent agreement with theory over their entire range. In the

tests with low charge density filters (Section C), the comparison depends on the filter's fixed charge density, for which no previous data is available. A reasonable agreement is obtained by assuming that the particular filter type being tested had a constant fixed charge density over the whole range of fluid conductivity used in the experiments.

SECTION A. APPARATUS, FILTERS, AND FLUID

Charging experiments were conducted with plane filters mounted in two test cells, which simulated the essentially one-dimensional filtration assumed in our theory. The liquid was n-heptane, its conductivity controlled by doping with Shell ASA-3 antistatic additive. Various cellulose ester, nylon, and polyvinyl chloride filters manufactured by the Millipore company[1] were used (Table 1), largely because they are available in controlled thicknesses, pore sizes, and chemical compositions, and are relatively inert to most orgnaic solvents. All the Millipore filters turned out to have high fixed charge, in the terminology of our theory. Filters cut from an industrial pleated cartridge unit, Velcon FO-614PLF-2,[2] were also tested. These had low fixed charge under our experimental conditions.

Test cell 1, shown in Fig. 1, was used for low flow rate experiments and cell 2, shown in Fig. 2, for high flow rates. Both cells were made of plexiglas, the conductivity of which is much less than the fluid conductivities in our experiments. In cell 1 the filter was supported primarily at its edges where a viton O-ring sealed it against the cell wall. The exposed filter area was $1.02 \times 10^{-3} m^2$. In cell 2 a multiple channel system was employed, each of the 61 channels exposing a small, unsupported area of the filter (about $2.5 \times 10^{-6} m^2$) to the incident flow. The total exposed filter area was $1.51 \times 10^{-4} m^2$. This configuration allowed the use of high flow rates without a filter support screen which might have partly occluded

Filter Type	CATALOGUE DATA [1]			
	Material	Thickness µm	Porosity	Pore Radius µm
MF SS	mixed cellulose esters	150	0.83	1.5
MF RA		150	0.82	0.6
MF PH		150	0.77	0.15
MF VC		130	0.74	0.05
NR	nylon	150	0.63	0.5
BD	PVC	135	0.73	0.3
EA	cellulose acetate	130	0.74	0.5
Velcon FO-614PLF-2	resin impregnated paper	390†	not known	~ 1

† Our measurement

TABLE 1. Filter Properties

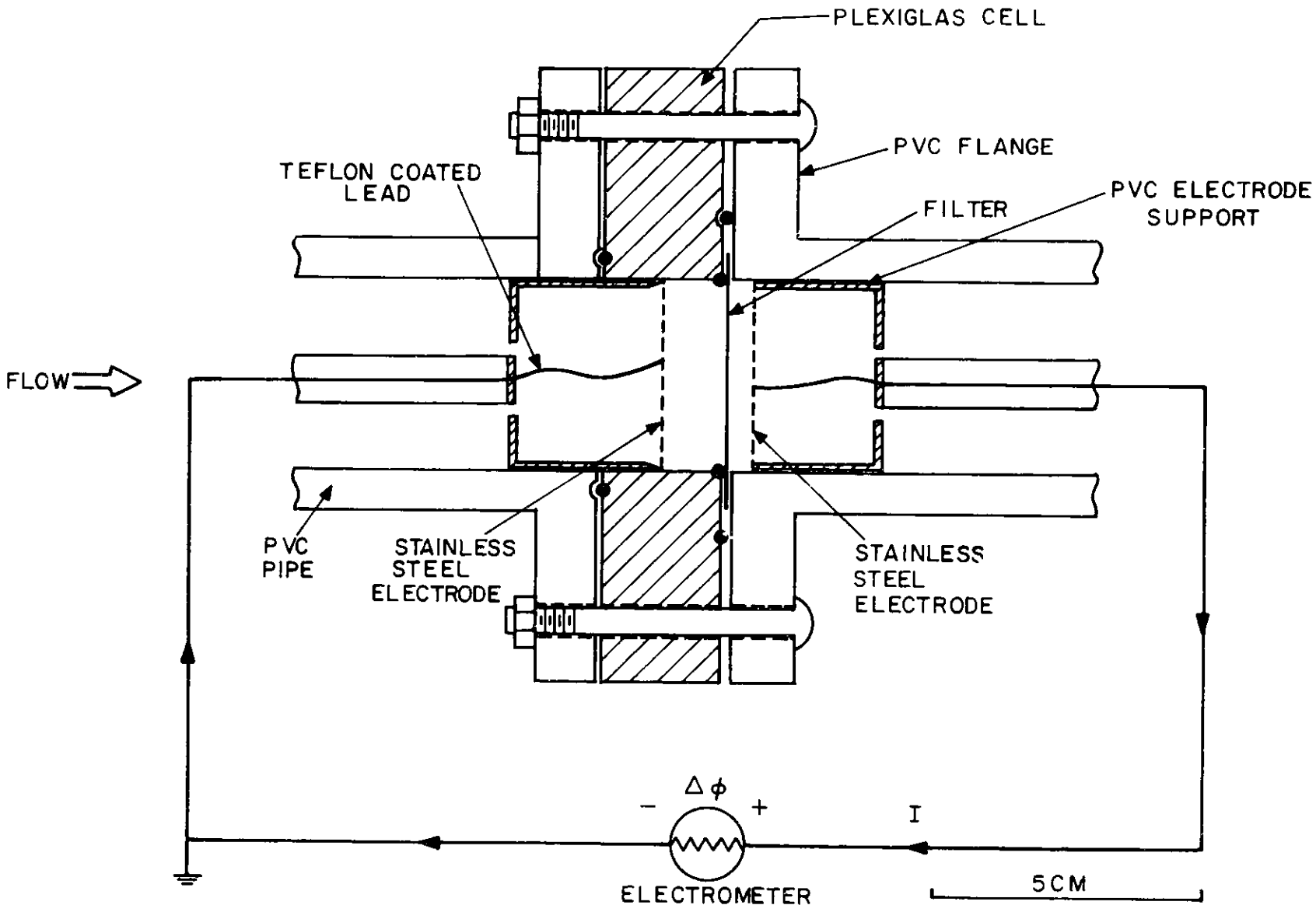


FIGURE 1. Test Cell 1.

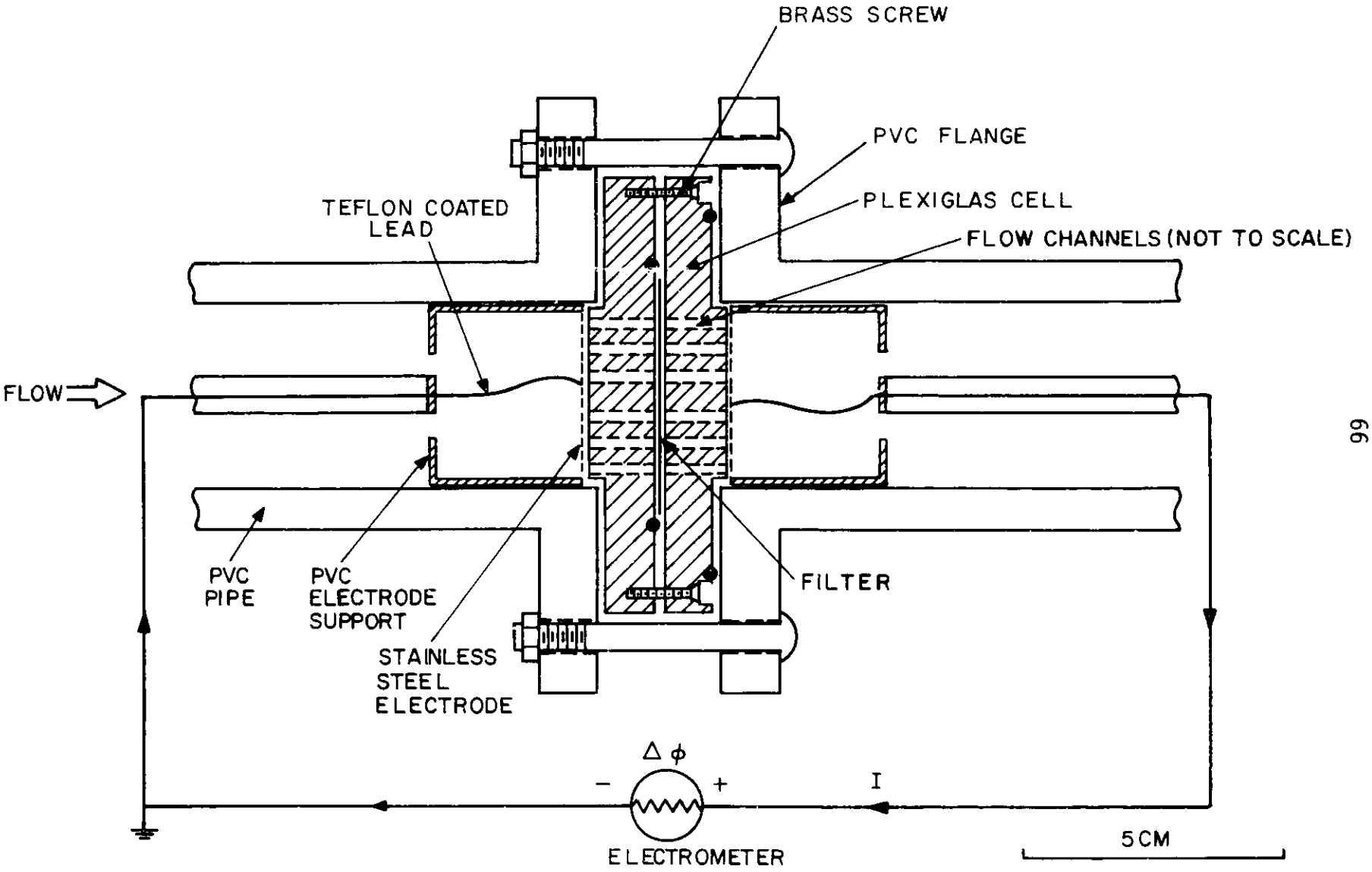


FIGURE 2. Test Cell 2.

the filter or affected the decay of charge downstream.

Fluid was stored upstream of the test cell in a large stainless steel reservoir pressurized with nitrogen. It was conducted to the test cell via nylon and PVC tubing and collected in another reservoir downstream of the cell. All points upstream of the filter, including the upstream electrode, were grounded, while points downstream of the test cell were well insulated from ground. The downstream electrode led to the electrometer (a Keithley 610B) via teflon-coated coaxial cable. Both electrodes consisted of 30 mesh stainless steel. Control experiments without filters indicated that the currents and potentials generated by flow through the electrodes and tubing upstream of the filter were several orders of magnitude less than those generated by the filter.

The heptane used was quoted by the manufacturer as being 99 mole % pure. Without additives it had a conductivity of about $10^{-10}\ \Omega^{-1}m^{-1}$, which is at least an order of magnitude higher than that of chemically pure heptane.[3] In all our experiments the conductivity was increased by a factor of five or more above the conductivity of the fluid as delivered, by the addition of small amounts of Shell ASA-3 ionizing additive.[4,5,6] The assumption was that all observed electrical effects would then involve primarily the ions of the known, controlled additive. Conductivities were measured by a standard d.c. method[7] which was adequate for the relatively high fluid conductivities used.

Figure 3 shows the room temperature conductivity of heptane as a function of the concentration of Shell ASA-3, in the range of concentrations

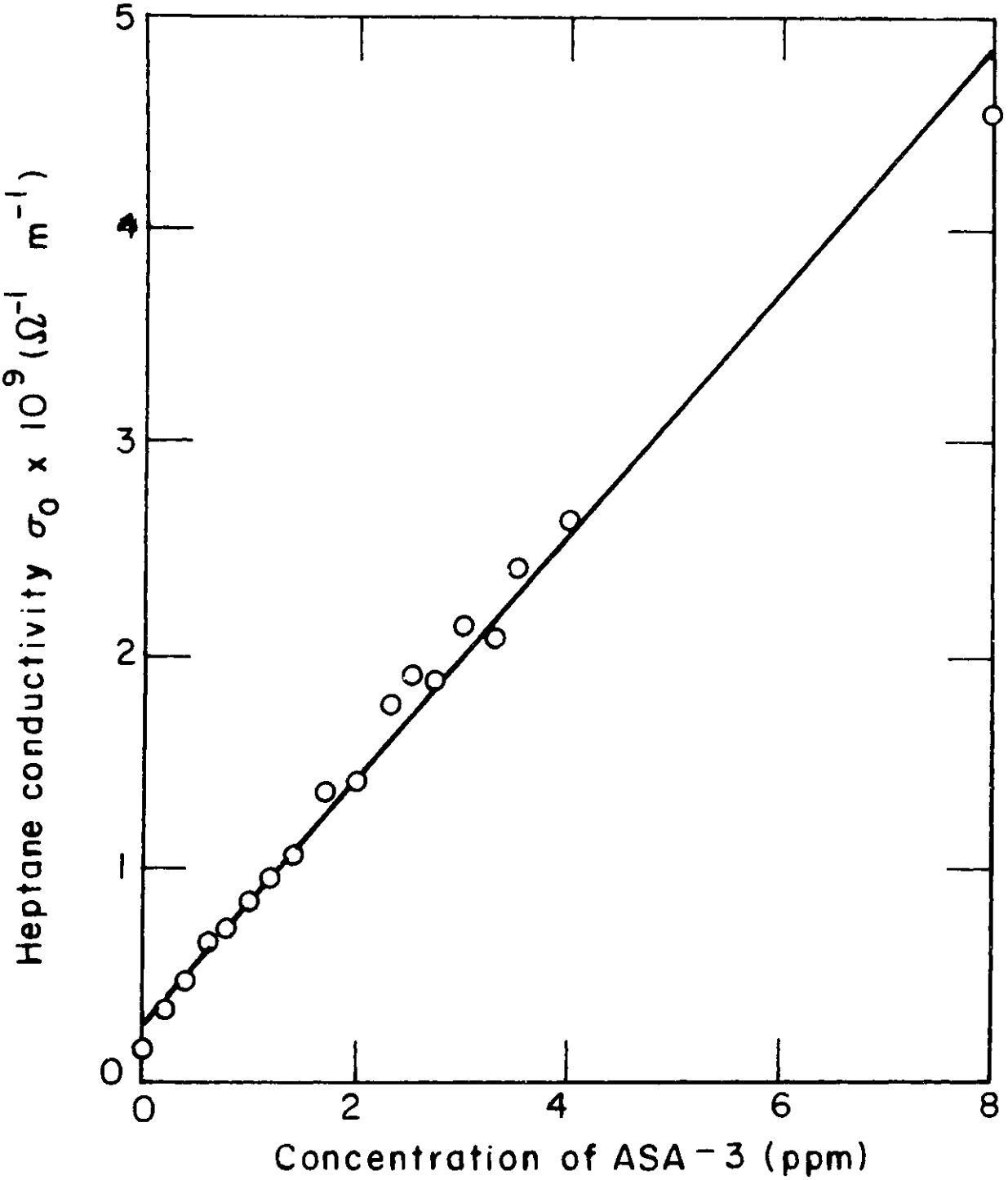


FIGURE 3. Conductivity of heptane as a function of the concentration of Shell ASA-3 antistatic additive measured at 24°C.

used in our experiments. Other hydrocarbon liquids have conductivities of the same order of magnitude at equivalent ASA-3 concentration. [5] ASA-3 is manufactured expressly for the purpose of increasing the conductivities of fuels so as to reduce charging hazards. It is a mixture of equal parts of chromium dialkyl salicylate ("Cr-Ac") and calcium didecyl sulfosuccinate ("Ca-Aerosol-OT") in copolymer of lauryl methacrylate and methyl vinyl pyriine. [6] The primary dissociating constituent appears to be Cr-Ac, with Ca-Aerosol-OT stabilizing the ionic products of the dissociated Cr-Ac via a bimolecular dissociation reaction. That Cr-Ac must be the primary dissociating constituent seems apparent from the fact that a conductivity of $10 \times 10^{-10} \Omega^{-1} m^{-1}$ can be attained by the addition of 1 mole m^{-3} of Ca-Aerosol-OT or about 0.004 mole m^{-3} of Cr-Ac or about 0.001 mole m^{-3} of a mixture of equal parts of the two compounds. [4] Bimolecular dissociation is indicated[8] by the linear variation of the conductivity with additive concentration (Figure 3). A square root variation would be expected if ionization of the additive occurred by binary dissociation.

In previous experiments, [9] we observed that the charging behavior of a filter is affected by the period of immersion in the hydrocarbon liquid. Transient behavior will typically disappear after a certain initial period of soaking. Since we were primarily interested in steady state behavior most of our filters were immersed in the working fluid for several hours or days before testing. The filters were then transferred directly to the test cell without being allowed to dry out. In many cases the filters were tested again after further soaking in the fluid. Special care was taken

in all our tests to ensure steady, reproducible results.

The electric circuit constituted by the filter, fluid, electrodes, and electrometer is shown schematically in Figure 4. The electrometer is characterized by a known external resistance R_e . R_0 is the resistance of all the fluid between the electrodes, both inside and outside the filter. Flow through the filter induces an emf $\mathcal{E}$ between the electrodes. Expressions for this emf are given in Eqs. (12) and (15), Ch. 1. Currents through, and potential differences across, the electrodes of our test cells were measured with a Keithley 610B electrometer, and, when necessary, a Keithley 6103A 1000:1 voltage divider (for potential differences greater than 100 V). Values for R_e were set on the electrometer, from a maximum of 10^{14} Ω (in the potential measuring mode for $\Delta\phi$ < 100 V) to a minimum of about 10^7 Ω . The inter-electrode fluid resistance R_0 was calculated from the neutral fluid conductivity σ_0 , the cross-sectional area of fluid between the electrodes A_f , and the distance between the electrodes. The insulating filter matrix and the charge cloud immediately downstream of the filter contributed an entirely negligible resistance to the total resistance R_0 , because of the large resistances of the <u>neutral</u> inter-electrode fluid upstream and downstream of the filter (see Tables 2 and 3).

In our theory the charging characteristics of a filter are described in terms of a charging emf $\mathcal{E}$ which depends on flow conditions and filter and fluid properties. The actual potential difference $\Delta\phi$ between the electrodes (Fig. 4) is given by

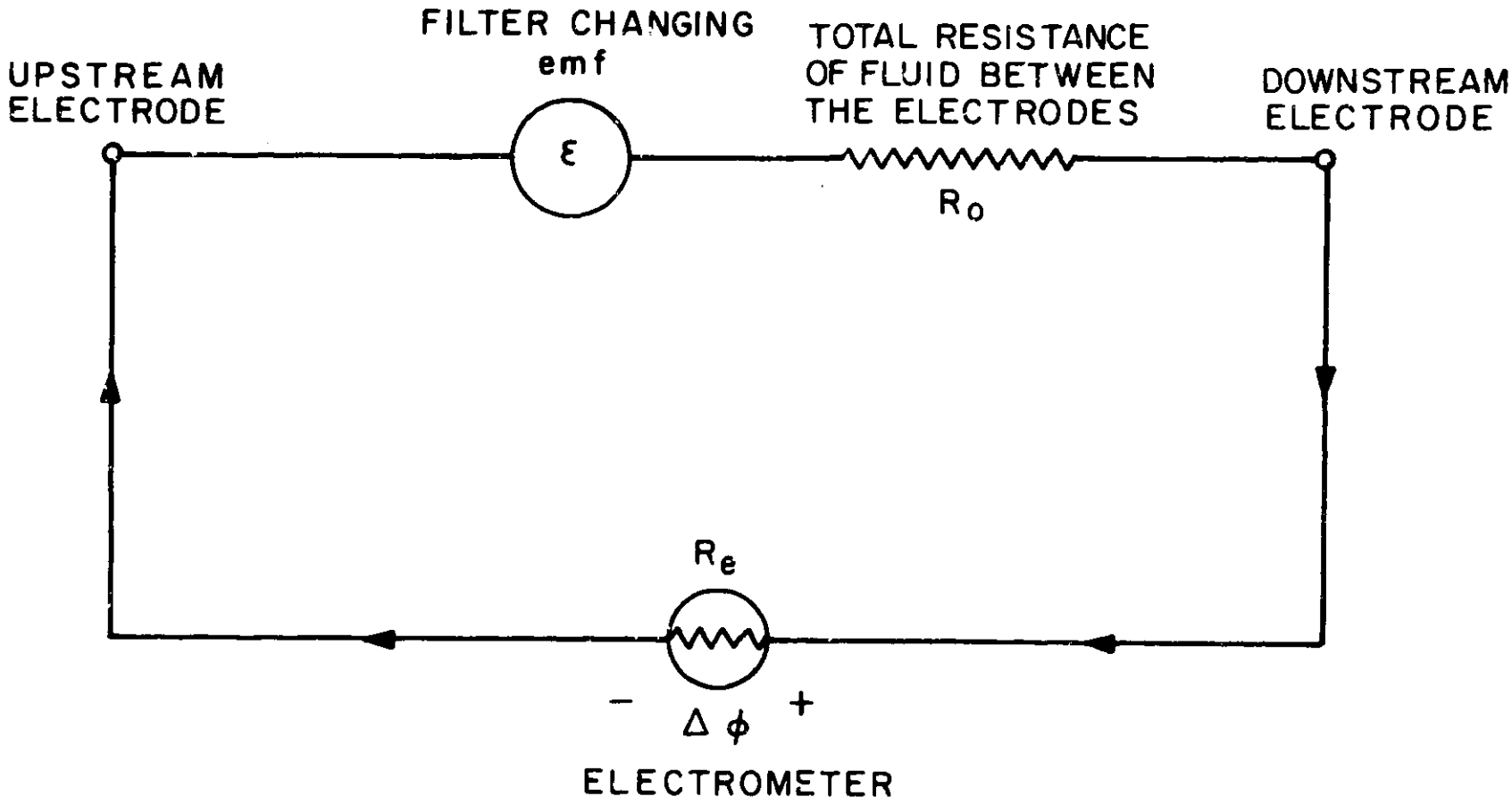


FIGURE 4. Schematic of the filter-fluid-electrometer electric circuit.

Neutral Fluid Conductivity σ_0 , $\Omega^{-1}m^{-1}$	Total Inter-electrode Fluid Resistance R_0 , Ω	Resistance of the Interstitial Fluid inside the Filter $h/PA_f\sigma_0$ [a], Ω	R_e "open" circuit Ω	R_e [b] "short" circuit Ω
6.0×10^{-10}	2.0×10^{10}	8.8×10^{8}	10^{14}	10^{7} - 10^{8}
12.1×10^{-10}	1.0×10^{10}	4.4×10^{8}	10^{14}	10^{7} - 10^{8}

(a) Maximum values for three filters in series. Based on the neutral fluid conductivity and omitting a factor of τ^2 from the estimate.[9]

(b) Maximum values. Currents were measured in both the "normal" and the "fast" current measuring mode. The latter reduces R_e substantially.

TABLE 2. Ranges of Circuit Parameters for experiments in cell 1

Neutral Fluid Conductivity σ_0 , $\Omega^{-1}m^{-1}$	Total Inter-electrode Fluid Resistance R_0 , Ω	Resistance of the Interstitial Fluid inside the Filter $h/PA_f\sigma_0$ [(a)], Ω	R_e "open" circuit Ω	R_e [(b)] "short" circuit Ω
6.0×10^{-10}	3.0×10^{11}	6.0×10^{9}	4.5×10^{11}	10^{7} - 10^{8}
11.9×10^{-10}	1.5×10^{11}	4.0×10^{9}	4.5×10^{11}	10^{7} - 10^{8}

(a) Maximum values for three filters in series. Based on the neutral fluid conductivity and omitting a factor of τ^2 from the estimate.[9]

(b) Maximum values. Currents were measured in both the "normal" and the "fast" current measuring mode. The latter reduces R_e substantially.

TABLE 3. Ranges of circuit parameters for experiments in cell 2

$$\Delta\phi = \mathcal{E} - IR_0 \tag{1}$$

where I is the current through the circuit. Since $\Delta\phi = IR_e$, one obtains from Eq. [1] that

$$\mathcal{E} = \left(1 + \frac{R_0}{R_e}\right) \Delta\phi \tag{2}$$

$$= (R_0 + R_e)I \tag{3}$$

That is, if R_0 and R_e are known, the charging emf can be related either to the potential between the electrodes or the current in the circuit. We note in particular that

$$\mathcal{E} \simeq \Delta\phi \quad \text{if} \quad R_0 \ll R_e \tag{4a}$$

$$\mathcal{E} \simeq IR_0 \quad \text{if} \quad R_0 \gg R_e \tag{4b}$$

Eq. [4] represents the "open-circuit" condition where the full charging emf appears across the electrodes, and Eq. [5] represents the "short-circuit" condition where the electrodes are essentially shorted, and the current adjusts itself to a value such that the charging emf developed by the filter is exactly balanced by the ohmic potential drop in the fluid between the electrodes.

In each of our experimental runs, the charging emf was inferred from two different measurements:

(a) A measurement of electrode potential $\Delta\phi$, with R_e as large as possible. In the lower flow rate experiments, R_e was the

internal resistance (about 10^{14} Ω) of the electrometer and the condition $R_e >> R_0$ applied, so that ζ could be deduced from Eq. (4). At higher flow rates the potential was so large that a 1000:1 voltage divider with $R_e = 4.5 \times 10^{11}$ Ω had to be used, and since this R_e was of the same order as R_0, ζ had to be deduced from Eq. (2). We will refer to this type of data as potential-current measurements, in contrast to measurements of open circuit potentials or of short circuit currents.

(b) A measurement of the short-circuit current or "streaming current" I_0, with the electrometer in the current measuring mode, where the condition $R_e << R_0$ applied ($R_e \sim 10^7$, 10^8 Ω), and ζ could be deduced from Eq. (5).

Care was taken in all our tests to satisfy the basic assumptions on which our theory is based.[1] These are discussed fully in Appendix A.

SECTION B. MILLIPORE FILTER EXPERIMENTS

1. Low θ Experiments

Table 4 (a) and (b) lists the experiments conducted with Millipore filters in cell 1. The heptane was doped at 1 and 2 ppm (by volume) of additive, giving conductivities in the range $6\text{-}12 \times 10^{-10}\Omega^{-1}m^{-1}$. As indicated in the table these were "low θ" experiments - the fluid relaxation length even at the highest flow speeds was always much less than the filter thickness.

Equation (15), Chapter 1, contains the theoretical prediction for the charging emf of a high fixed charge filter:

$$-Z_f \mathcal{E} = \frac{\tau^2}{P}\frac{\bar{u}h}{\kappa_a} + F(t_a)\frac{\varepsilon_0 \bar{u}^2}{k_a \sigma_0} \quad . \tag{5}$$

For "low θ" flows only the first term on the right hand side of Eq. (5) is important, thus:

$$-Z_f \mathcal{E}_{\text{low }\theta} \approx \frac{\bar{u}\, h}{P k_a}\tau^2 \tag{6}$$

[Eq. (80), Chapter 1].

Figure 5 shows open circuit potential versus flow rate data for all MF (mixed cellulose ester) filters tested. The steady state polarity was in every case positive, indicating a filter fixed charge polarity $Z_f = -1$. The simple linear dependence on $\bar{u}$ and h is clearly confirmed by the data. Variations in pore size by a factor of 30 and in conductivity by a

Filter Type	Number of Filters in Series	Period of Immersion	Temperature, °C	Fluid Conductivity $\sigma_0 \times 10^{10}\,\Omega^{-1}m^{-1}$	Sign of Fixed Charge Z_f	$\frac{\lambda_D}{a}$ (a)	$R_0 \times 10^{-10}$ Ω	Minimum Tested	Maximum Tested
SS	1	2 days	19.5	6.0	⊖	2.0	2.0	0.0070	0.079
	1	13 days	20.8	6.0		2.0	2.0	0.012	0.13
	2	13 days	19.6	6.0		2.0	2.0	0.0036	0.07
	3	13 days	20.3	6.0		2.0	2.0	0.0050	0.043
RA	1	15 minutes	21.2	6.6	⊖	4.7	1.9	0.015	0.076
	1	3 days	20.1	6.6		4.7	1.9	0.012	0.12
	2	9 days	21.6	6.4		4.8	1.9	0.0060	0.06
	3	9 days	24.1	6.4		4.8	1.9	0.0030	0.043
	1	6 days	21.0	12.0		3.5	1.0	0.0052	0.12
	1	10 days	24.3	12.0		3.5	1.0	0.042	0.12
	1	11 days	23.1	12.1		3.5	1.0	0.017	0.11
	3	11 days	23.1	12.1		3.5	1.0	0.0040	0.022
	4	6 days	21.0	12.0		3.5	1.0	0.0015	0.0070
PH	1	1 day	21.2	6.6	⊖	19	1.9	0.0077	0.077
	2	12 days	18.3	6.0		20	2.0	0.0037	0.060
	3	12 days	18.8	6.0		20	2.0	0.0040	0.047
	1	10 days	22.9	12.0		14	1.0	0.0078	0.12
	3	10 days	22.9	12.0		14	1.0	0.0020	0.024
VC	1	12 days	20.4	6.0	⊖	59	2.0	0.013	0.13
	2	12 days	21.8	6.0		59	2.0	0.0055	0.060
	3	13 days	21.4	6.0		59	2.0	0.0027	0.028
	1	7 days	21.5	12.0		42	1.0	0.0034	0.13
	3	7 days	26.1	12.0		42	1.0	0.0021	0.027

(a) Assuming $D = 3 \times 10^{-10} m^2 s^{-1}$

$\varepsilon_0 = 1.8 \times 10^{-11} C^2 N^{-1} m^{-2}$

TABLE 4a. Low n experiments with MF filters

Filter Type	Number of Filters	Period of Immersion	Temperature, °C	Fluid Conductivity $\sigma_0 \times 10^{10} \Omega^{-1} m^{-1}$	Sign of Fixed Charge Z_f	$\frac{\lambda_D}{a}$ (a)	$R_0 \times 10^{-10}$ Ω	Minimum Tested	Maximum Tested
	1	2 hours	21.6	6.5		5.8	1.9	0.013	0.21
	1	3 days	18.6	6.5		5.8	1.9	0.018	0.21
	2	2 days	18.6	6.5		5.8	1.9	0.0034	0.11
NR	3	1 day	22.7	6.6	⊖	5.7	1.9	0.0057	0.037
	3	1 day	18.2	6.6		5.7	1.9	0.0017	0.053
	3	2 days	22.6	6.6		5.7	1.9	0.0020	0.018
	1	3 days	18.8	11.5		4.3	1.1	0.011	0.12
	3	3 days	18.8	11.5		4.3	1.1	0.0028	0.040
	1	1 day	22.0	6.5		9.6	1.9	0.021	0.099
	1	3 days	19.5	6.5		9.6	1.9	0.037	0.080
	2	one hour	21.0	6.5		9.6	1.9	0.016	0.043
	2	2 days	20.6	6.5		9.6	1.9	0.018	0.038
BD	2	3 days		6.5	⊕	9.6	1.9	0.0075	0.042
	3	2 hours	21.7	6.5		9.6	1.9	0.0037	0.060
	3	3 days	20.6	6.5		9.6	1.9	0.0093	0.083
	1	5 days	21.5	12.0		7.1	1.0	0.028	0.13
	3	5 days	21.5	12.0		7.1	1.0	0.0093	0.037
	1	3 hours	21.9	6.6		5.7	1.9	0.015	0.095
	2	1 day		6.6		5.7	1.9	0.010	0.044
	2	7 days	21.8	6.6		5.7	1.9	0.0030	0.070
EA	3	7 days	22.3	6.4	⊖	5.8	1.9	0.0063	0.050
	3	8 days	21.1	6.4		5.8	1.9	0.0043	0.050
	1	3 days	18.4	11.5		4.3	1.1	0.097	0.14
	3	3 days	18.4	11.5		4.3	1.1	0.032	0.047

(a) Assuming $D = 3 \times 10^{-10} m^2 s^{-1}$

$\varepsilon_0 = 1.8 \times 10^{-11} C^2 N^{-1} m^{-2}$

TABLE 4b. Low θ experiments with NR, BD, EA Filters

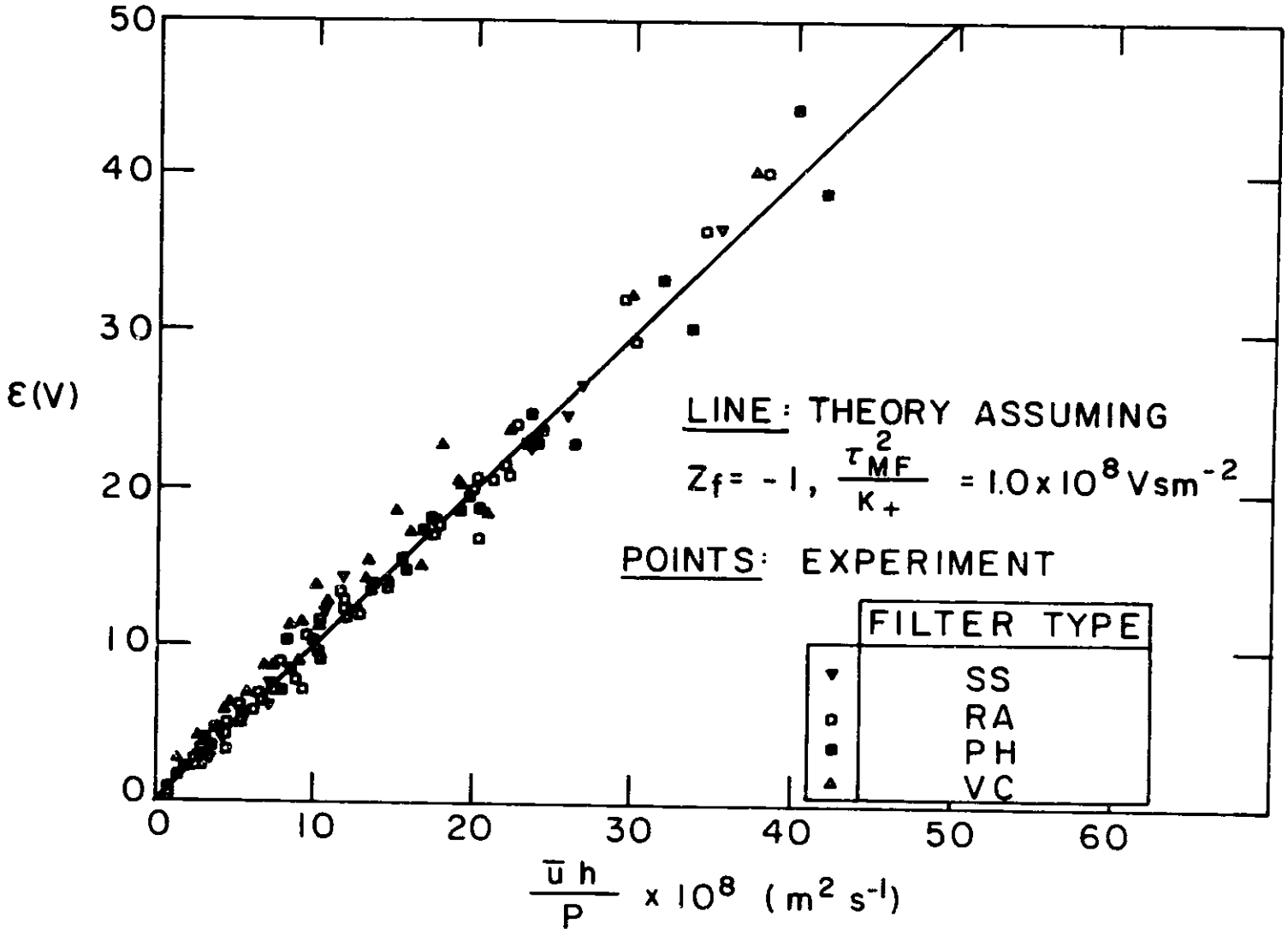


FIGURE 5. Filter emf versus reduced flow speed. Open circuit potential data from MF filters. $0.0015 \leq \theta \leq 0.13$.

factor of 2 had no observable effect on the filter emf, as expected from Eq. (6). To make an <u>absolute</u> comparison between the data in Figure 5 and Eq. (6), a value for the ratio τ^2_{MF}/κ_+ is required (the cation mobility κ_+ is the appropriate counterion property for flows through a negative fixed charge filter and all MF filters appear to have the same tortuosity τ_{MF}). A good fit to the data is obtained by assuming:

$$\frac{\tau^2_{MF}}{\kappa_+} = 1.0 \pm 0.14 \times 10^8 \text{ V s m}^{-2} \quad . \tag{7}$$

Unfortunately, no information on the mobilities of ASA-3 ionic products in heptane or on the Millipore filter tortuosities of interest appears to exist in the open literature. Physically reasonable ranges for these quantities are $0.5 \times 10^8 m^2 V^{-1} s^{-1} \lesssim \kappa_a \lesssim 5 \times 10^8 m^2 V^{-1} s^{-1}$ and $1 \lesssim \tau \lesssim 1.6$. Clearly, the ratio of τ^2/κ inferred from our data, Eq. (7), is well within the physically reasonable range. More detailed comment on Eq. (7) must await analysis of the high θ charging data.

Figure 6 shows short circuit current data for the same MF filters. The measured currents have been reduced to filter emf's according to Eq. (4b) to allow a direct comparison with Eq. (6). The data of Figure 6 are clearly in good agreement with the theory, and confirm the value of τ^2_{MF}/κ_+ already inferred from the potential data, in Figure 5.

The most important possible sources of consistent error in these experiments are probably in the catalogue values of the filter thickness

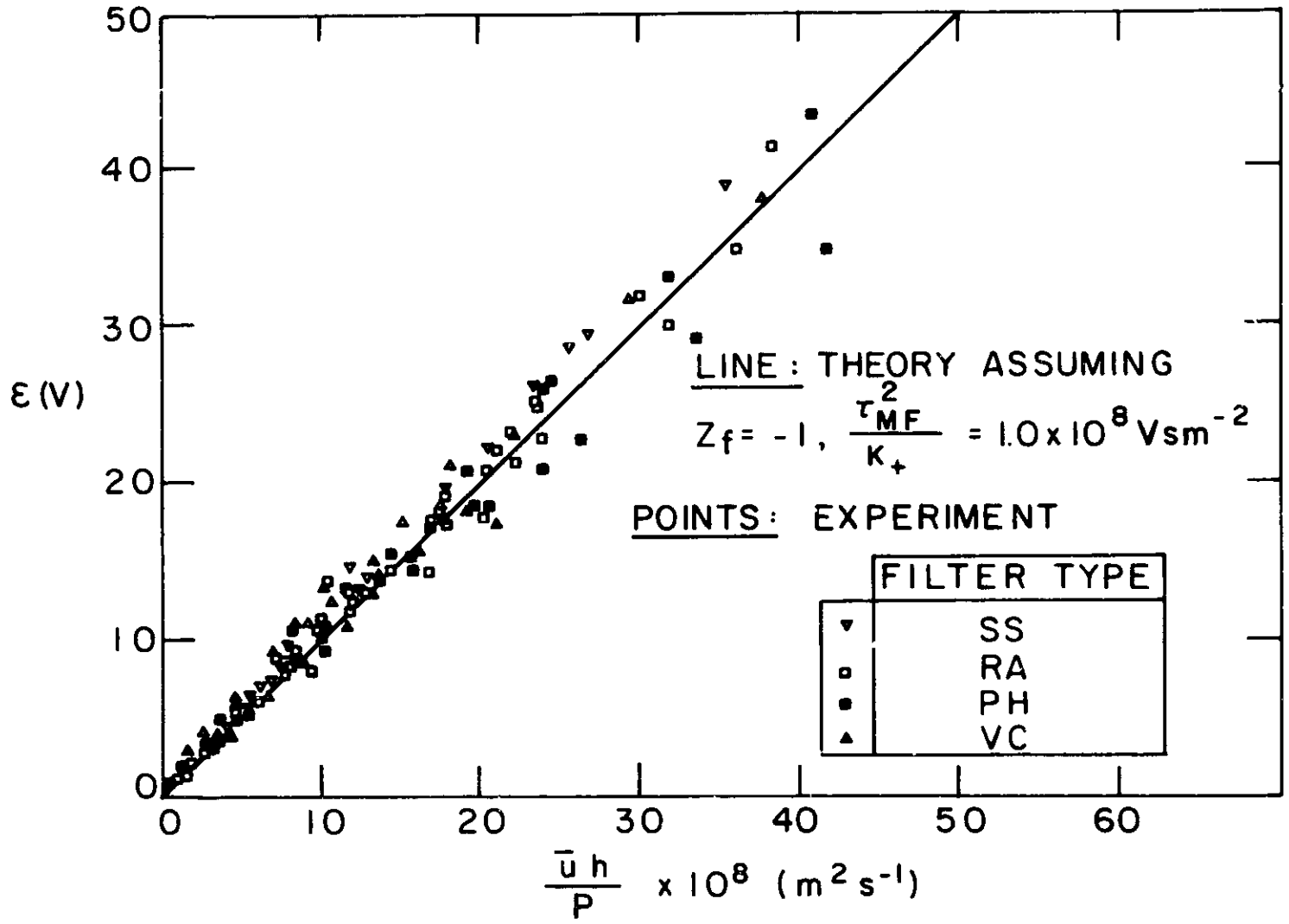


FIGURE 6. Filter emf versus reduced flow speed. Short circuit current data from MF filters. $0.0015 \leq \theta \leq 0.13$.

h and porosity P , which were used in the data reduction, values which are accurate to within about ±10%.† Thus the maximum error in our estimate for τ^2_{MF}/κ_+ is about 20%, with a most probable error[10] of about 14% as indicated in Eq. (7).

Figures 7 and 8 show open circuit potential and short circuit current data for EA (pure cellulose acetate), NR (nylon), and BD [poly (vinyl chloride)] filters. These filters developed negative potentials and currents at steady state, indicating a fixed charge polarity $Z_f = +1$. The NR and BD filters exhibit almost identical behavior, and show good agreement with the theory assuming

$$\frac{\tau^2_{NR,BD}}{\kappa_-} = 0.5 \pm 0.07 \times 10^8 \text{ V s m}^{-2} \qquad (8)$$

while data for the EA filter falls on a line of higher slope indicating

$$\frac{\tau^2_{EA}}{\kappa_-} = 0.91 \pm 0.13 \times 10^8 \text{ V s m}^{-2} \quad . \qquad (9)$$

The rough error analysis in Eqs. (8) and (9) is the same as for the MF filters.

---

†The Millipore catalogue[1] quotes thicknesses to within ±7%. Our own measurements have indicated variations of about ±10% from the median catalogue values across a single dry filter or from filter to filter. Quoted values of P are accurate to about ±10% (private communication with the Millipore Corporation).

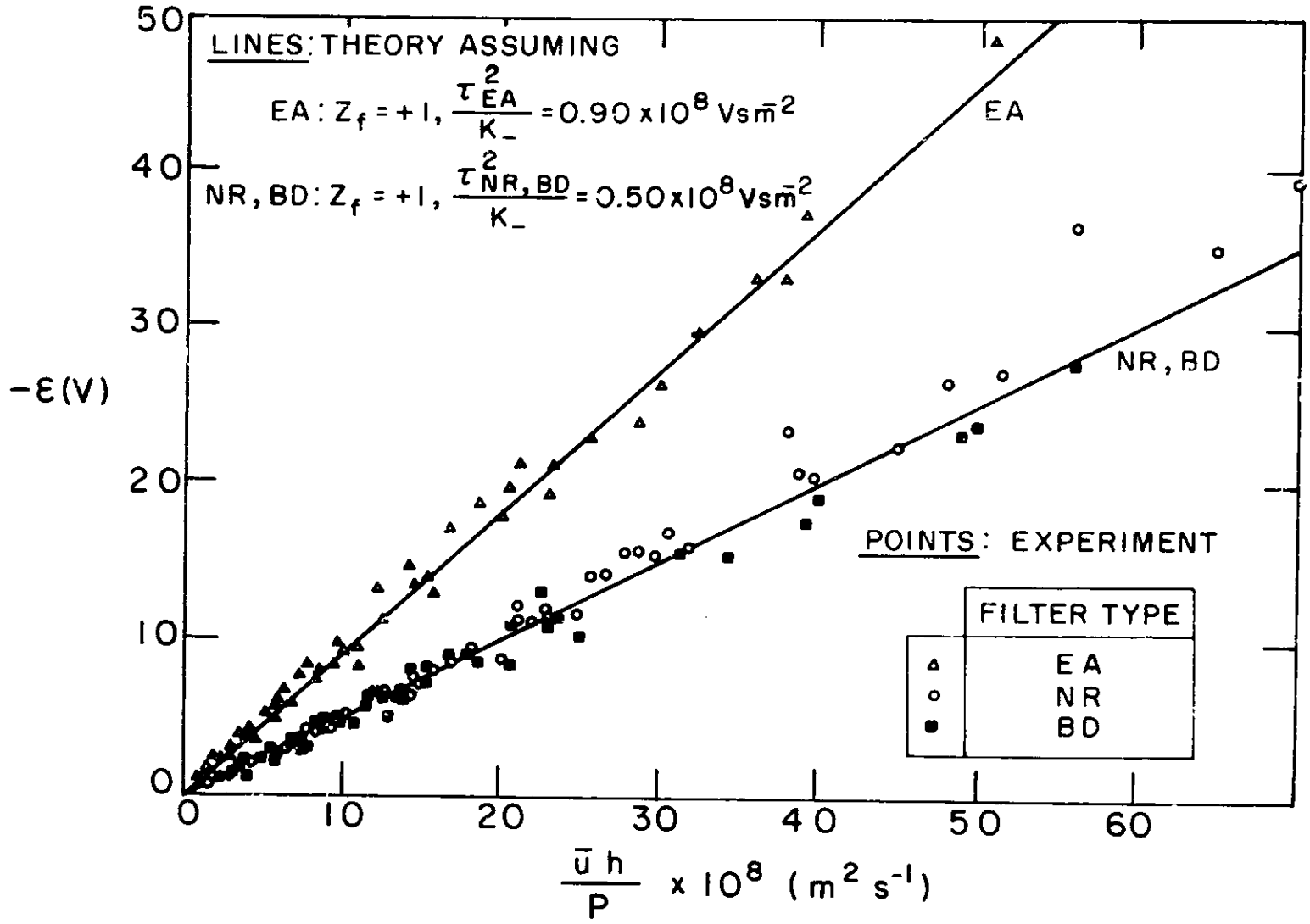


FIGURE 7. Filter emf versus reduced flow speed. Open circuit potential data from NR, BD, and EA filters. $0.0017 \leq \theta \leq 0.21$.

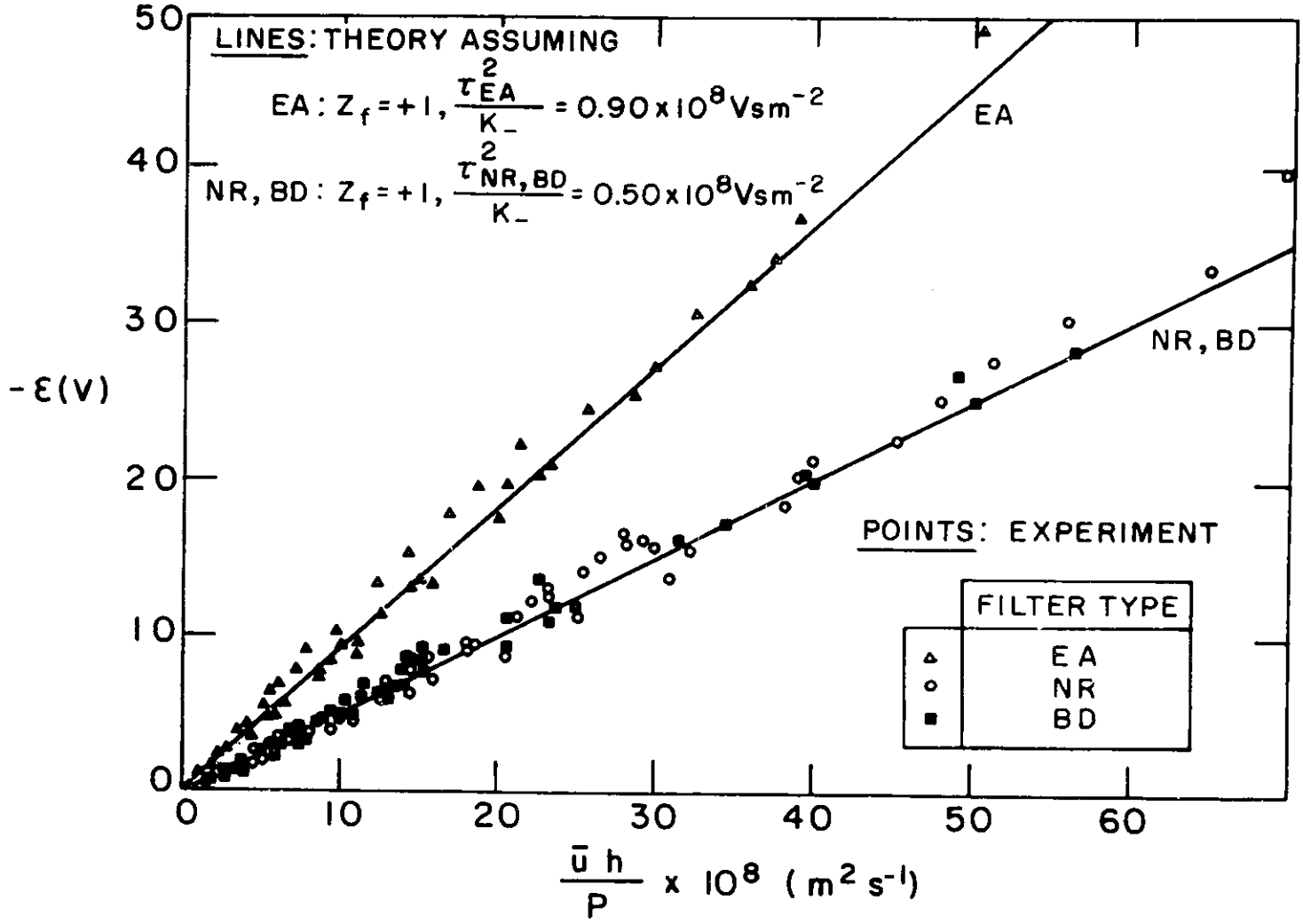


FIGURE 8. Filter emf versus reduced flow speed. Short circuit current data from NR, BD, and EA filters. $0.0017 \leq \theta \leq 0.21$.

2. High θ Experiments

Table 5 (a) and (b) lists the experiments conducted with Millipore filters in cell 2. While these experiments did overlap with the low θ data discussed above, maximum values for θ in these tests were well beyond the "low θ" range of Figures 5 - 8.

Equations (5) and (6) can be rewritten:

$$- Z_f \frac{\mathcal{E}P}{\bar{u}h} \frac{\kappa_a}{\tau^2} = 1 + \frac{\bar{u}\,\varepsilon_0\,P}{\sigma_0 h} \frac{F(t_a)}{\tau^2} = 1 + P\theta \frac{F(t_a)}{\tau^2} \quad . \qquad (10)$$

Adopting reduced variables indicated by Eq. (10), we plot in Figure 9 $- Z_f \frac{\mathcal{E}P}{\bar{u}h} \frac{\kappa_a}{\tau^2}$ against $P\theta$ for the high θ MF filter tests. The closed and open points distinguish emfs deduced from potential-current data [Eq. (2)] and those deduced from short circuit current data [Eq. (4b)]. The experimentally determined value for τ^2_{MF}/κ_+ [Eq. (7)] was used in Eq. (10).

The data in Figure 9 confirm the theoretically predicted dependence of $\mathcal{E}$ on $\bar{u}$, σ_0, and h. The polarity is consistent with $Z_f = -1$ as indicated by the low θ experiments. To make an absolute comparison between theory and experiments a value for the group $F(t_+)/\tau^2_{MF}$ is required. A good theoretical fit to the data of Figure 9 is obtained by assuming

$$\frac{F(t_+)}{\tau^2_{MF}} = 0.94 \pm 0.17 \qquad (11)$$

Filter Type	Number of Filters	Period of Immersion	Temperature, °C	Fluid Conductivity $\sigma_0 \times 10^{10} \Omega^{-1} m^{-1}$	Sign of Fixed Charge Z_f	$\frac{\lambda_D}{a}$ (a)	$R_0 \times 10^{-10}$ Ω	θ Minimum Tested	θ Maximum Tested
SS	1	15 days	17.0	6.0	⊖	2.0	3.0	1.3	6.5
	2	15 days	18.7	6.0		2.0	3.0	0.65	3.3
	3	16 days	17.0	6.0		2.0	3.0	0.43	2.2
RA	1	13 days	18.9	6.0	⊖	5.0	3.0	2.0	6.4
	1	14 days	20.0	6.0		5.0	3.0	0.54	6.4
	2	14 days	20.1	6.0		5.0	3.0	0.28	3.2
	3	14 days	21.0	6.0		5.0	3.0	0.43	2.1
	1	12 days	23.2	11.5		3.6	1.6	0.67	3.3
	3	12 days	23.2	11.5		3.6	1.6	0.22	1.1

(a) Assuming $D = 3 \times 10^{-10} m^2 s$

$\varepsilon_0 = 1.8 \times 10^{-11} C^2 N^{-1} m^{-2}$

TABLE 5a. High θ experiments with MF filters. No experiments were conducted with PH or VC filters in this flow regime. The differential pressures required with these filters to obtain high θ flows caused rupture of the filter discs.

Filter Type	Number of Filters	Period of Immersion	Temperature, °C	Fluid Conductivity $\sigma_0 \times 10^{10}\,\Omega^{-1}m^{-1}$	Sign of Fixed Charge Z_f	$\frac{\lambda_D}{a}$ (a)	$B_0 \times 10^{-10}$	Minimum Tested	Maximum Tested
NR	1	2 hours		6.5	Φ	7.4	2.7	0.064	5.7
	1	7 days	22.0	6.5		7.4	2.7	0.13	4.5
	2	3 hours	18.9	6.5		7.4	2.7	0.012	2.93
	3	2 hours	18.6	6.5		7.4	2.7	0.091	2.0
	1	2 hours	23.4	11.9		5.5	1.5	0.65	3.3
	1	2 hours	24.4	11.9		5.5	1.5	0.65	3.3
	1	1 day	23.8	11.9		5.5	1.5	1.0	3.3
	3	30 days	22.5	11.9		5.5	1.5	0.049	1.1
BD	1	1 hour	18.2	6.5	O	12	2.7	0.54	6.6
	1	3 days	19.5	6.5		12	2.7	0.51	6.6
	2	2 hours	18.8	6.5		12	2.7	0.44	1.8
	2	60 days	20.7	6.5		12	2.7	0.63	1.8
	3	1 hour	21.0	6.5		12	2.7	0.42	1.0
	3	1 day	21.4	6.5		12	2.7	0.42	1.1
	3	3 days	20.1	6.5		12	2.7	0.69	0.96
	3	5 days	18.5	6.5		12	2.7	0.57	1.1
	3	60 days	19.7	6.5		12	2.7	0.44	1.7
	1	18 days	24.3	11.0		9.5	1.6	0.74	3.6
	3	19 days	27.6	11.8		9.1	1.51	0.24	0.59
EA	1	40 minutes	18.9	6.6	Θ	7.3	2.7	0.92	6.7
	1	1 day	18.7	6.6		7.3	2.7	0.13	6.8
	2	15 minutes	18.7	6.6		7.3	2.7	0.38	3.4
	2	1 day	18.2	6.6		7.3	2.7	0.65	3.4
	3	7 days	20.5	6.4		7.4	2.8	0.72	2.3
	3	3 days	19.6	6.4		7.4	2.8	0.46	2.3
	1	14 days	22.1	11.0		5.7	1.6	0.85	4.1
	1	17 days	24.0	11.0		5.7	1.6	1.2	4.1
	3	17 days	24.0	11.0		5.7	1.6	0.28	1.4

(a) Assuming $D = 3 \times 10^{-10} m^2 s$

$\varepsilon_0 = 1.8 \times 10^{-11} C^2 N^{-1} m^{-2}$

TABLE 5b. High Θ experiments with NR, BD, EA Filters

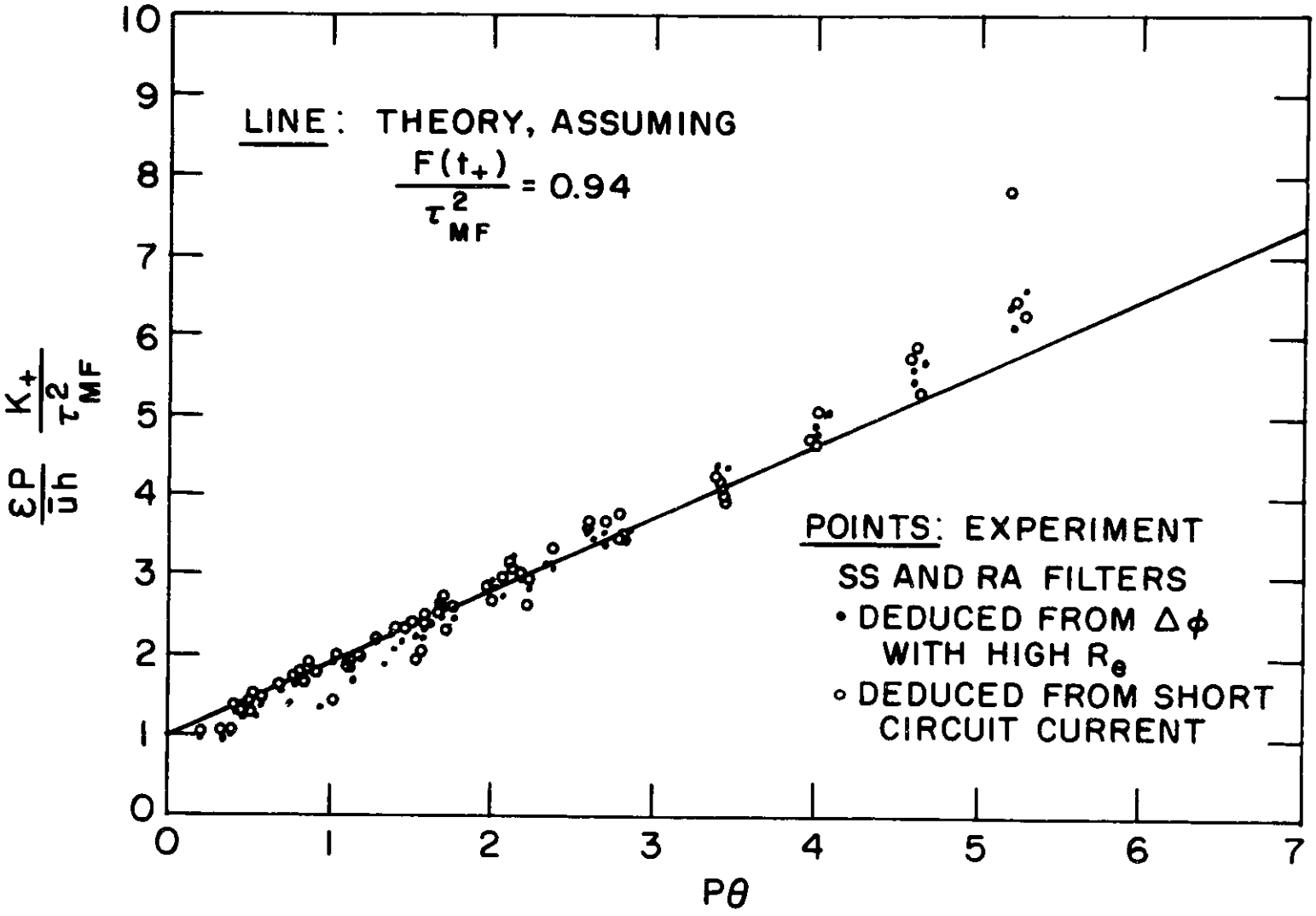


FIGURE 9. Reduced filter emf versus reduced flow speed. MF filters. $0.22 \leq \theta \leq 6.5$.

in Eq. (10). For physically reasonable ranges of t_a, $F(t_a)$ is of order unity (Table 1, Chapter 1), as are typical tortuosities. Thus the experimentally inferred value for $F(t_+)/\tau^2_{MF}$ is well within a physically reasonable range; again we defer until the next section a more detailed analysis of this aspect of our experimental results.

The error analysis in Eq. (11) involves the same uncertainties in h and P ($\pm$ 10%) and additional possible error in the measured conductivity σ_0 which we estimate to be at most $\pm$10%. Thus the maximum possible error in Eq. (11) would be about 30%, with a most probable error of about 18% as indicated.

Figure 10 shows similar emf data for NR and BD filters. The data indicate:

$$\frac{F(t_-)}{\tau^2_{NR,BD}} = 0.93 \pm 0.17 \quad . \tag{12}$$

Again, the predicted theoretical dependence on $\bar{u}$, σ_0, and h appears to be confirmed, and the charging polarities agree with the low θ data.

Emf data for EA filters are shown in Figure 11. The best theoretical fit corresponds to

$$\frac{F(t_-)}{\tau^2_{EA}} = 0.59 \pm 0.11 \quad . \tag{13}$$

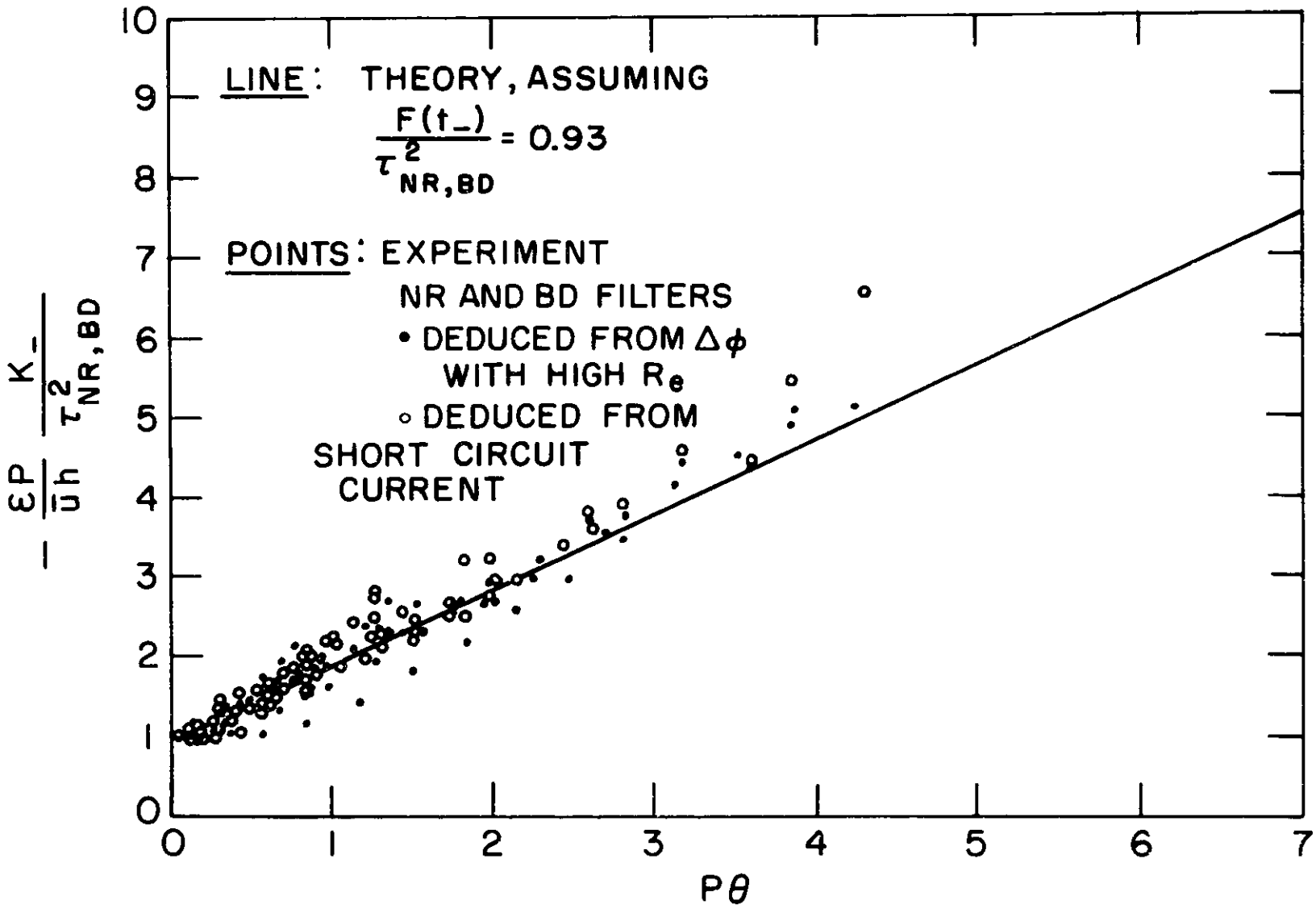


FIGURE 10. Reduced filter emf versus reduced flow speed. NR and BD filters. $0.012 \leq \theta \leq 6.6$.

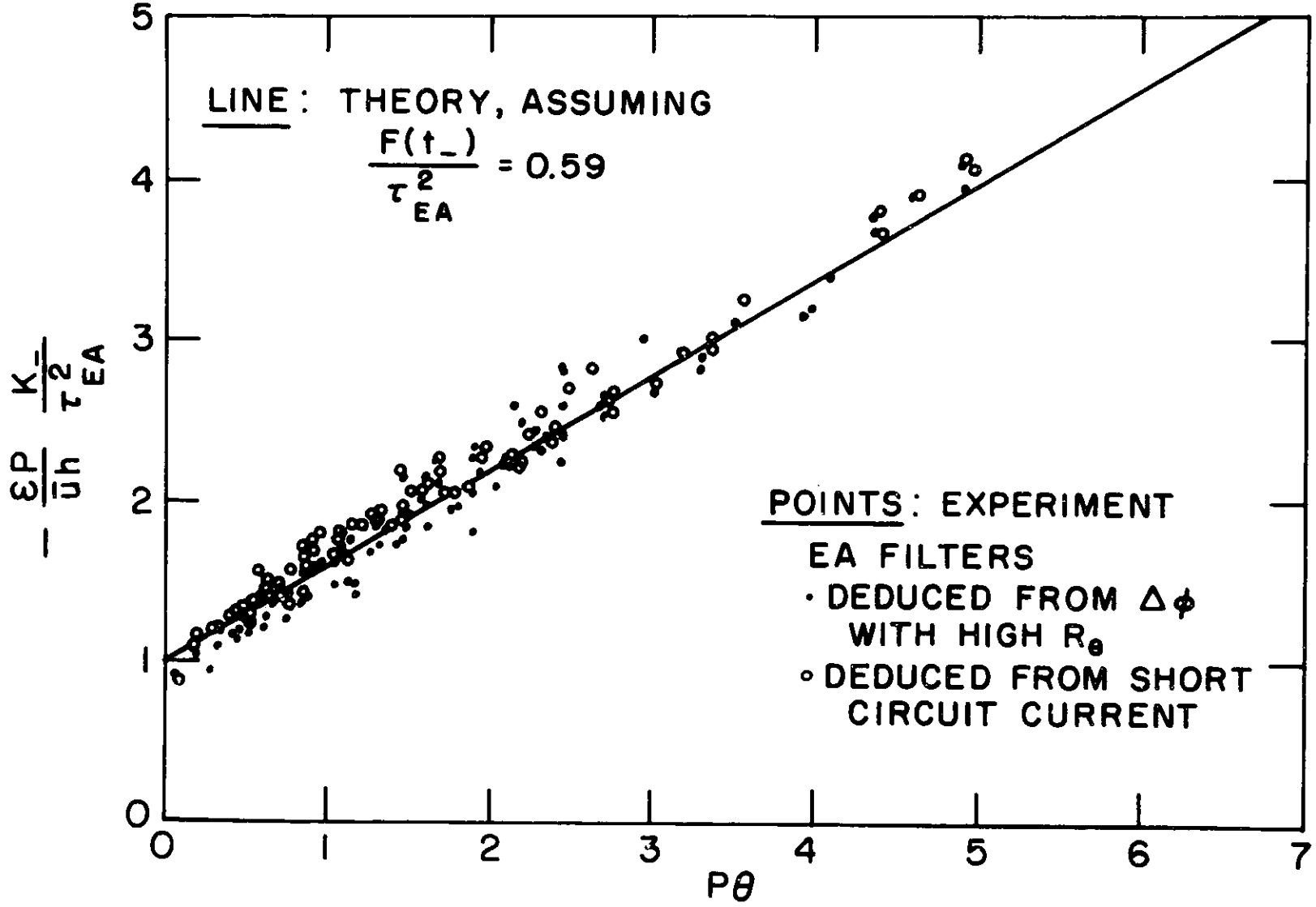


FIGURE 11. Reduced filter emf versus reduced flow speed. EA filters. $0.13 \leq \theta \leq 6.8$.

3. Tortuosities and Mobilities Inferred from the Data

From the experimental data in Figures 5 - 11 it is possible to infer distinct values for the cation and anion mobilities of ASA-3 dissociation products in heptane and to identify separate tortuosities for MF filters, NR and BD filters, and EA filters. Table 6 lists the values of τ^2/κ_a and $F(t_a)/\tau^2$ determined by the comparison of our charging data with the theoretical predictions. Using these six values and the theoretical function $F(t_a)$ (Table 1, Chapter 1) the five unknowns κ_+, κ_-, τ_{MF}, $\tau_{NR,BD}$, and τ_{EA} can be determined. The unknowns are not, however, uniquely defined since there is one redundant equation. If we solve for the unknowns assuming the behavior of the positive fixed charge filters to be best characterized by the data from BD and NR filters (which provided the larger fraction of the data for positive fixed charge filters) we arrive at values for the filter tortuosities and ionic mobilities listed in Table 6. Because of the experimental redundancy, two slightly different values for τ_{EA} are ultimately inferred.

In the "Discussion" we comment further on the magnitudes of the mobilities and tortuosities listed in Table 6. Suffice it to say at this stage that the values are in physically reasonable ranges. The mobilities are close to those predicted by empirical correlations for these quantities; the tortuosities are certainly of the right order of magnitude and encompass within the error bars physically plausible values.

Filter Type	Fixed Charge Polarity Z_f	EXPERIMENTAL RESULTS		INFERRED VALUES	
		τ^2/κ_a $\times 10^{-8}$ V s m^{-2}	$\frac{F(t_a)}{\tau^2}$	Tortuosity τ	co-ion mobility $\kappa_a \times 10^8$ $m^2V^{-1}s^{-1}$
SS, RA	-1	$\frac{\tau^2_{MF}}{\kappa_+} = 1.0\pm0.14$	$\frac{F(t_+)}{\tau^2_{MF}} = 0.94\pm0.17$	$\tau_{MF} = 0.95\pm0.11$	$\kappa_+ = 0.91\pm0.21$
PH, VC	-1		—	$\tau_{MF} = 0.95\pm0.11$	$\kappa_+ = 0.91\pm0.21$
NR, BD	+1	$\frac{\tau^2_{NR,BD}}{\kappa_-} = 0.50\pm0.07$	$\frac{F(t_-)}{\tau^2_{NR,BD}} = 0.93\pm0.7$	$\tau_{NR,BD} = 0.89\pm0.11$	$\kappa_- = 1.6\pm0.37$
EA	+1	$\frac{\tau^2_{EA}}{\kappa_-} = 0.90\pm0.13$	$\frac{F(t_-)}{\tau^2_{EA}} = 0.59\pm0.11$	1.1 or 1.2 $\Rightarrow \tau_{EA} = 1.2 \pm 0.14$	$\kappa_- = 1.6\pm0.37$

TABLE 6. Tortuosities and mobilities inferred from the charging data.

4. Summary of Results

Figure 12 compares charging data from all of the Millipore filter tests with the theoretical predictions of Eq. (5) over the whole range of parameters investigated. The data in this figure are the open circuit potential and potential-current measurements, made with $R_e \gg R_0$ in the low θ experiments and $R_e \gtrsim R_0$ in the high θ tests. Values for filter tortuosities and cation and anion mobilities listed in Table 6 have been used. The data in Figure 12 are in convincing agreement with the theoretical predictions. The agreement is uncertain only insofar as the chosen tortuosities and mobilities may differ from the actual values.

In Figure 13 the short circuit current data (data for which $R_e \ll R_0$) from all Millipore filters are presented. On the abscissa is the charging emf inferred from our short circuit current data [Eq. (4b)], on the ordinate the theoretically predicted emf. The agreement between theory and experiment is very satisfactory.

5. Discussion of Millipore Filter Experiments

There appears to be good agreement between the theoretical predictions for high fixed charge density filters and the potentials and currents measured in experiments with Millipore filters of various types. Any physically reasonable choice of ionic mobilities and filter toruosities will give reasonable agreement between the theory and experiments and to

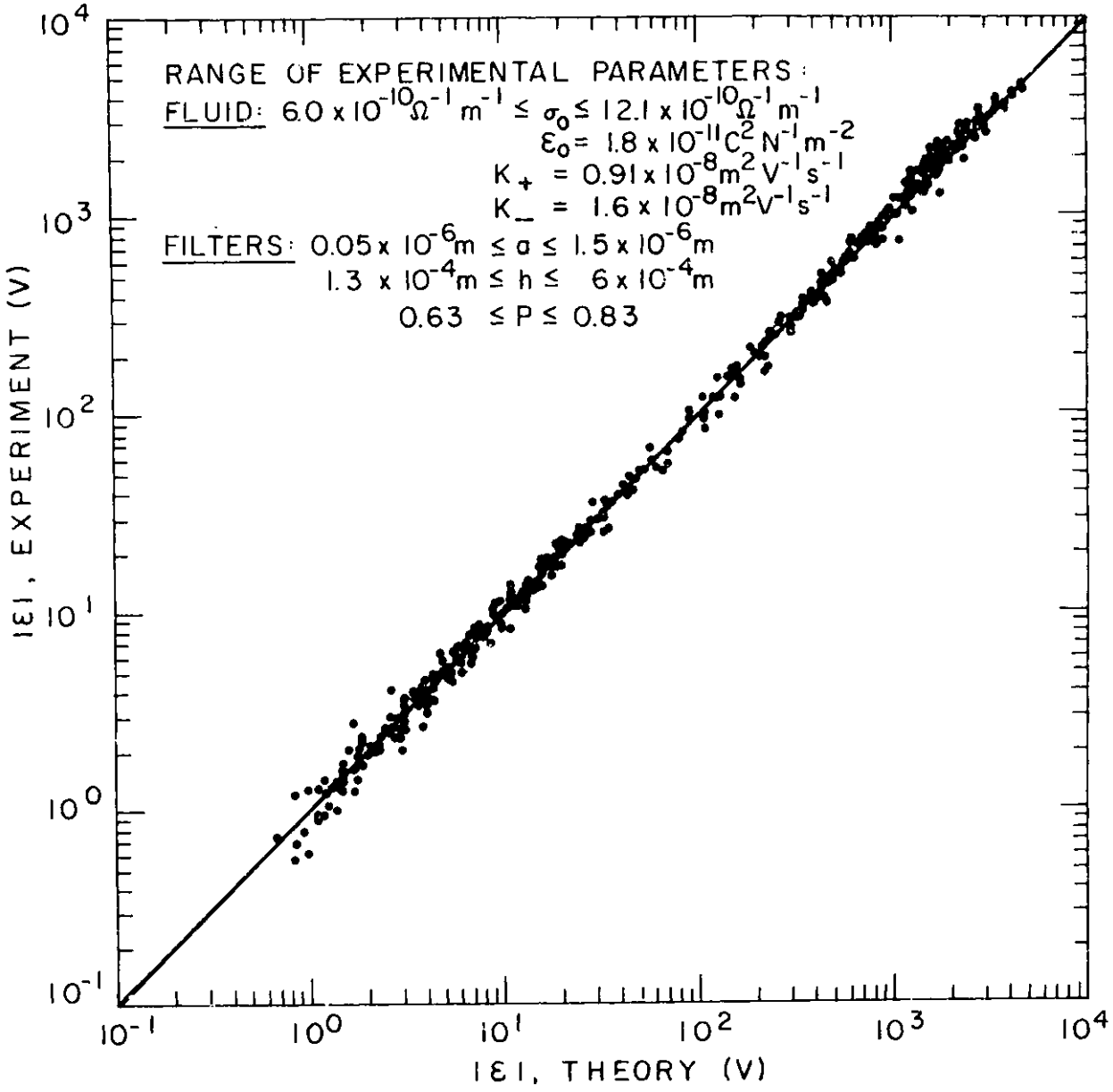


FIGURE 12. Experiment versus theory. Open circuit potential and potential current data ($R_e \geq R_o$) from Millipore filters. $0.0015 \leq n \leq 6.8$.

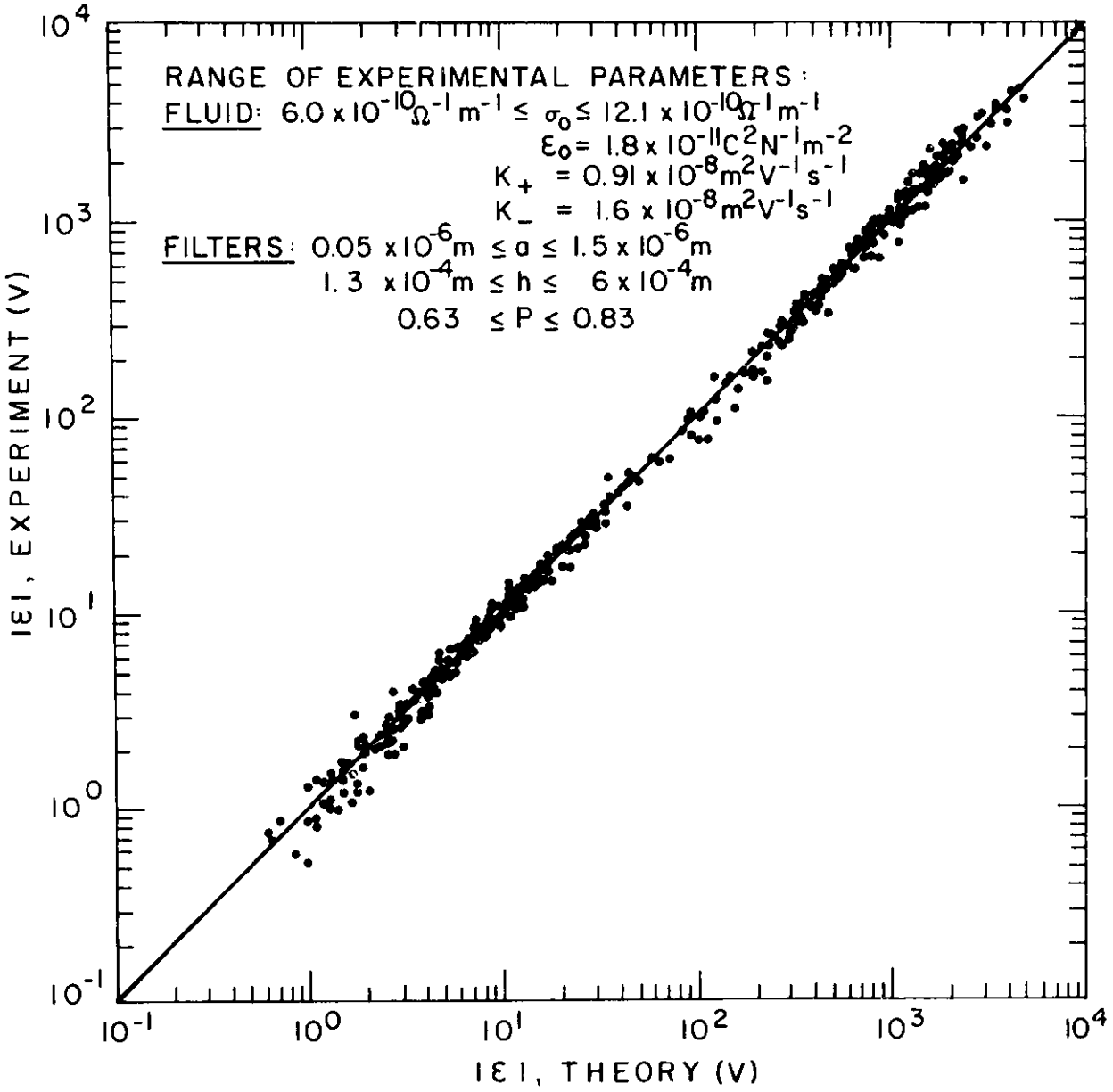


FIGURE 13. Experiment versus theory. Short circuit current data ($R_e \ll P_e$) from Millipore filters. $0.0015 \leq A \leq 6.8$.

this extent the confirmation of the theory can be regarded as an absolute one.

It is possible to estimate values of ionic mobilities from empirical correlations of measured diffusivities in hydrocarbon solutions. The American Petroleum Institute,[11] on the basis of earlier work by Wilke and Chang,[12] recommends the following equation for dilute binary solutions in hydrocarbon solvents:

$$D = \frac{1.2 \times 10^{-16} \, (M_2)^{0.5} \, T}{\mu \left(\frac{M_1}{\rho_1} \right)^{0.6}} \; m^2 s^{-1} \quad . \qquad (14)$$

Here M_1 and M_2 are the molecular weights of the solute and solvent respectively, ρ_1 is the density of the solute at its normal boiling point (k m^{-3}), μ is the viscosity of the solution (k $m^{-1}s^{-1}$) and T is the temperature (°K).† The "apparent" molecular weights of Ca-Aerosol-OT and Cr-Ac - the ASA-3 electrolyte constituents - have been reported[4] as 2000 and 2500 k $kmole^{-1}$. If bimolecular dissociation of these species occurs the ions will have similar ionic weights, perhaps in the range 1500-3000 k $kmole^{-1}$. The cation, probably containing the heavy metallic atoms and associated aliphatic and aromatic groups to stabilize the positive charge in the hydrocarbon liquid, may be substantially heavier

---

†Original equation is in f.p.s. units with T in °R.

than the anion. Taking $\mu = 4.1 \times 10^{-4}$ k $m^{-1} s^{-1}$ and $M_2 = 100$ for heptane, and estimating $M_1 = 1500 - 3000$ and $\rho_1 = 9 \times 10^2$ k m^{-3} † for the additive ions, Eq. (14) predicts $D = 4.2 - 6.2 \times 10^{-10} m^2 s^{-1}$ at 290°K, corresponding to ionic mobilities in the range $1.7 - 2.5 \times 10^{-8}$ $m^2 V^{-1} s^{-1}$ (from Einstein's relation $\kappa = FD/RT$). This estimate is, of course, only as accurate as the approximate solute data available and the precision of the empirical correlation used. There is, however, surprisingly close agreement with the mobilities indicated by our charging experiments, $\kappa = 0.91 - 1.6 \times 10^{-8}$ $m^2 V^{-1} s^{-1}$ (Table 6).

The median values of the filter tortuosities inferred from the charging experiments are at first sight surprising. In our model τ represents the ratio of the average distance traveled by a fluid particle as it passes through the filter to the filter thickness, a ratio which cannot be less than unity. The three tortuosities listed in Table 6 encompass physically reasonable values within the error bars, but the median values of τ_{MF} and $\tau_{NR,BD}$ are slightly less than unity. Permeability data for Millipore filters highlights some of the uncertainties in the capillary model and filter data we have used. Conventional capillary models[13] relate the tortuosity of a filter τ to the mean pore radius a, filter porosity P,

---

†This value is the density of the ASA-3 solution as delivered.[5] In fact the density of the ionic products should be used in Eq. (14). Since we are dealing with organometallic compounds we expect that ρ_1 is close to 1×10^3 k m^{-3} and that no substantial error is introduced by using the average additive density.

thickness h and permeability π according to:

$$\tau = \left(\frac{P\, a^2}{8\pi}\right)^{\frac{1}{2}} \quad . \tag{15}$$

The Millipore Company catalogues[1] provide information on filter permeability as well as the values for h, a, and P used in the analysis of our charging data. Values of τ, inferred from Eq. (15) and the catalogue data are listed in Table 7. Most of the values are less than unity - a result which is physically inconsistent with a capillary model. Inconsistencies between the catalogue data and the capillary model may, of course, be reflected in the analysis of our charging data and in the tortuosities ultimately inferred.

It is noteworthy that the steady state polarity of the fixed charge of all the filters tested appears to depend only on the chemical nature of the filter-fluid combination. The fact that the mixed cellulose ester filters (MF) acquire a fixed charge of polarity opposite to that of the chemically similar cellulose acetate filter (EA) suggests that very sensitive surface chemistry may determine the sign of the adsorbed charge. In no case did we observe a steady state fixed charge polarity which was dependent on flow speed or fluid conductivity. Transient changes in fixed charge polarity were observed when a fresh filter was tested after only a very short period of immersion in the fluid, but the steady state polarity, attained after a sufficient period of immersion, was invariant.

Filter[a]	"Flow Rate"[b]	Permeability Π (m^2)	Inferred tortuosity
SS	296	1.1×10^{-13}	1.5
RA	222	8.0×10^{-14}	0.68
PH	29.6	1.1×10^{-14}	0.44
VC	1.5	4.7×10^{-16}	0.70
NR	200	7.2×10^{-16}	0.52
EA	178	5.6×10^{-14}	0.64
BD	33.3	6.5×10^{-15}	1.1

(a) Values of α , P , h are shown in Table 1.

(b) From Reference 1. Values are in mℓ of water per minute per cm^2 of filter at an applied pressure of 52 cm of mercury. The BD filter flow rate is based on methanol instead of water.

TABLE 7. Tortuosities inferred from permeability data.

The theoretical prediction with which we have compared the charging data from Millipore filters, Eq. (15), Chapter 1, assumes a high filter fixed charge density. We validate this assumption for our Millipore filter tests only implicitly, by the agreement between the theory based on this assumption and the experiments. It is possible, however, to estimate the minimum fixed charge densities in the Millipore filters by inspection of Figure 2, Chapter 1. In our tests θ attained a maximum value of about 7, and the high fixed charge theoretical solution remained applicable. From Figure 2, Chapter 1, this would indicate a minimum fixed charge $\gamma_f \gtrsim 100$, or $\rho_f \gtrsim 5$ C m^{-3} of filter void [Eq. (10), Chapter 1]. If the fixed charge arises by adsorption in the filter, the charge density on the internal filter surfaces will be of order $a\rho_f/2$, where a is the mean pore radius in the filter. Thus for RA filters, for example, the surface charge density was of the order of, or greater than, about 10^{-6} C m^{-2} of of internal surface area or about one adsorbed ion per square micron of surface.[†]

[†]In experiments with VF grade mixed cellulose ester Millipore filters saturated with bromobenzene and immersed in an aqueous solution of potassium chloride, Ilani[14] estimated that the filters acquired about 10^{-7} moles of fixed anions, which would correspond to about 3×10 m^{-3} of filter void or about 7.5×10^{-4} C m^{-2} of internal surface area. We note that the polarity of the fixed charge is consistent with the polarity we inferred, and the magnitude is considerably higher than our estimated lower limit.

SECTION C. VELCON FILTER EXPERIMENTS

The Velcon filter[2] (Table 1) is a pleated "resin impregnated paper" cartridge, used in industrial filtration of Avgass, turbine oil, diesel fuels, and other hydrocarbon liquids. From the "2-micron" rating of this filter we infer a pore radius of about 10^{-6}m; the filter thickness is about 3.9×10^{-4}m. No information on the filter porosity or tortuosity is available. Tests with filters cut from a Velcon cartridge were conducted in cells 1 and 2 (Table 8) in the same ranges of fluid conductivity and flow rate used in the Millipore filter experiments. One or two filters in series were used.

The charging behavior of the Velcon filters was quite different from that of the Millipore filters. First, the data obtained with Velcon filters exhibited considerably more scatter. Day to day changes of up to 200% in the magnitudes of potentials and currents generated by a filter were observed. Second, the potentials and currents were considerably lower than those generated by the Millipore filters - lower by about a factor of three to five at the lowest flow rates and by an order of magnitude or more at the highest flow rates tested. We attribute this difference in behavior to the fact that the Velcon filters acquired only a <u>low</u> fixed charge density when immersed in heptane of conductivity $6 - 12 \times 10^{-10}\Omega^{-1}m^{-1}$. Again, we have made no <u>direct</u> measurements of filter fixed charge densities - our inference is based on the agreement between the Velcon charging data

Number of Filters in Series	Period of Immersion	Temperature, °C	Fluid Conductivity $\sigma_0 \times 10^{10} \Omega^{-1} m^{-1}$	$\frac{\lambda_D}{a}$ (a)	$R_0 \times 10^{-10}$ Ω	Minimum Tested	Maximum Tested
1	4 days	19.6	6.6	2.8	1.9	0.0033	0.042
1	16 days	19.8	6.4	2.9	1.9	0.0083	0.008
1	1 day	20.7	6.4	2.9	1.9	0.0049	0.046
1	1 day	19.5	6.6	2.8	2.7	0.43	2.0
1	3 days	21.0	6.6	2.8	2.7	0.19	2.0
1	4 days	20.0	6.6	2.8	2.7	0.30	2.0
1	20 days	19.7	6.6	2.8	2.7	0.30	2.2
1	21 days	20.6	6.6	2.8	2.7	0.16	2.2
1	22 days	20.3	6.6	2.8	2.7	0.084	2.0
1	30 days	20.7	6.4	2.9	2.8	1.42	2.3
1	31 days	18.2	6.4	2.9	2.8	0.61	2.4
1	5 days	20.0	6.6	2.8	2.7	0.30	2.0
2	10 days	21.6	6.4	2.9	1.9	0.0026	0.14
2	15 days	19.9	6.4	2.9	1.9	0.0043	0.049
2	16 days	20.5	6.4	2.9	1.9	0.0032	0.049
2	3 days	19.9	6.4	2.9	1.9	0.46	2.3
1	7 days	23.6	11.5	2.1	1.1	0.0052	0.049
1	69 days	23.5	12.1	2.1	1.0	0.0029	0.037
1	30 days	26.7	12.1	2.1	1.5	1.1	1.3
1	31 days	26.5	12.1	2.1	1.5	0.21	1.3
1	32 days	25.2	12.1	2.1	1.5	0.21	1.3
2	8 days	23.5	11.5	2.1	1.1	0.0023	0.049

(a) Based on $a = 1 \times 10^{-6}$ m
$D = 3 \times 10^{-10} m^2 s^{-1}$

TABLE 8. Experiments with Velcon filters

and the low charge density theory.

Equation (12), Chapter 1, is the theoretical prediction for the charging emf of a low fixed charge density filter:

$$-Z_f \mathcal{E} = \frac{\tau^2}{P} \frac{\rho_f \bar{u}h}{\sigma_0} \left[1 - \left(1 - \frac{P^2}{\tau^2} \right) \frac{\varepsilon_f}{\varepsilon_0 P^2} \theta \left(1 - e^{-\frac{\varepsilon_0 P^2}{\varepsilon_f \theta}} \right) \right] \tag{16}$$

$$= \frac{\tau^2}{P} \rho_f \frac{\bar{u}h}{\sigma_0} \qquad \text{when} \quad \theta << 1 \tag{17}$$

$$= \frac{P \rho_f \bar{u}h}{\sigma_0} \qquad \text{when} \quad \theta >> 1 \tag{18}$$

Figures 14 and 15 show our Velcon filter charging data. At steady state (after several days of immersion in the working fluid) the Velcon filters acquired a positive fixed charge ($Z_f = +1$) in all tests. Figure 14 shows filter emfs deduced from open circuit potential and potential current data [Eqs. (2) and (4a)] while Figure 15 shows emfs calculated from short circuit current measurements [Eq. (4b)]. Data indicated by $\cdot$ in Figures 14 and 15 correspond to $\theta < 1$ [and should thus approach the Eq. (17) limit]; points marked as $\times$ are for $\theta \geq 1$ [approaching the Eq. (18) limit]. There is considerable scatter in the data - up to 200% in both limits. Furthermore, the maximum value of θ tested was about 2.4 and thus the high θ limit is not well defined by the data. Certain trends are, however, clearly indicated. A simple linear dependence $\mathcal{E} \propto \frac{\bar{u}h}{\sigma_0}$ is evident in the low θ limit and appears to apply also in the high θ limit, with a lower constant of proportionality, as expected from Eqs. (17) and (18). Despite

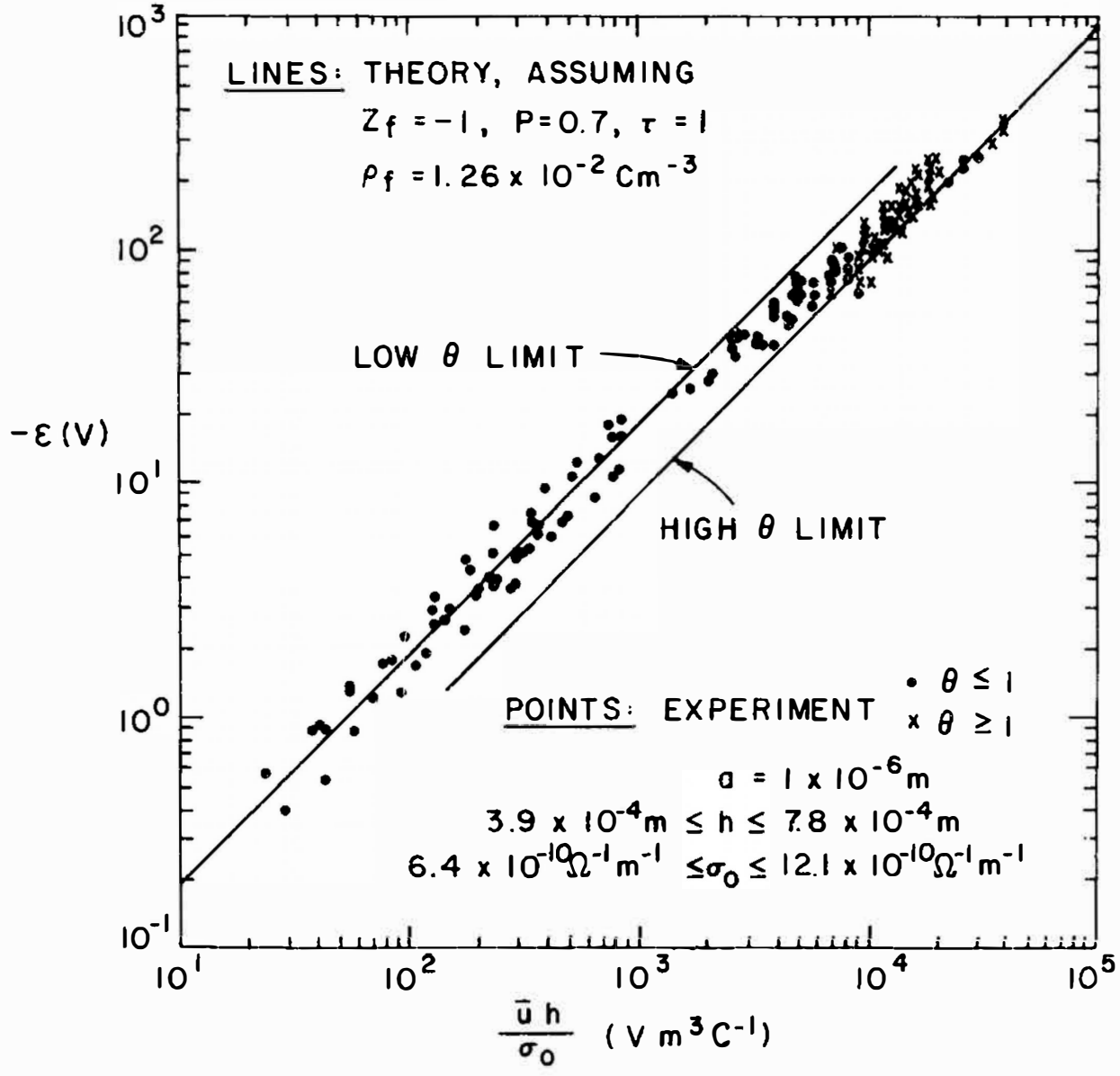


FIGURE 14. Filter emf versus reduced flow speed. Open circuit potential and potential current data ($R_e \geq R_o$) from Velcon filters. $0.0029 \leq \theta \leq 2.4$.

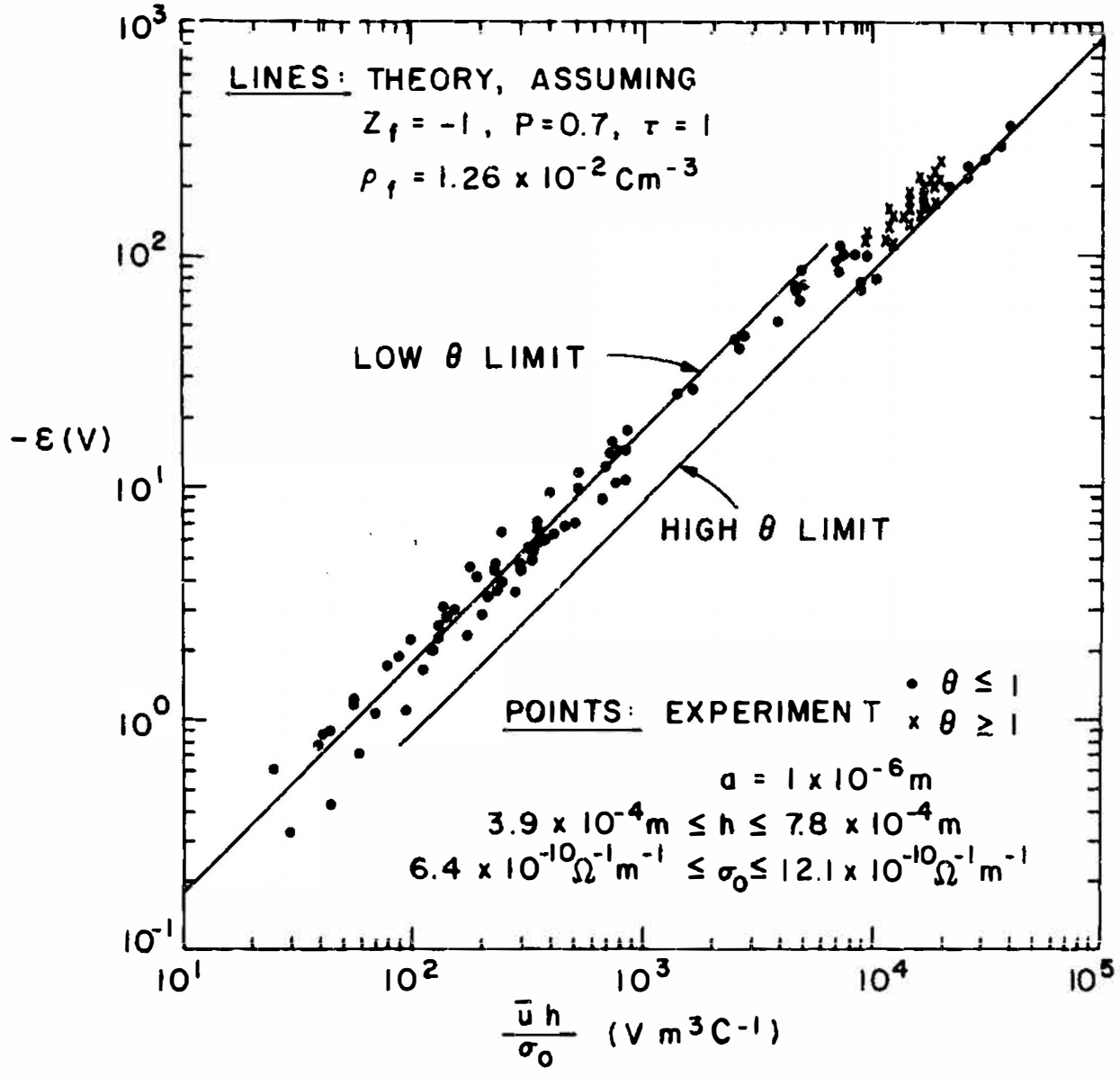


FIGURE 15. Filter emf versus reduced flow speed. Short circuit current data ($R_e \ll R_0$) from Velcon filters. $0.0029 \leq \theta \leq 2.6$.

the scatter in the data, the theoretically predicted dependence on conductivity σ_0 and filter thickness h appears to be supported - any reduction of the data excluding either of these variables gives a significantly less good correlation. This Velcon filter behavior is in marked contrast with the Millipore filter results, for which there was no dependence on fluid conductivity in the low θ limit and a definite quadratic dependence on flow speed for $\theta \geq 1$.

Comparing the $\theta < 1$ (•) points in Figures 14 and 15 and Eq. (17) we infer:

$$\frac{\tau_v^2 \rho_{f_v}}{P} = 1.8 \times 10^{-2} \text{ C m}^{-3} \qquad (19)$$

where τ_v and ρ_{f_v} are the tortuosity and fixed charge density of the Velcon filter. The low θ theory line drawn in Figures 14 and 15 is based on this value. Since we have no information on the Velcon filter porosity and only limited high θ charging data, the high θ line drawn in Figures 14 and 15 is rather speculative and is based on Eqs. (18) and (19), and an assumed porosity $P = 0.7$ and tortuosity $\tau_v = 1$. The most we can say is that the agreement between experiment and theory (given the assumed parameters) is not discouraging. From these assumed values for P and τ_v we deduce a filter fixed charge density from Eq. (19), $\rho_{f_v} = 1.26$ C m^{-3}. As expected, this is lower than the ion density ρ_0 in the neutral permeant fluid in our tests [see Eq. (26) Chapter 1] which was in the range 5×10^{-2} C m^{-3} $< \rho_0 <$ 10×10^{-2} C m^{-3} .

In Figure 16 we replot all the Velcon filter data from Figures 14 and 15 to compare the experiments directly with Eq. (16). The solid points are data for a fluid conductivity $\sigma_0 = 6.4 - 6.6 \times 10^{-10}\ \Omega^{-1}\ m^{-1}$, the open points for $\sigma_0 = 11.5 - 12.1 \times 10^{-10}\ \Omega^{-1} m^{-1}$. Insofar as the scatter in the data does not negate our conclusion it appears that the filter fixed charge density was reasonably independent of fluid conductivity. We attribute the scatter in the data to day to day changes in ρ_{f_v}, caused by changes of temperature or of other uncontrolled variables on which ρ_{f_v} may depend. Assuming $P = 0.7$, $\tau = 1$, $\rho_{f_v} = 1.26 \times 10^{-2}$ $C\ m^{-3}$ as before, and also assuming $\varepsilon_f = \varepsilon_0$ we can draw the solid line in Figure 16 based on the theoretical prediction, Eq. (16).

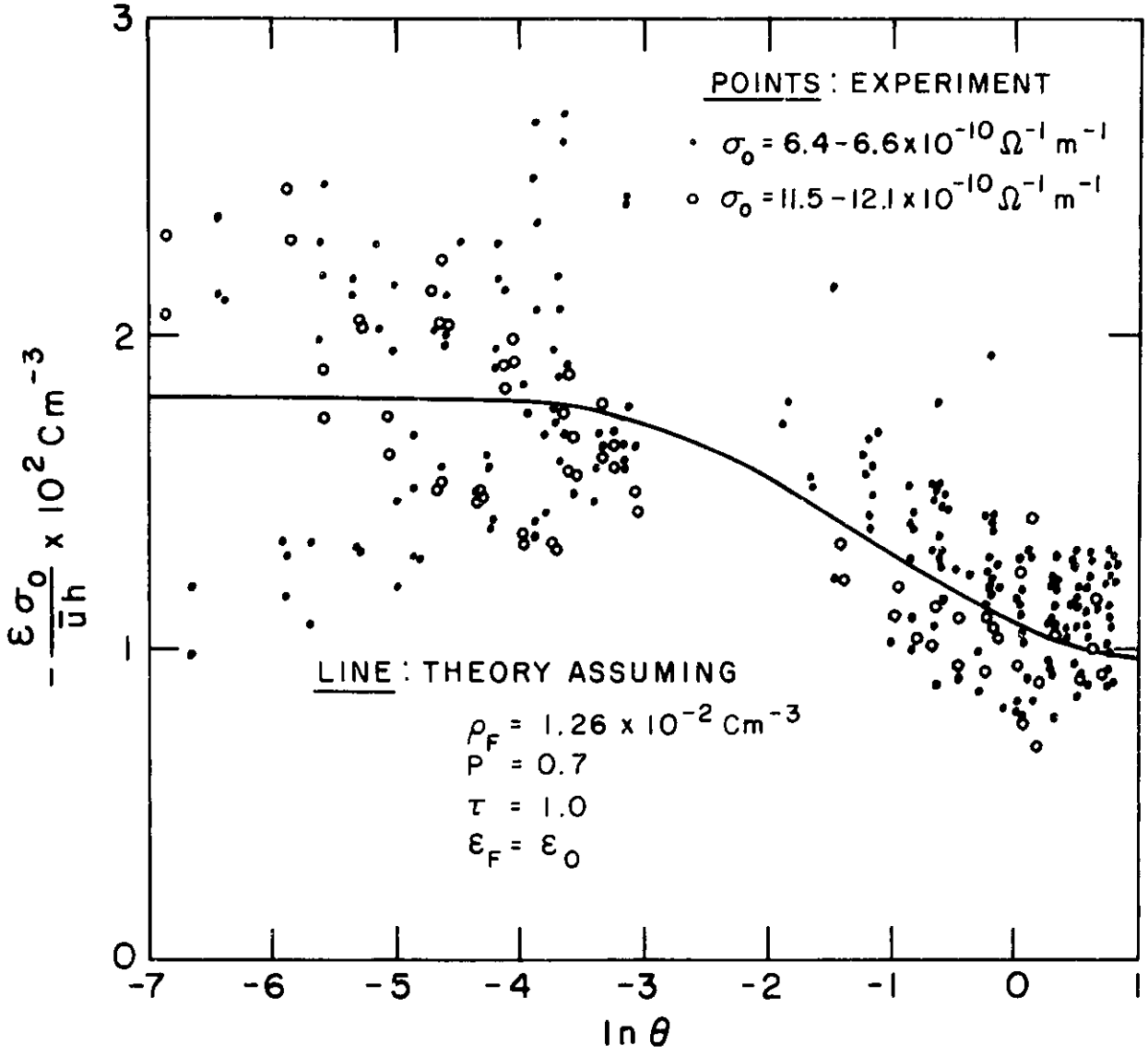


FIGURE 16. Filter emf versus ℓn θ . Velcon filters. $0.0024 \leq \theta \leq 2.4$.

CONCLUDING REMARKS

Within the range of parameters tested our model and theory appear to be well supported by the charging data. The agreement between the high fixed charge density theory and the Millipore filter results is convincing. The theoretically predicted dependence on flow speed, fluid conductivity, filter thickness, and porosity appears to be confirmed and the tortuosities and mobilities inferred from our charging data are within the physically reasonable ranges expected. The behavior of the Velcon filter is in interesting contrast to the Millipore filter data, and appears to support the low fixed charge density theory. We do not, however, have sufficient data from low charge density filters to claim a categorical confirmation of this part of the theory.

It should be noted that the high and low fixed charge filter classes distinguished in our theory depend on the ion density in the permeant fluid as well as on the charge density in the filter. For example, if the fixed charge density in the Velcon filters is insensitive to permeant fluid conductivity and remains close to 10^{-2} C m^{-3} its behavior will change to that of a high fixed charge density filter for fluid conductivities less than about $10^{-11}\Omega^{-1}m^{-1}$. Similarly, at sufficiently high fluid conductivities we expect the Millipore filters to act as low fixed charge density filters, if we assume again that the fixed charge density is not a strong function

of permeant fluid conductivity.

If our theory is to be used for detailed assessment of charging hazards in practical filtration conditions, filter fixed charge densities as functions of the filter/fluid combination and the fluid conductivity will be required as handbook information. There is, however, a theoretical upper bound to the filter charging emf, contained in the high charge density solution which is independent of the fixed charge densities. In no instance have we measured filter emfs that significantly exceeded this limit.

APPENDIX A

TEST CONDITIONS AND THE THEORETICAL ASSUMPTIONS

In Chapter 1 Section 2 we list the assumptions that underlie our theoretical predictions for charging in fuel filtration. The experiments described in this chapter, conducted to verify the theory, were contoured to satisfy these initial assumptions, at least to the extent that the relevant parameters could be measured and controlled.

Assumption (a); Large Debye Lengths [Eq. (2), Chapter 1]

As indicated in Tables 4, 5, and 8, the ratio of the Debye length to the filter pore radius ranged in our experiments from about two in the highest conductivity and largest pore radius tests to sixty in the opposite limit. It was therefore always larger than unity. The Debye ratios listed in Tables 4, 5, and 8 have been calculated from Eq. (3) Chapter 1, assuming an average ionic diffusivity $3 \times 10^{-10} m^2 s^{-1}$ (corresponding to a mobility of $1.2 \times 10^{-8} m^2 V^{-1} s^{-1}$, the arithmetic average of κ_+ and κ_- inferred from our data, Table 6). We note, in this context, that the large Debye length assumption as stated in Chapter 1 does not consider the fluid conductivity increase and corresponding Debye length decrease inside the filter pores for flows through high fixed charge density filters [see Eqs. (3) and (24), Chapter 1]. Since we do not have a precise measure of the fixed charge densities in the filters tested it is difficult to quantify this factor.

We have estimated that the minimum fixed charge density in the Millipore filter tests was $\rho_f \gtrsim 5$ C m^{-3} (Section B5), which would imply a pore fluid conductivity of about 6×10^{-8} Ω^{-1}m^{-1} and a Debye length of order 3×10^{-7} m, less than the largest pore radius $a = 1.5 \times 10^{-6}$m. However, when the charge density in the fluid is high, the governing equations become independent of the magnitude of the charge density; thus the requirement $a < \lambda_D$ can be replaced by the less strict condition that λ_D/a be sufficiently large to ensure a high charge density at the center of a pore (where the charge density is a minimum). We note that the results of our charging tests <u>are</u> independent of pore size and thus the simplified Debye length criterion of Eq. (3) Chapter 1 appears to be adequate.

<u>Assumption (b): Insulating Filters [Eq. (5) Chapter 1]</u>

Table 9 lists the bulk conductivities of the solid constituents of the filters we tested and the range of neutral fluid conductivities investigated. The table also includes our own rough estimates of filter resistances based on direct ohmic measurements on dry filters.[†] Clearly

---

[†]A direct resistance measurement of a dry filter allows us to infer[9] a value for the quantity $(1 - P)\sigma_s/\tau_s^2$ where τ_s is the tortuosity of the solid matrix. Surface conduction is neglected in the calculation - possibly a bad assumption for filters which always have very large internal surface areas.

Filter	$\frac{(1-P)\sigma_s}{\tau_s^2}$ (a) $\Omega^{-1}\ m^{-1}$	Material	Bulk Conductivity of Solid Constituent[15]	Neutral Fluid Conductivity in our Tests
SS, RA, PH, VC (MF)	1×10^{-13}	mixed cellulose esters	7.1×10^{-14} to $1.4 \times 10^{-12}\ \Omega^{-1}m^{-1}$ (b)	$6 - 12.0 \times 10^{-10}\Omega^{-1}m^{-1}$
NR	7×10^{-13}	nylon	$10^{-12} - 5 \times 10^{-15}$	$6.4\text{-}12.0 \times 10^{-10}\Omega^{-1}m^{-1}$
BD	2×10^{-13}	poly vinyl chloride	1×10^{-14}	
EA	7×10^{-14}	cellulose acetate	1.4×10^{-12}	
Velcon	2×10^{-12}	resin impregnated paper	2×10^{-12} (b)	

(a) Estimate based on direct ohmic measurements on a dry filter

(b) See Table II, Chapter 1.

TABLE 9. Filter Conductivities

$\sigma_s \ll \sigma_0$ in all cases, and thus Eq. (5) Chapter 1 should certainly be satisfied.

Assumptions (c) and (d): One-dimensional Conditions and a Remote Downstream Electrode

Both of our test cells allowed us to mount a plane filter in a constant area tube that extended well beyond the charge cloud developed downstream of the filter. Experiments conducted in cell 1 involved very short relaxation lengths, only a fraction of a filter thickness, in no case more than about 3×10^{-5}m. In cell 2 the maximum relaxation length was about 10^{-3}m while the downstream electrode was mounted 1.25×10^{-2}m downstream of the filter. Eq. (6), Chapter 1 was clearly satisfied in all tests.

One problem which we have not addressed in detail involves the possible effect of a non-uniform flow field (any deviation from ideal slug flow) downstream of the filter. Radial gradients in the charge density distribution downstream of the filter would tend to arise if the axial flow speed is not perfectly uniform, with the charge cloud at the center of the pipe where the flow speed is highest extending further than at the periphery. Our assumption here is that the radial charge gradients will not be sustained in the downstream charge cloud because both coulombic forces (migration in any radial field that is set up) and diffusion will tend to re-establish radial homogeneity.

Assumption (e): High Péclet Numbers [Eq. (8), Chapter 1]

The minimum superficial flow speed in our tests was about 3.4×10^{-5} m s^{-1} , giving a minimum Péclet number of about 14 (based on $D_{av} \approx 3 \times 10^{-10}$ m^2 s^{-1} and $h \gtrsim 1.3 \times 10^{-4}$m). Eq. (8) Chapter 1 was thus satisfied in all our tests.

Assumption (f): Weak Electrolyte in Thermodynamic Equilibrium

Only a small fraction of the Ca-Aerosol-OT and Cr-Ac molecules added to the heptane did in fact dissociate, justifying the weak electrolyte assumption. We base this conclusion on the following.

A conductivity of about $6 \times 10^{-10} \Omega^{-1} m^{-1}$ was attained at a nominal additive concentration of 1 ppm by volume (Figure 3), that is, at a concentration of about 5×10^{-4} mole m^{-3} (assuming a density of order one for the additive and solvent and an additive molecular weight of order 2000. See Section B5). Had the additive been fully dissociated the corresponding cation and anion concentrations would have been about 2×10^{-4} mole m^{-3} . Assuming an average ionic mobility of $1.2 \times 10^{-8} m^2 V^{-1} s^{-1}$ (Section B4), these ionic products would have resulted in a conductivity of about $6 \times 10^{-7} \Omega^{-1} m^{-1}$, a conductivity three orders of magnitude higher than that actually attained. We conclude, therefore, that the ASA-3/heptane solution did behave as a weak electrolyte, in which about 0.1% of the additive dissociated.

The assumption of local thermodynamic equilibrium [Eq. (22) Chapter 1] cannot be tested without a knowledge of rate constants for the ASA-3 dissociation reactions,† data which do not appear to exist in the open literature. Thus we can only justify this assumption a posteriori, by the good agreement between the theory and the charging experiments.

---

†If the reaction proceeds in a characteristic time τ_r, then Eq. (22) Chapter 1 should be a valid approximation for flows in which $\tau_r \ll \varepsilon_0/\sigma_0$.

REFERENCES

1. "Millipore Catalogue MF-68" and "1974 Millipore Catalogue and Purchasing Guide," No. LMC 0174/P, Millipore Co., Bedford, Mass., 1968 and 1974.
2. Velcon Filters, Inc. Sales Catalogue, San Jose, California.
3 Washburn, E.W. (Ed.), "International Critical Tables of Numerical Data, Physics, Chemistry, and Technology," Vol. VI, p. 144.
4. Klinkenberg, A. and Poulston, B.V., J. Inst. Petrol. 44, 379 (1958).
5. "Shell Anti-Static Additive ASA-3," Shell Technical Bulletin ICSX:69:5, Revised, Charlmont Press, London, 1969.
6. Chem. Week, p. 45, December 26, 1964.
7. Gavis, J. and Wagner, J.P., Chem. Eng. Sci. 23, 381 (1968).
8. Klinkenberg, A., in "Static Electrification, 1967," Proc. 2nd Conf. on Static Electrification, Conference Series No. 4, Inst. of Physics and Phys. Soc., London, 1967.
9. Huber, P.W. and Sonin, A.A., J. Coll. Int. Sci. 52, 415 (1975).
10. Cook, N.H. and Rabinowicz, E., "Physical Measurement and Analysis," Addison-Wesley, Reading, Massachusetts, 1963.
11. "Technical Data Book - Petroleum Refining," Chapter 13: "Diffusivity"; and Documentation Report No. 13-66, American Petroleum Institute, Division of Refining, New York, 1964.
12. Wilke, C.R. and Chang, P., AIChE Journal 1, 264 (1955).

13. Jacazio, G.; Probstein, R.F.; Sonin, A.A.; and Yung, D., J. Phys. Chem. 76, 4015 (1972).

14. Ilani, A., Biochim. et Biophys. Acta 94, 405 (1965).

15. Bikales, N.M. (Ed.), "Encyclopedia of Polymer Science and Technology," Vol. 5, p. 524, Wiley-Interscience, New York, 1964.

CHAPTER III

A NEW LOOK AT SOME OLD DATA ON ELECTRIC CHARGING IN FUEL FILTRATION

INTRODUCTION

Most of our theoretical predictions and experimental results described in Chapters I and II are, at first sight, contradicted by previous experimental work in this area conducted by Gavis and Wagner (hereinafter referred to as G&W),[1-4] who appear to offer the only comprehensive scheme other than our own for quantitatively predicting charging in filtration. A person attempting to assess hazards or to propose modifications in system design and operating conditions on the basis of our work would learn from G&W's published work that in some instances his efforts were tending to aggravate rather than to abate the charging problem. This condition of uncertainty is clearly unacceptable in a field concerned with important industrial hazards.

In this chapter, we analyze G&W's work in terms of our own model and theory. We compare G&W's unreduced charging data first with the empirical correlation that they proposed for this data and then with our own theoretical predictions.

SECTION A. SUMMARY OF GAVIS AND WAGNER'S WORK

1. Experiments and Results

Gavis and Wagner conducted a series of experiments, summarized in Table I, using heptane doped with Shell ASA #1 flowing through Millipore cellulose ester filters. They measured streaming currents as a function of flow rate, fluid conductivity, and filter structure (thickness, pore size, and porosity) and proposed an empirical correlating equation for some of their data.

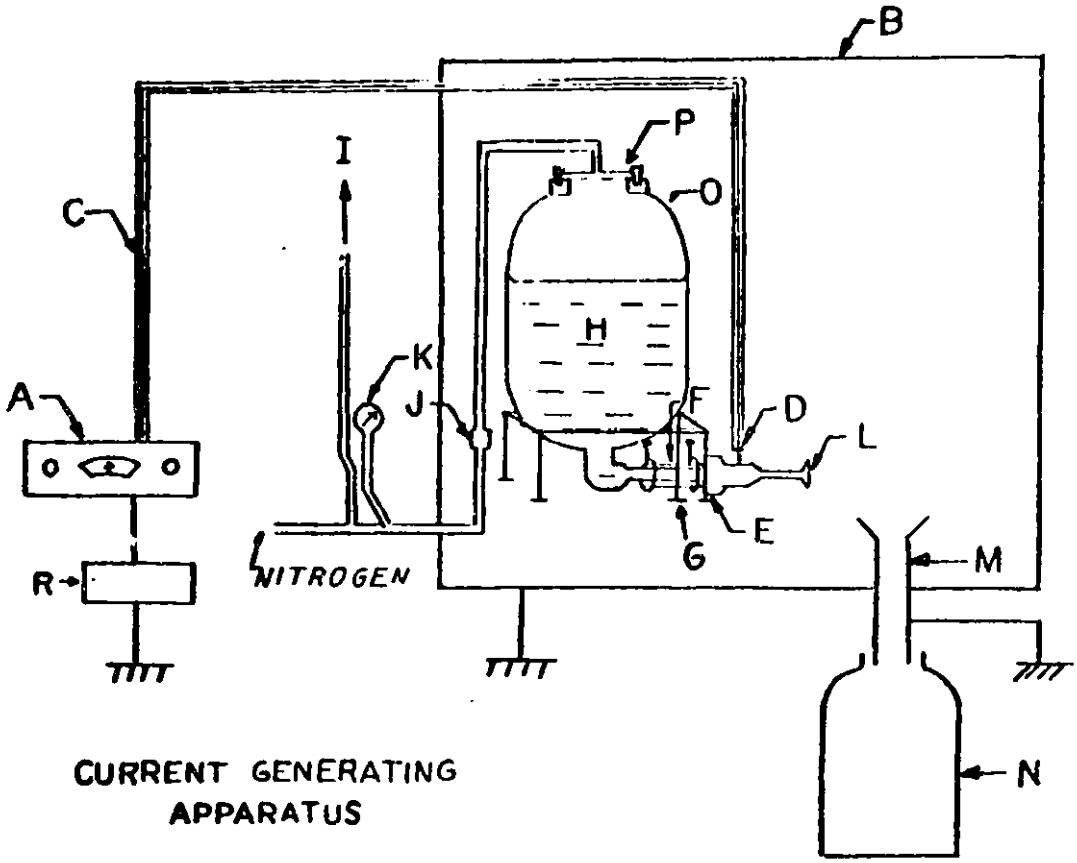
The experimental set-up used in G&W's charging tests is shown in Figure 1. Figure 2 shows the filter holder that was used, Millipore A-H micro-analysis filter holder # XX5002500. Note that the entire filter holder, including the filter support screen, is made of metal.

In each experimental run a single filter was mounted in the filter holder and heptane was passed through the filter and collected in the receiving vessel. The current that flowed from the filter holder to ground at a fixed flow rate was measured by the electrometer. Flow speeds through each filter were varied by about one order of magnitude in most runs, starting at an applied pressure of 5 psi and increasing in 5 psi intervals to 60 psi.

Apparently it was G&W's intention to convect charge of one sign from the filter to the receiving vessel where it would discharge against the grounded metal walls of the funnel and tank. Charge of the opposite sign would discharge on the solid filter matrix, and would then be conducted through the filter to the filter holder and hence to ground via the electro-

RUN #	Filter type & properties d=pore size μm h=thickness μm P=porosity	Range of flow rates tested 10^{-6} m^{3}s^{-1} Q_{min}	Q_{max}	Neutral fluid conductivity Ω^{-1} m^{-1}	Range of relaxation lengths 10^{-1}m $\lambda_{r_{min}}$	$\lambda_{r_{max}}$	Number of Data Points total measured	in correlated region of Fig. 3	with $\lambda_r \geq 0.2$ m
1		11	110	7.1×10^{-11}	69	700	11	11	11
2	AA	11	110	1.0×10^{-10}	49	500	11	11	11
3	d = 8.0	11	120	2.9×10^{-10}	17	190	12	12	11
4	h = 150	11	120	3.8×10^{-10}	13	140	12	12	11
5	P = 0.82	11	120	9.7×10^{-10}	5.1	56	12	12	8
6		11	120	6.6×10^{-9}	0.074	0.82	12	7	0
7		11	120	1.4×10^{-8}	0.034	0.38	12	1	0
8		5.2	62	2.2×10^{-11}	110	1300	12	12	12
9		5.2	62	4.6×10^{-11}	51	610	12	12	12
10		5.2	62	1.0×10^{-10}	23	270	12	12	12
11		5.2	62	2.2×10^{-10}	21	120	12	12	11
12	DA	5.2	62	3.1×10^{-10}	7.7	91	12	12	10
13	d = 6.5	5.2	62	5.1×10^{-10}	4.7	55	12	12	8
14	h = 150	5.2	62	6.9×10^{-10}	3.4	40	12	12	7
14a	P = 0.81	5.2	62	6.9×10^{-9}	0.034	0.4	12	4	0
15		5.2	62	1.0×10^{-8}	0.023	0.27	12	0	0
16		5.2	62	1.2×10^{-8}	0.020	0.24	12	0	0
17		5.2	62	1.2×10^{-8}	0.020	0.23	12	0	0
18		5.2	62	1.2×10^{-8}	0.019	0.23	12	0	0
19		5.2	62	1.3×10^{-8}	0.018	0.21	12	0	0
20		5.2	62	1.5×10^{-8}	0.016	0.19	12	0	0
21		5.2	62	1.7×10^{-8}	0.014	0.17	12	0	0
22		2.4	28	3.1×10^{-11}	35	400	12	12	12
23		2.4	28	4.9×10^{-11}	22	260	12	12	12
24	HA	2.4	28	4.0×10^{-11}	0.27	3.2	12	12	0
25	d = 4.5	2.4	28	2.3×10^{-10}	0.047	0.54	12	7	0
26	h = 150	2.4	28	3.8×10^{-10}	0.029	0.33	12	5	0
27	P = 0.79	9.3	51	2.6×10^{-10}	0.17	0.91	18	0	0
28		2.4	28	6.1×10^{-10}	0.018	0.21	12	1	0
29		9.3	54	7.1×10^{-10}	0.059	0.34	19	9	0
30		2.4	28	7.7×10^{-10}	0.014	0.16	12	0	0
31		2.4	28	1.7×10^{-8}	0.0065	0.075	12	0	0
32		2.4	28	2.1×10^{-8}	0.0051	0.059	12	0	0
33		2.4	28	4.1×10^{-8}	0.0026	0.031	12	0	0
34	TW d = 4.5 h = 100 P = 0.43	1.3	15	3.6×10^{-11}	17	200	12	12	11
35		1.3	15	9.7×10^{-11}	6.3	72	12	12	9
36		0.95	11	2.2×10^{-11}	20	240	12	12	11
37	GS	0.95	11	3.8×10^{-11}	11	130	12	12	11
38	d = 2.2	0.95	11	8.7×10^{-11}	5.0	60	12	12	9
39	h = 135	0.95	11	1.6×10^{-10}	2.7	33	12	12	5
40	P = 0.75	0.95	11	1.3×10^{-9}	0.34	4.0	12	12	0
41		0.95	11	1.8×10^{-9}	0.23	2.8	12	12	0
42	VC d = 1.0 h = 130 P = 0.74	0.15	1.8	2.4×10^{-10}	0.28	3.5	12	12	0
43	VM d = 0.5	0.12	1.5	1.5×10^{-10}	0.36	4.4	12	12	0
44	h = 130 P = 0.72	0.042	0.51	7.9×10^{-10}	0.024	0.29	12	12	0

TABLE 1. Gavis and Wagner's Charging Experiments



CURRENT GENERATING APPARATUS

A) Keithley #610-B electrometer
B) Aluminum sheet Faraday cage
C) Amphenol #140/U co-axial cable
D) Teflon insulated banana plug
E) Millipore microanalysis filter holder
F) Teflon approach tube: 7/32" I.D., with adjustable clamps leading to 1/2" O.D. copper pipe nipple
G) Teflon legs
H) A.S.A. #1 solution dissolved in purified heptane
I) Relief valve
J) Teflon separation forced fitted over copper tubing
K) Ashcroft 60 PSIG test gauge
L) Threaded teflon plug
M) Conical copper funnel; 2 1/4" diameter
N) Storage vessel
O) Stainless steel reservoir, 40 l. capacity, with a steel ring welded on its top
P) Steel cover over a rubber gasket held in place by hexagonal bolts threaded into the steel ring on top of the reservoir.
R) Bausch and Lomb vom-6 laboratory chart recorder

FIGURE 1. Charging Apparatus[1] (Scale: E-L appears to be the filter holder base, which was about 6-7 cm long).

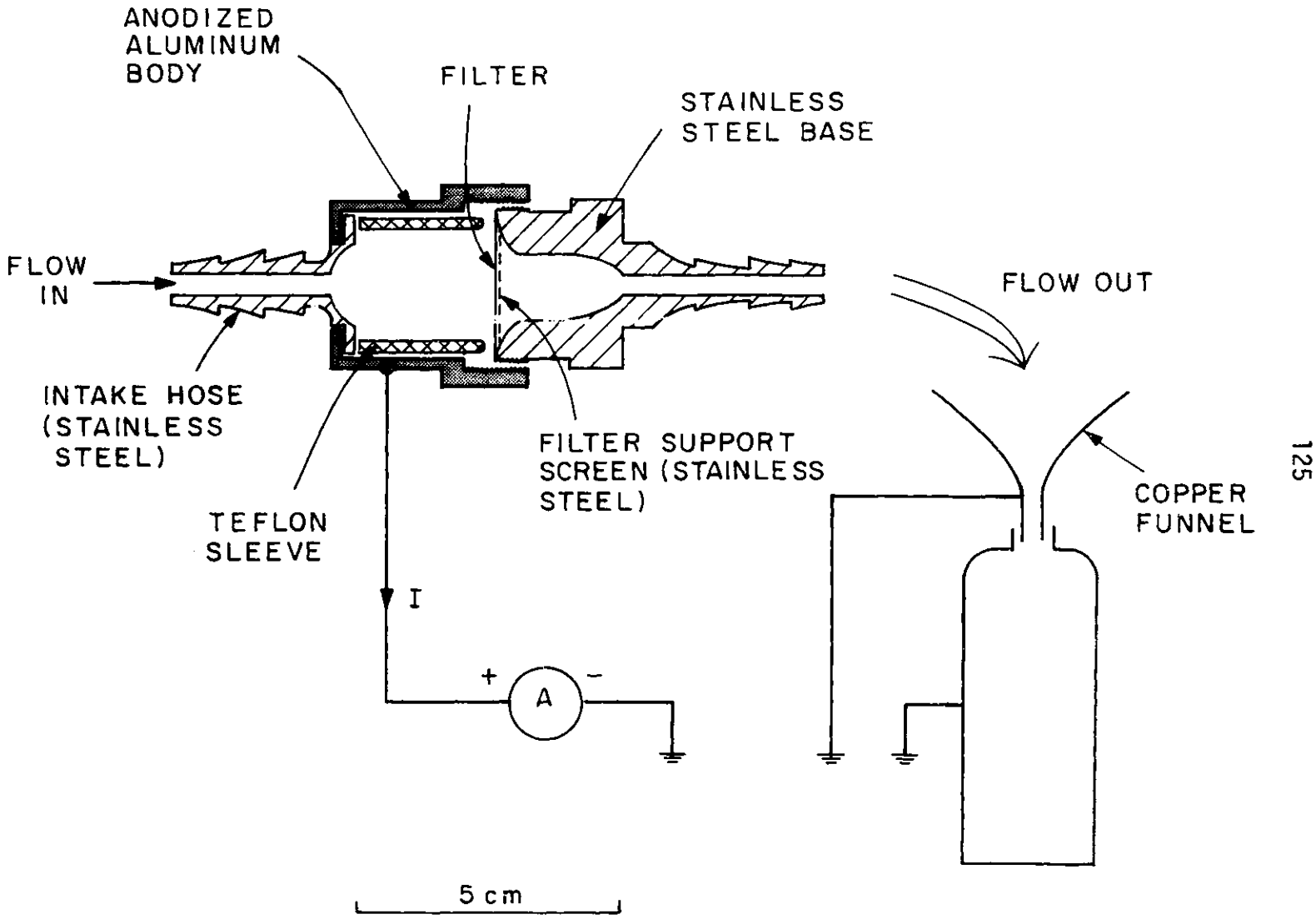


FIGURE 2. Filter holder (Millipore Filter Holder # XX500 2500) and schematic of the funnel and receiver.

meter.

Thus the current through the electrometer to ground would be equal in magnitude and opposite in sign to the current emanating from the filter.

Figure 3 shows G&W's charging data as presented in references (1) to (4).† On the abscissa is a reduced current $I\varepsilon_0\kappa/d\sigma_0^2AP$, where I is the current measured by the electrometer, ε_0 the permittivity of the fluid (1.8×10^{-11} C $N^{-1}m^{-2}$ for heptane), κ the ionic mobility (assumed to be $5 \times 10^{-8} m^2V^{-1}s^{-1}$ by G&W), d the nominal pore diameter of the filter, σ_0 the neutral fluid conductivity, A the total cross-sectional area of the filter (3.88×10^{-4} m^2), and P the filter porosity. The ordinate is

---

†Here, and in other equations and figures, including quotations from G&W's text, we have replaced G&W's symbols with our own. In many cases we have also rearranged the variables using the relationships

$$\tau_0 = \frac{\varepsilon_0}{\sigma_0} \quad \text{(ref. 1, p. 53)} \qquad \sigma_0 = \kappa F c_0 \quad \text{(ref. 1, p. 95)} \qquad v \equiv \frac{\bar{u}}{P} \quad \text{(ref. 1, p. 25)}$$

In these equations τ_0 is the fluid relaxation time, F is Faraday's constant, and c_0 is the total ion concentration in the electrically neutral hydrocarbon. G&W define the symbol v as the "superficial flow speed." We term the quantity $\bar{u}$ the superficial flow speed.

For example, G&W represented their reduced current as

$$\frac{\frac{I\tau_0}{APd}}{Fc_0},$$

and the reduced flow speed as $v\tau_0/d$, groups which we rewrite as

$$\frac{I\varepsilon_0\kappa}{Ad\sigma_0^2P} \quad \text{and} \quad \frac{\bar{u}\varepsilon_0}{Pd\sigma_0}.$$

the reduced flow rate, $\bar{u}\varepsilon_0/Pd\sigma_0$. Here $\bar{u}$ is the superficial flow speed (defined as the flow rate divided by the total cross-sectional area of the filter). All the data is reported in unreduced form in the Appendix of Reference 1.

G&W draw attention to two facets of their data as presented in Figure 3. First, "[t]he reduced current could be plotted as a function of $\bar{u}\varepsilon_0/P\sigma_0 d$ alone over the entire range of data obtained" (Ref. 2, p. 388). Second, Figure 3 appears to be divided into two distinct parts. G&W attach a physical significance to the existence of distinct, high flow rate behavior (Ref. 2, p. 390).

For the right hand part of the curve in Figure 3, that is, for $\bar{u}\varepsilon_0/Pd\sigma_0 > 5 \times 10^3$, G&W propose the following correlating equation:

$$\frac{I\varepsilon_0\kappa}{\sigma_0^2 dAP} = 2.00 \times 10^{-4} \left(\frac{\bar{u}\varepsilon_0}{P\sigma_0 d} \right)^{1\ 3/4} , \qquad (1)$$

which can be rewritten to give an expression for the unreduced superficial current;

$$\frac{I}{A} = \frac{c_1\ \sigma_0^{\frac{1}{4}}\ \bar{u}^{1\ 3/4}}{(Pd)^{3/4}} \qquad (2)$$

$$c_1 = \frac{2.0 \times 10^{-4}}{\kappa} (\varepsilon_0)^{3/4} \qquad (3)$$

$$\kappa \equiv 5 \times 10^{-8}\ m^2 V^{-1} s^{-1} \qquad (4)$$

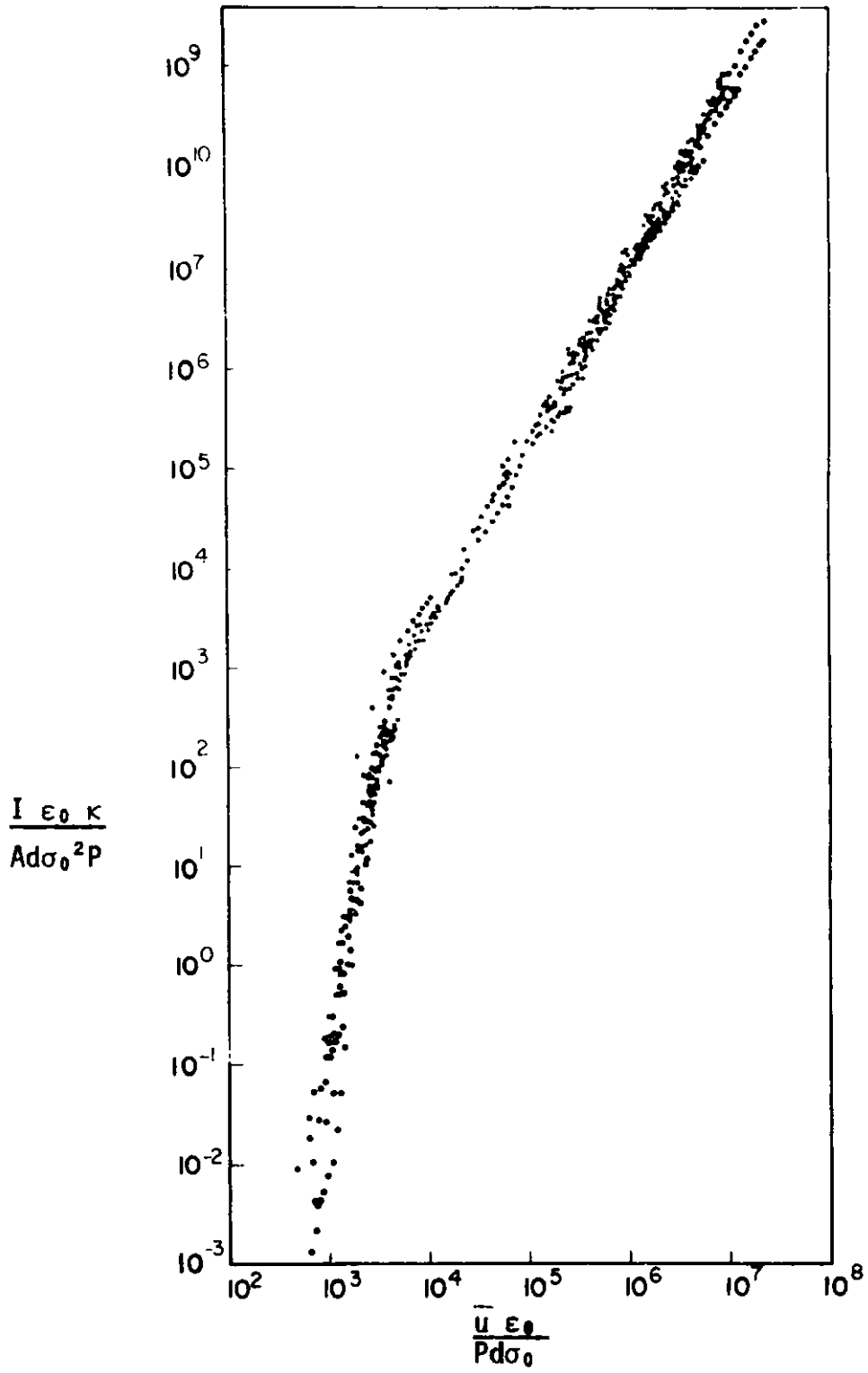


FIGURE 3. Gavis and Wagner's reduced charging data[1-4]

G&W suggest (Ref. 2, p. 390) that Eq. (1), subject to the restriction $\bar{u}\,\varepsilon_0/Pd\sigma_0 > 5 \times 10^3$, should correctly predict streaming currents for all combinations of filters and hydrocarbon liquids. Reference 2 also includes some sample charging data in unreduced form, shown in Figure 4. Streaming current-flow rate curves for various filters in a wide range of conductivities are shown. For purposes of comparison, Figure 5 shows the same curves but omits all data that do not fall in the correlated range of Figure 3, that is, points for which $\bar{u}\,\varepsilon_0/Pd\sigma_0 < 5 \times 10^3$.

2. Gavis and Wagner's Assumptions and the Actual Experimental Conditions

Underlying Gavis and Wagner's charging experiments and their model of the charging process are two assumptions--first, that in their experiments charge was transported primarily by convection between the filter and the downstream receiving vessel; second, that the solid filter matrix offered a path for electrical conduction from the fluid to the metal filter holder, and hence to the electrometer.

It is, in fact, unlikely that either of these assumptions was valid in all, or even in a substantial majority of their tests. Charge existing as a net ion imbalance in a fluid cannot be convected over indefinitely large distances. The fluid relaxation length λ_r, related to the conductivity and characteristic flow speed by

$$\lambda_r = \bar{u}\tau_0 = \frac{\bar{u}\,\varepsilon_0}{\sigma_0} \quad , \tag{5}$$

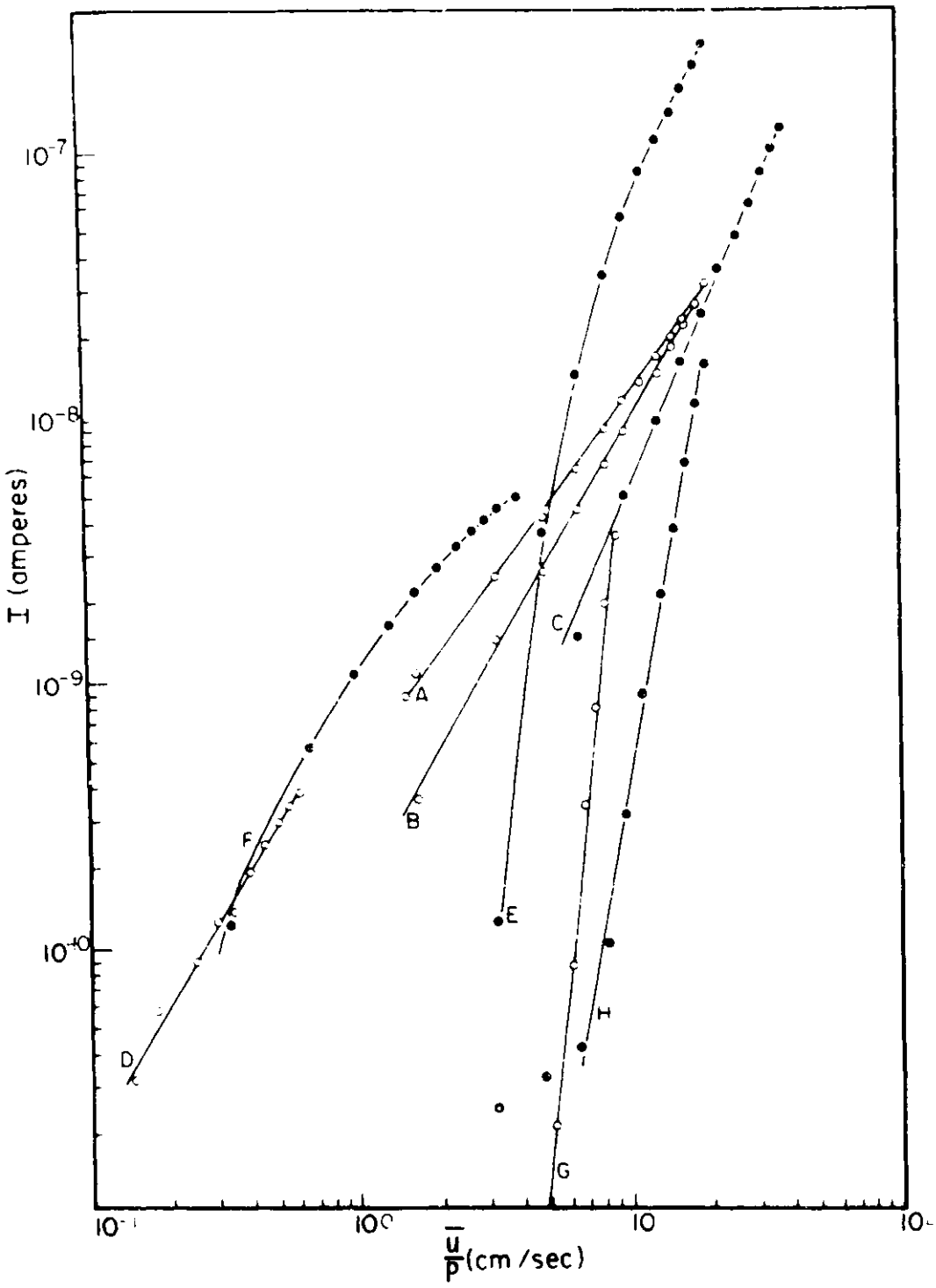


FIGURE 4. Measured Current versus Flow Speed

curve	run#	curve	run #
A	14	E	14A
B	8	F	41
C	1	G	31
D	42	H	21

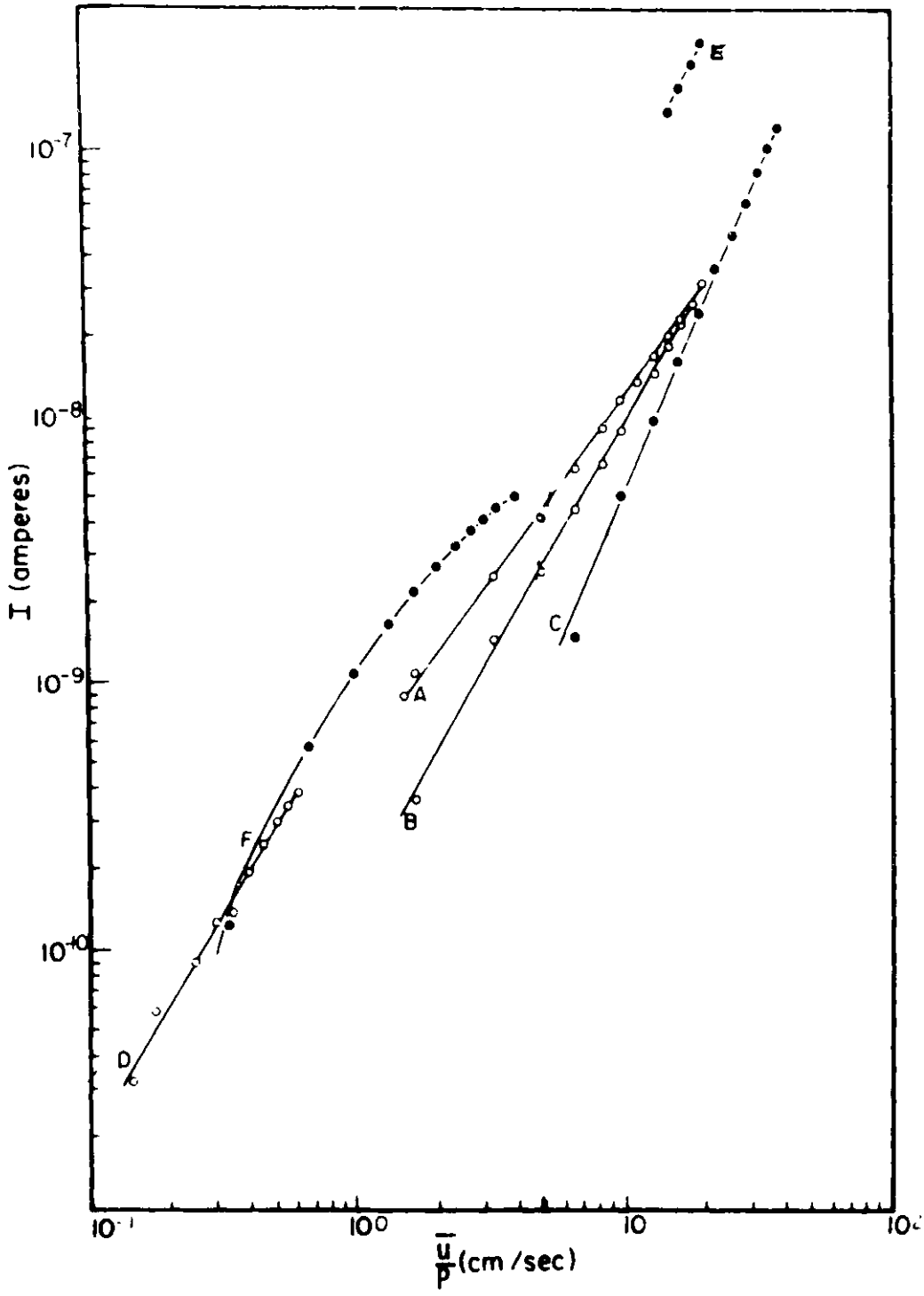


FIGURE 5. Data from Figure 4 for which

$$\frac{\bar{u}\,\varepsilon_0}{Pd\sigma_0} > 5 \times 10^3$$

curve	run #	curve	run #
A	14	D	42
B	8	E	14A
C	1	F	41

determines how far charge will be convected in a flow before a significant electric potential is built up in the fluid to counteract charge convection by backward conduction through the liquid stream (Chapter 1). No net charge can remain in the fluid at distances greater than about four relaxation lengths from the source of the charge. Currents driven by ionic migration in an electric field can, of course, flow through the fluid at any point, regardless of the local net charge density.

In G&W's experiments λ_r † ranged from about 13 m (run #8, Q = 62 × $10^{-6} m^3 s^{-1}$) to 2.6 × 10^{-5} m (run #33, Q = 2.4 × $10^{-6} m^3 s^{-1}$). Table 1 shows the minimum and maximum values of λ_r in each of the 44 runs conducted. A value for the distance between the filter and the grounded receiving vessel was not reported but appears to have been of the order of 0.1 m (Figure 1; see also Section C).

Further questions are raised by G&W's implicit assumption relating to the matrix conductivity of the filters tested. In their discussion of the physical mechanism for charging (Ref. 2, p. 289), G&W appear to suggest that current conduction through the solid filter matrix occurs quite readily. The implication seems to be that the filter conductivities in their

---

†Relaxation lengths in Table 1 have been calculated on the basis of the superficial flow speed immediately downstream of the filter, using the flow area 3.88 × $10^{-4} m^2$ reported by G&W. The flow area is reduced considerably in the exit nozzle of the filter holder (Figure 2) and charge relaxation in the fluid jet will therefore occur over distances correspondingly larger than the quoted values of λ_r. Unless otherwise noted in this chapter, relaxation lengths will be tacitly based on the flow speed immediately downstream of the filter.

experiments were high compared with those of the test fluids. Subsequent investigators[5] commenting on G&W's work have restated this suggestion as though it had been factually established.

The fluid conductivities in G&W's experiments ranged from 2.2×10^{-13} $\Omega^{-1}m^{-1}$ (runs #8, 36) to $4.1 \times 10^{-9}\Omega^{-1}m^{-1}$ (run #33). The bulk conductivities of cellulose esters - the chemical constituents of the Millipore filters tested by G&W [6] - are typically in the range 10^{-12} - $10^{-14}\Omega^{-1}m^{-1}$ (Ref. 7 and Table 2, Chapter 1). Furthermore, the filters were in most cases more than 70% porous (one filter had an exceptionally low porosity of 43%) For these highly porous filters, the solid matrix would have a total conductance about three times lower than that of a fluid of the same bulk conductivity permeating the filter. Given the low conductivities of the solid constituent and the low filter porosities, it seems unlikely that significant current conduction through the filter matrix would occur when a path of lower resistance through the fluid existed, that is, in most of G&W's experiments.

SECTION B. CORRELATION OF GAVIS AND WAGNER'S DATA

A careful examination of Gavis and Wagner's unreduced data (Ref. 1, Appendix) reveals charging behavior that is quite different from G&W's correlation, Eq. (2). For example, the claimed dependence $I \propto \sigma_0^{1/4}$ is not substantiated by the data; the claimed dependence $I \propto (Pd)^{-3/4}$ is poorly supported; the claim that I is independent of h turns out to be sheer speculation.

In this section we present our own, detailed analysis of G&W's data and outline our conclusion regarding the importance of variables such as fluid conductivity, filter pore size, and filter thickness in G&W's experiments. Only a qualitative comparison with the predictions of our theory is made at this stage.

Based on our analysis of the current-conductivity behavior (in subsection 1, below), we can identify the flow regime in which meaningful charging data were obtained by G&W. All data obtained in this regime are summarized in Section C; quantitative comparisons with our theory can then be made.

1. Fluid Conductivity, $I \propto \sigma_0^{1/4}$

Figure 6 shows sample plots of measured currents versus conductivity for all filters tested by Gavis and Wagner at more than one conductivity (all but VC filters). Each curve is for a constant flow rate through one filter type at one applied pressure. For example, the curve marked AA60,

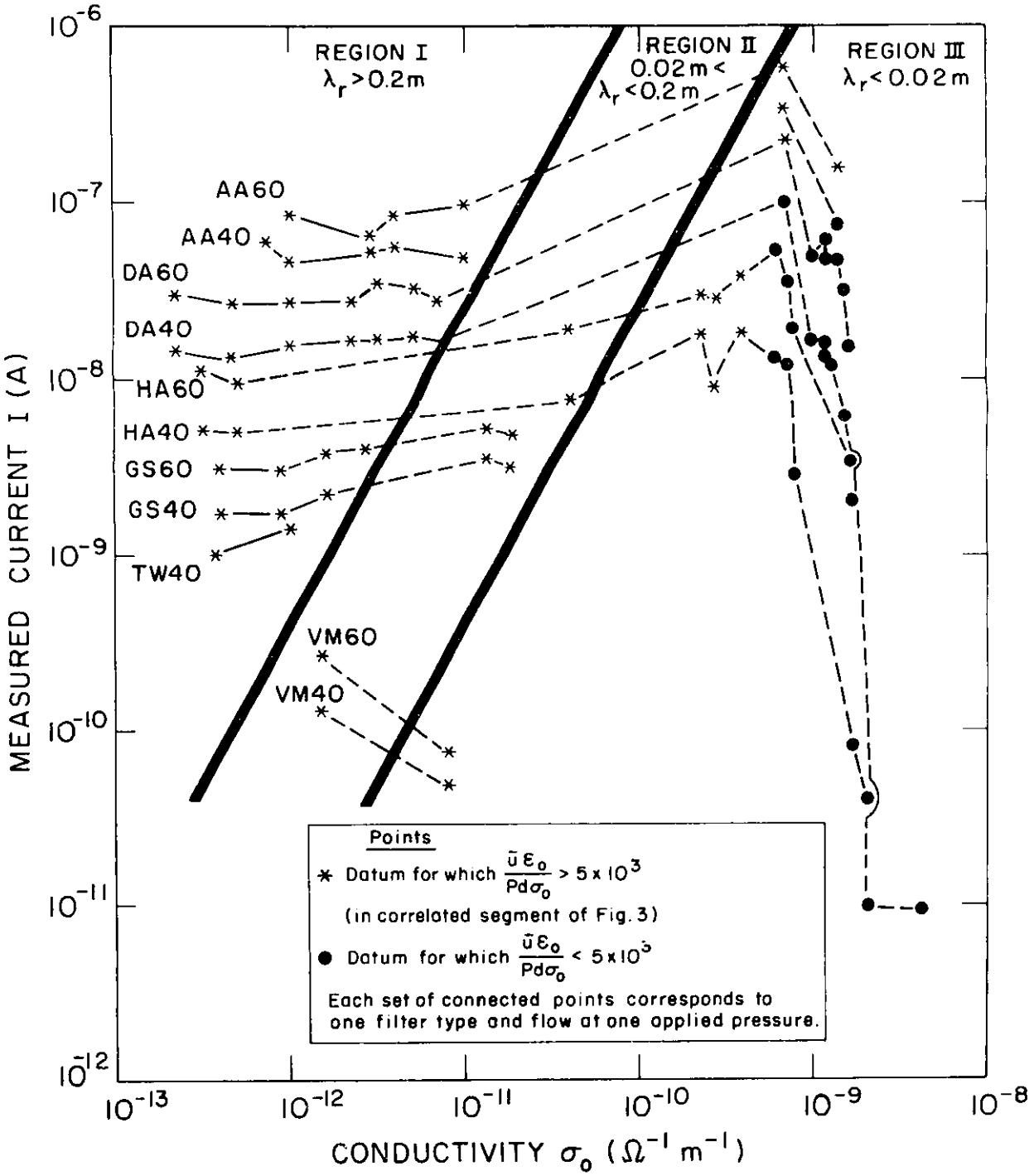


FIGURE 6. Measured current versus neutral fluid conductivity for various filters and flow speeds.

Figure 6, is a plot of streaming currents developed through an AA filter at an applied pressure of 60 psi. Data points marked with a * would fall in the high flow rate segment of Figure 3 [and should thus be correlated by Eq. (2)], and those marked with a • land in the low flow rate segment of Figure 3. While Figure 6 includes only selected charging data from G&W's tests, the current-conductivity behavior shown is typical of all of G&W's tests, over the whole range of flow rates through each filter type. Thus our conclusions based on Figure 6 are generally applicable to G&W's results.

Figure 6 can be separated into three regions - one of low conductivity, one of intermediate conductivity, and one of high conductivity, as indicated by the diagonal lines drawn. In region I it is clear that to a good approximation I is independent of σ_0. There is certainly no confirmation of $I \propto \sigma_0^{1/4}$, despite the fact that all data in this region are purportedly correlated by Eq. (2).

There is an increase of current with conductivity in region II (something like $I \propto \sigma_0$ or $I \propto \sigma_0^{1/2}$) followed by an extremely rapid decrease in region III. G&W have tacitly attempted to correlate all the data from region I and some of the lower conductivity data from regions II and III by the simple power law $I \propto \sigma_0^{1/4}$. This is a poor fit in regions I and III and largely speculative in region II.

The diagonal lines that we have drawn in Figure 6 to separate regions I, II, and III are based on a simple criterion. All data points in region I were measurements for which the fluid relaxation length λ_r was greater

than 0.2 m. Data points in region II were obtained when $0.02\ m < \lambda_r < 0.2\ m$, those in region III when $\lambda_r < 0.02$ m. For example, curve AA60 of Figure 6 corresponds to an applied pressure of 60 psi across an AA filter, giving a superficial flow speed $\bar{u} = 0.31\ m\ s^{-1}$. On this curve, the fluid conductivity must therefore be less than $2.7 \times 10^{-11} \Omega^{-1} m^{-1}$ if the fluid relaxation length $\lambda_r = \bar{u}\epsilon_0/\sigma_0$ is to exceed 0.2 m. These 0.2 m and 0.02 m relaxation lengths can be roughly related to dimensions in G&W's charging apparatus. The distance from the filter and metal support screen to the downstream edge of the metal filter holder was about 0.05 m in Figure 2. Disregarding changes in flow rate inside the filter holder and assuming an exponential decay of charge in this region, less than 30% of the charge in the fluid will be convected beyond the downstream edge of the filter holder when the fluid relaxation length is less than 0.02 m. When the fluid relaxation length exceeds about 0.2 m, at least 80% [†] of the charge will be convected out of the filter holder.

Thus G&W's experiments demonstrate the following dependence on conductivity. When most of the charge was convected out of the metal filter holder (region I in Figure 6), the streaming current was <u>independent</u> of conductivity. When most of the charge remained inside the filter holder (region III, Figure 6), the <u>measured</u> streaming current <u>was</u> dependent

---

[†]In fact, even more than 80%, since the flow rate increases substantially as the flow area is reduced, about 2×10^{-2} m downstream of the filter, Figure 2. The assumption is that discharge against the metal filter holder will be slight in this flow regime.

on conductivity, decreasing very rapidly as the conductivity was increased. In the intermediate relaxation length tests, when charge was distributed inside and downstream of the filter holder, insufficient data were obtained to establish the relationship between the fluid conductivity and the measured streaming currents.

It seems probable that the charging data from regions II and III depend not only on the characteristics of the filter and fluid but on the process of charge relaxation and current conduction in the fluid inside the metal filter holder, a process which may be very sensitive to the geometry of the filter holder and the kinetics of discharge on the metal surfaces. Current conducted in the closed loop formed by the upstream fluid, the filter, the downstream fluid, and the metal filter holder would not, of course, be detected by the electrometer (Figure 2). We attribute the very rapid decrease of measured currents in region III of Figure 6 to this problem. The measured current would become relatively insensitive to the dimensions of the charging apparatus only when the relaxation length was sufficiently large ($\lambda_r \gtrsim 0.2$ m) to ensure that most of the charge was convected beyond the confines of the filter holder.

In Section C we will discuss in detail an explanation of G&W's high relaxation length data in terms of our theory. Suffice it to say at this stage that according to our theory the charging emf $\mathcal{E}$ of a filter depends on conductivity according to $\mathcal{E} \propto 1/\sigma_0$ when the relaxation length is much greater than the filter thickness. If this emf drives a current through a fluid loop of conductivity close to σ_0, the streaming current is, to a

good approximation, independent of σ_0 . Thus our theory appears to offer an adequate explanation for the current-conductivity behavior indicated in region I of Figure 6.

The "threshold" phenomenon

In seventeen of their forty-four runs, Gavis and Wagner found that no current at all could be measured at the lowest flow rates although currents were measured at the highest flow rates in all runs. From this G&W claim to have identified a general "threshold" condition below which streaming currents cannot be developed (Ref. 2, p. 388) and attach a physical significance to the existence of such a threshold (Ref. 2, p. 390).

Figure 7 shows all of G&w's data that pertains to the "threshold" phenomenon. Measured streaming currents are plotted against fluid relaxation length in the flow regime in which the "threshold" was observed, that is, at the lowest relaxation lengths investigated. It is evident that when the fluid relaxation length decreased to a value lower than about 2.3×10^{-4}m, no current was measurable in G&W's charging apparatus. As the relaxation length increased above this value the measured current increased vary rapidly, changing almost discontinuously from less than 10^{-15} A (noise on the electrometer) to 10^{-12}A or higher. Further increases in fluid relaxation length gave fairly smooth, relatively slow increases in measured current. We note that the thickness of the metal filter support screen (Figure 2) was 1.9×10^{-4}m (our own measurement made cn a filter holder of the same

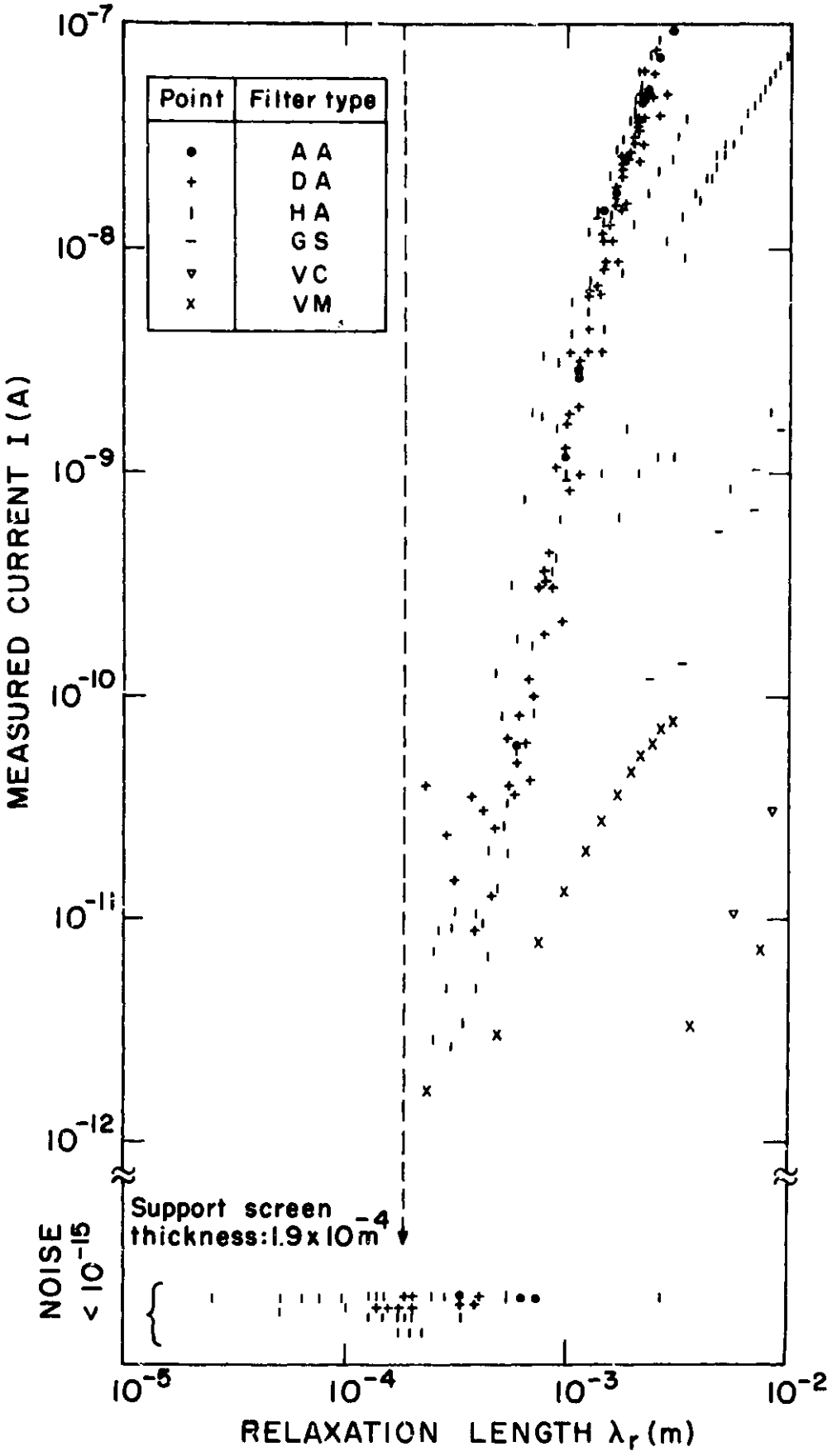


FIGURE 7. Low relaxation length data and the "threshold" phenomenon.

model). This thickness is strikingly close to the "threshold" relaxation length that is manifest in Figure 8. It appears that the threshold phenomenon reported by G&W was a direct result of discharge against the filter support screen--when no charge was convected beyond the support screen, no current was measurable. The presence of the fine metal grid allowed for a path of very low resistance from the fluid close to the grid to the filter holder and back into the fluid upstream of the filter. Significant current conduction through the loop formed by the fluid jet, receiver, and electrometer (Figure 2) occurred only when the full streaming potential was developed beyond the conducting metal grid.

G&W report (Ref. 2, p. 383) that several experiments were performed using a teflon filter holder base and teflon-coated support screen to test specifically for possible discharge against the filter holder and screen. "No discernable difference in current could be detected..." Unfortunately, references (1)-(4) do not report the details of these experiments so we cannot assess their implications. If they were, in fact, conducted in a high relaxation length flow regime [more or less the regime in which G&W felt that their data could be correlated by Eq. (1)], the results from the insulating filter holder tests were not surprising and would not contradict our interpretation of the low relaxation length data. At sufficiently high relaxation lengths it is unlikely that discharge against the filter holder screen and walls was a significant problem even in tests with the metal filter holder.

2. Filter Structure

Pore size and porosity, $I \propto (Pd)^{-3/4}$

Gavis and Wagner report that the streaming current from a filter depends on two filter parameters - pore diameter d and porosity P according to:

$$I \propto (Pd)^{-3/4} \qquad (6)$$

[Eq. (2)]. The ranges of these variables tested by G&W are

$$0.43 < P < 0.82$$

$$0.5 \times 10^{-7}\text{m} < d < 8 \times 10^{-7}\text{m} \ .$$

A direct assessment of Eq. (6) requires streaming current data for a range of values of Pd with all other variables - flow speed, fluid conductivity, and filter thickness - held constant.

Unfortunately, such data are not readily available from G&W's experiments, since their high flow rate data is exclusively from filters of large pore size and the low flow rate data are from filters of small pore size. However, by selecting two flow rates $Q = 10.6 \times 10^{-6}\text{m}^3\text{s}^{-1}$ and $Q = 1.5 \times 10^{-6}\text{m}^3\text{s}^{-1}$, it is possible to make comparisons of streaming current data for a significant range of filter properties.

Table 2 shows data obtained by Gavis and Wagner at a superficial flow rate close to $10.6 \times 10^{-6}\ \text{m}^3\text{s}^{-1}$. We have tabulated all data obtained at this flow rate that fall in the correlated segment of

Filter	σ_0 $\Omega^{-1}m^{-1}$	Q $10^{-6}m^3s^{-1}$	I 10^{-9} A	$I(Pd)^{3/4}$ $10^{-14}A\ m^{3/4}$	$I(Pd)^{3/4}/\sigma_0^{1/4}$ $10^{11}\ A\ m\ \Omega^{1/4}$	Data for which $\lambda_r > 0.2$ m
	7.1×10^{-12}		1.4	3.2	3.5	x
AA	1.0×10^{-12}		1.6	3.7	3.7	x
Pd =	2.9×10^{-12}	10.9	2.0	4.7	3.5	
6.6×10^{-7}	3.8×10^{-12}		1.5	3.5	2.5	
m	9.7×10^{-12}		1.0	2.3	1.3	
	2.2×10^{-13}		1.4	2.8	4.0	x
	4.6×10^{-13}		1.4	2.8	3.3	x
DA	1.0×10^{-12}		1.4	2.8	2.8	x
Pd =	2.2×10^{-12}	10.4	1.9	3.7	3.1	
5.3×10^{-7}	3.1×10^{-12}		1.6	3.1	2.4	
m	5.1×10^{-12}		2.3	4.5	3.0	
	6.9×10^{-12}		2.4	4.7	2.9	
	3.1×10^{-11}	9.3, 10.6, 11.7	1.8, 2.1[a], 2.4	3.1	4.1	x
HA Pd = 3.6×10^{-7} m	4.9×10^{-11}	9.3, 10.6, 11.7	1.8, 2.1[a], 2.4	3.1	3.7	x
	4.0×10^{-11}	9.3, 10.6, 11.7	2.7, 3.4[a], 4.0	5.0	2.0	
TW Pd = 1.9×10^{-7} m	3.6×10^{-13}	10.3	1.0	0.91	1.2	x
	9.7×10^{-13}		1.4	1.3	1.3	x
	2.2×10^{-13}		2.7	2.3	3.3	x
	3.8×10^{-13}		2.6	2.2	2.8	x
GS	8.7×10^{-13}	10.4	2.7	2.3	2.3	x
Pd =	1.6×10^{-12}		3.4	2.8	2.5	x
1.7×10^{-7} m	1.3×10^{-11}		4.8	4.0	1.8	
	1.9×10^{-11}		4.5	3.8	1.8	
	AVERAGE:		2.2	3.2	2.7	

[a] Estimate, by interpolation of G&W's data

TABLE 2. Current dependence on pore size and porosity. G&W's data for which $u\epsilon_0/Pd > 5 \times 10^3$ and $Q \approx 10.6 \times 10^{-6} m^3 s^{-1}$.

Figure 3 $\left(\frac{\bar{u}\epsilon_0}{Pd\sigma_0} > 5 \times 10^3\right)$. Also tabulated are reduced currents $I(Pd)^{3/4}$ and $I(Pd)^{3/4}/\sigma_0^{1/4}$ and the <u>average</u> streaming currents and reduced streaming currents at this flow rate:

$$\bar{I} \quad , \quad \overline{I(Pd)^{3/4}} \quad , \quad \text{and} \quad \overline{I(Pd)^{3/4}/\sigma_0^{1/4}} \quad .$$

Figure 8 shows plots of the reduced and unreduced currents divided by the appropriate average value against the parameter Pd. According to G&W's data correlation, Figure 8(c) should be a horizontal line while (a) and (b) would deviate substantially from horizontal lines of best fit.

It is quite clear that for the limited data presented, there is no demonstrated dependence on pore size or porosity. Certainly the high relaxation length data (indicated by a $\cdot$ in Figure 8) shows no more scatter in plot (a) (unreduced) than in plot (c) (reduced according to G&W's correlating equation). A careful analysis of VM, VC, GS, and TW filters at a constant flow rate $Q = 1.5 \times 10^{-6} m^3 s^{-1}$ leads to the same conclusion. In fact, any reduction of the high relaxation length data ($\lambda_r > 0.2$ m) <u>excluding</u> pore size as a parameter will tend to collapse the data onto a single line <u>as effectively</u> as a corresponding reduction that includes pore size (see discussion in Section C, particularly Figure 9).

Our own theory and experiments indicate that charging effects should be independent of pore size when the Debye ratio is high, that is, when

$$\frac{2\lambda_D}{d} = \left(\frac{4D\epsilon_0}{d^2\sigma_0}\right)^{1/2} > 1 \quad , \qquad (7)$$

where D is the ionic diffusion coefficient. In G&W's experiments the

• Datum for which $\lambda_r \geq 0.2\,m$ and $\frac{\bar{u}\varepsilon_o}{Pd\sigma_o} > 5 \times 10^3$

* Datum for which $\lambda_r < 0.2\,m$ and $\frac{\bar{u}\varepsilon_o}{Pd\sigma_o} > 5 \times 10^3$

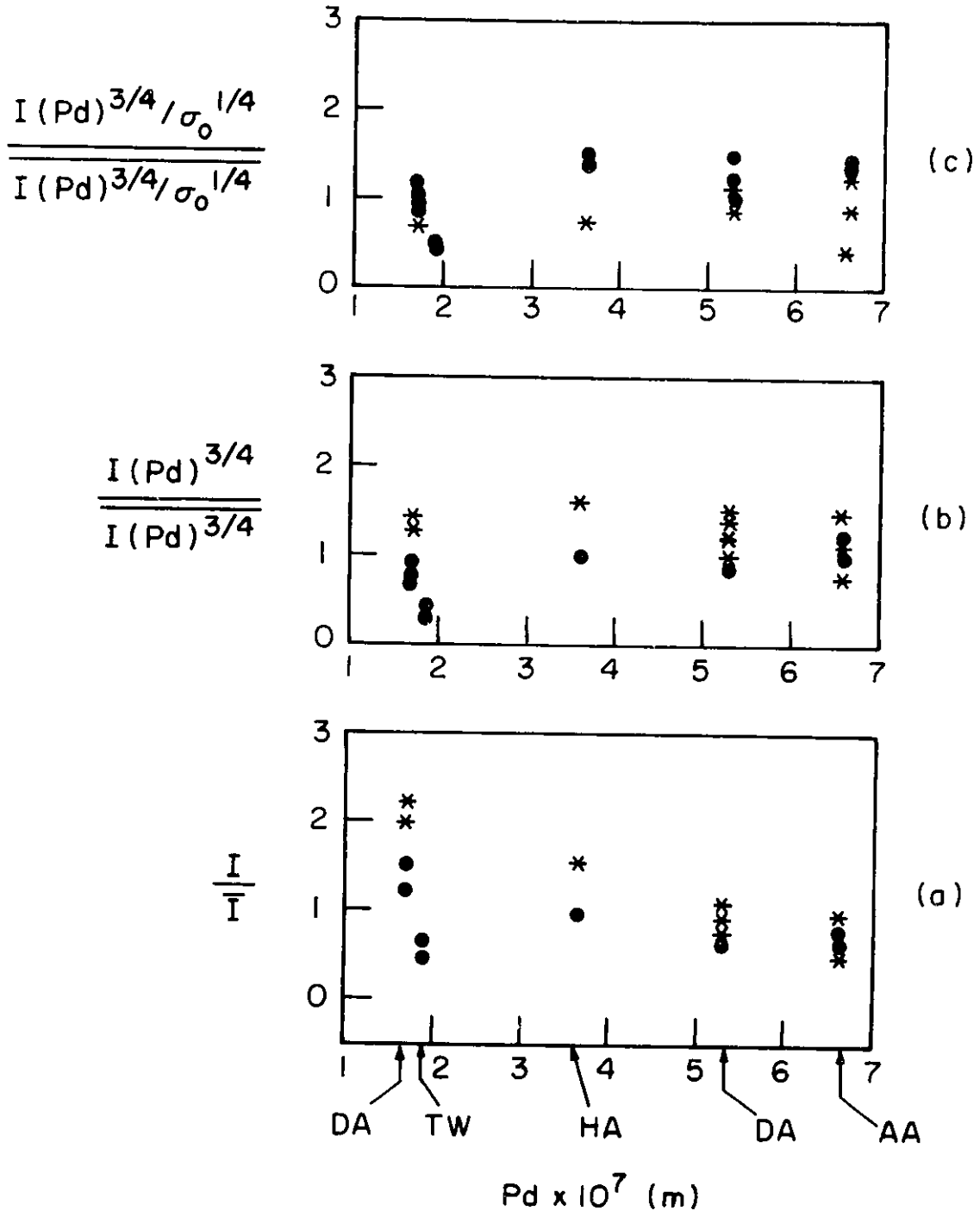


FIGURE 8. Unreduced and reduced measured currents versus porosity × pore diameter. $Q = 10.6 \pm 0.3 \times 10^{-6}\,m^3 s^{-1}$.

Debye ratio varied from 20 to 5×10^6 (Ref. 2, p. 388).† Furthermore, as discussed in Section C, our theory indicates that in some ranges of flow conditions charging effects depend primarily on the flow rate outside the filter and are to a good approximation independent of the filter porosity. All of G&W's high relaxation length data are in this range.

Filter thickness (I independent of h)

Little can be said about G&W's claim that streaming currents are generally independent of filter thickness (Ref. 2, p. 388). Their conclusion has no support whatsoever in their experimental tests. The range of filter thicknesses tested by G&W was $1.0 \times 10^{-4}\,m \leq h \leq 1.5 \times 10^{-4}\,m$, while the scatter in G&W's results (Figures 3 and 9) is at least a factor of 2 in the correlated, high flow rate region of their curve, vastly more in the uncorrelated region. We note, also, that for the filters tested by G&W the ratio of the filter porosity to the filter thickness is almost constant. Thus any claimed dependence on P could equally well be an inverse dependence on h.

Our own theory and experiments indicate that charging phenomena may be strongly dependent on filter thickness h in some flow regimes and independent of h in others. Most of G&W's data that fall in the correlated

---

†G&W used a value $D \sim 1.3 \times 10^{-9}\,m^2s^{-1}$ in calculating the values reported. We believe that $D \sim 0.2 - 0.5 \times 10^{-9}\,m^2s^{-1}$ is more realistic. The inequality of Eq. (7) is satisfied in either case.

region of Figure 3 should, in fact, be quite insensitive to filter thickness (see discussion in Section C). This theoretical prediction cannot, however, be verified or contradicted by experiments in which the scatter in the data is greater than the range of filter thicknesses tested.

3. Filter Fixed Charge and Reaction Kinetics

Gavis and Wagner claim that their charging data were demonstrably independent of kinetic parameters (Ref. 2, p. 389) and suggest that their correlation should be generally applicable to all filters and hydrocarbon liquids (Ref. 2, p. 390), thus excluding physico-chemical properties of the solid/fluid interface from the variables that could affect charging. Both conclusions are speculative, since no physico-chemical properties or kinetic parameters were varied in their tests, which involved only one hydrocarbon, one additive, and filters of only one composition tested at one temperature.

Streaming currents measured by G&W in large relaxation length flows ($\lambda_r \gtrsim 0.2$ m) were consistently negative [†] (Ref. 2, p. 386). According to our model this would indicate a negative fixed charge in all the filters tested, an observation which agrees with our own experiments conducted with identical solid/fluid combinations.[††]

[†]We are using G&W's definition of polarity--a current from the filter holder body to ground is defined as positive. Figure 2.

[††]We used Shell ASA #3 as our additive, G&W used Shell ASA #1. It appears that the ionic constituents of both additives are, however, the same.[8]

At lower relaxation lengths, streaming currents measured by G&W were in most cases negative. In run #25 a polarity shift occurred from negative currents at lower flow speeds to positive at higher speeds (Ref. 2, p. 386). The lowest relaxation length (highest fluid conductivity) data was of erratic polarity (Ref. 2, p. 387). We are unable to explain G&W's observed polarity shift in run #25 or the erratic current polarity at lower relaxation lengths. Our own experiments gave consistent and repeatable steady state current polarities, corresponding to a negative filter fixed charge in mixed cellulose ester filters. These experiments were in the range of conductivities in which G&W found "no observable regularity" (Ref. 2, p. 387) in streaming current polarity. Considering that at large relaxation lengths G&W did not encounter this anomolous behavior, it is possible that these polarity shifts are a further reflection of problems concomitant with low relaxation length experiments performed in an electrically conducting test cell.

SECTION C. SUMMARY AND ANALYSIS OF GAVIS AND WAGNER'S DATA IN TERMS OF OUR THEORY

We have argued in the previous section that Gavis and Wagner's streaming current data appear to be independent of pore size and porosity and, in the high relaxation length flow regime, also independent of fluid conductivity. Figure 9, which shows all data for which the relaxation length exceeded 0.2 m, bears this out. All 204 data points obtained by G&W in this flow regime are plotted <u>twice</u> in Figure 9. On line A the data are presented in the reduced variables adopted by G&W. The ordinate and abscissa are at the top and on the left-hand side of the figure. Line A is the empirical fit proposed by G&W, Eq. (1). In connection with the data points on line A we emphasize:

(1) <u>All</u> the data fall in the range $\bar{u}\epsilon_0/Pd\sigma_0 > 5 \times 10^3$ as required by G&W's correlating equation, Eq. (1).

(2) The reduced data points were calculated directly from the <u>unreduced</u> current and volume flow rate records given in the appendix of Reference (1). They were <u>not</u> taken from Figure 3.

(3) G&W's proposed value, $\kappa = 5 \times 10^{-8} m^2 V^{-1} s^{-1}$ was used in the data reduction, since the purpose of the plot is to compare the data with their empirical correlating equation, which implicitly contains this number.

On line B, Figure 9, the <u>same</u> 204 data are shown in <u>unreduced</u> form. The abscissa for this plot, on the right-hand side of the figure, is G&W's

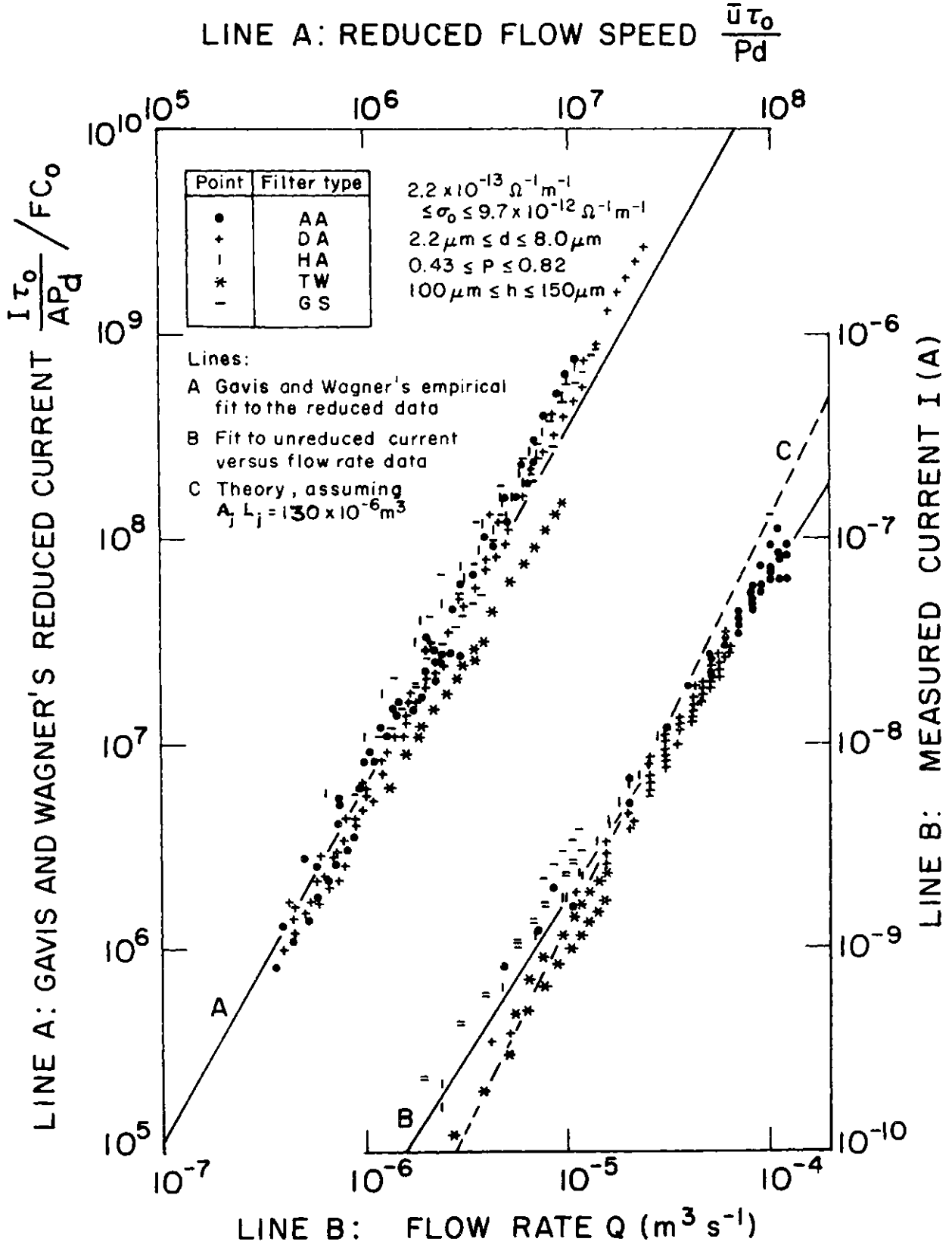


FIGURE 9. Comparison of G&W's proposed correlation with a plot of their unreduced, high relaxation length data.

measured streaming current; the ordinate at the bottom of the figure is the volume flow rate.

A simple visual comparison of lines A and B suffices - line B, which tacitly assumes that the current was independent of all variables except flow rate, correlates the data at least as well as does line A, proposed by G&W to take into account the influence of fluid conductivity, pore size, and filter porosity, as well as flow rate. Our conclusions based on the detailed Figures 6 and 8 are thus reaffirmed in Figure 9.

The theoretical equation for the charging emf $\mathcal{E}$ developed by an insulating filter of high negative fixed charge in one-dimensional flow is

$$\mathcal{E} = \frac{\bar{u}\, h\tau^2}{\rho\kappa_a} + \frac{\overline{u^2}\, \varepsilon_0}{\sigma_0\kappa_a} F(t_a) \qquad (8)$$

(Chapter 1) where τ is the filter tortuosity, κ_a the counterion mobility, and $F(t_a)$ a function of the counterion transport number, of order unity for physically reasonable values of t_a (Table 1, Chapter 1).

When the flow rate and conductivity are such that the fluid relaxation length greatly exceeds the filter thickness, only the $\overline{u^2}$ term of Eq. (8) is important. Accepting the values for the mobilities of ASA-3 † ions in heptane inferred from <u>our</u> charging experiments (Chapter 2) and requiring that $\lambda_r = \bar{u}\varepsilon_0/\sigma_0 \gg h$, Eq. (8) can be rewritten as:

---

†While G&W worked with ASA-1, it appears that the ionic constituents of ASA-1 and ASA-3 are the same.[8]

$$\mathcal{E} \approx \frac{0.86\ \varepsilon_0}{\sigma_0\ \kappa_+}\ \frac{Q^2}{A_j^{\,2}} \qquad (9)$$

$$\kappa_+ = 0.91 \times 10^{-8}\ m^2\ V^{-1}\ s^{-1} \quad .$$

Here the superficial flow speed $\bar{u}$, which in G&W's experiments varied considerably because of changes in flow area downstream of the filter, has been replaced by the ratio of the volume flow rate Q to a characteristic jet area downstream of the filter A_j.

Let us assume that in G&W's charging experiments the fluid attained a fully relaxed condition at some point in the fluid far downstream of the filter. Given the complex, three dimensional downstream flow field in G&W's charging apparatus, we specify only that the fully relaxed condition be distant from the metal filter holder, presumably in the fluid in the receiving vessel. In the absence of any current flow through the system the potential difference between the electrically neutral fluid far downstream of the filter and fluid upstream of the filter would be predicted by Eq. (9), given an appropriate, average value for A_j. However, the electric circuit constituted by the fluid in the filter holder, the jet, and the receiving vessel, and the electrometer connecting the receiver to the filter holder body (through ground) <u>will</u> allow current flow. If the resistance of the circuit is sufficiently high, so that the current flow through it is much less than the maximum streaming current that could be generated by the filter, the product of the open circuit charging emf and

the electric conductance of the loop through which the current flows should correctly predict the streaming current. (This is a simple restatement of the arguments in Chapter 1, used to drop the current terms when the measuring electrodes are distant from the filter and the charge cloud.)

The ohmic conductance of the fluid circuit will be proportional to the conductivity of the fluid it contains. If most of the fluid is only slightly charged its average conductivity will be close to σ_0, even if some of the fluid immediately downstream of the filter is highly charged. The circuit conductance will also be proportional to an appropriate aspect ratio of the fluid in the jet and reservoir, A_j/L_j, where A_j is the effective cross-sectional area of the fluid downstream of the filter and L_j is the effective length of this region of fluid. We neglect the contributions of the electrometer and of the thin, insulating filter matrix to the total circuit resistance. Thus we can transform Eq. (10) into an approximate current equation:

$$I \approx \frac{\mathscr{E}\,\sigma_0\,A_j}{L_j} = \frac{0.86\,\varepsilon_0\,Q^2}{\kappa_+\,(A_jL_j)} \qquad (11)$$

where A_jL_j is a measure of the volume of fluid between the filter and the regions of the funnel and receiving vessel to which most of the current is conducted.

Referring again to Figure 9, the unreduced data on Line B can be circumscribed approximately by

$$I = (8 - 40\ A\ s^2 m^{-6})\ Q^2 \qquad (12)$$

with a reasonable (although not the best possible) fit provided by

$$I = (13\ A\ s^2 m^{-6})\ Q^2 \qquad (13)$$

as shown by the dashed line C.

Substituting $\varepsilon_0 = 1.8 \times 10^{-11}\ C^2 N^{-1} m^{-2}$ and $\kappa_+ = 0.91 \times 10^{-8} m^2 V^{-1} s^{-1}$ into Eq. (11) and comparing with Eq. (12) we conclude that $A_j L_j$ was typically about $130 \times 10^{-6} m^3$, with lower and upper values about $43 \times 10^{-6} m^3$ to $210 \times 10^{-6} m^3$. Considering the dimensions of G&W's charging apparatus these numbers are quite plausible. The flow area varied from $3.88 \times 10^{-4} m^2$ immediately downstream of the filter to about $0.36 \times 10^{-4} m^2$ at the exit of the filter holder and presumably back to some larger value in the funnel and receiving vessel. Wagner reports in a private communication that the length of the fluid jet alone varied from "essentially zero for the lowest flow rates and smallest pore diameter filters to around several inches or more." Thus the total length of the fluid stream (including the fluid in the filter holder upstream and downstream of the filter) was probably about 0.1 to 0.2 m in the high relaxation length tests. On this basis we would expect $A_j L_j$ to be of order 10 to $100 \times 10^{-6} m^3$, a range reasonably close to the $43 - 210 \times 10^{-6} m^3$ indicated by the charging experiments.

The fact that $A_j L_j$ was not systematically controlled in G&W's experiments may explain much of the scatter in the data, as well as the fact that the dependence on Q is closer to $Q^{1.75}$ than Q^2. Note that if $A_j L_j$

increased as Q increased the deviation from our theoretical line C in Figure 10 can be explained quite satisfactorily.

Some observations by Gavis, Koszman, and Wagner in their highest conductivity experiments also relate to the influence of the quantity $A_j L_j$ on the streaming current measurements. In a publication describing charging in hydrocarbon flows through capillaries Koszman and Gavis[9] reported that "the current...measured was a function of the distance between the tube and the receiver." In a private communication Wagner mentions that a similar phenomenon was observed in some of the experiments described in references (1)-(4). Koszman and Gavis attribute this type of behavior to "a 'battery current'... between the end of the tube from which the liquid flowed and the grounded receiving tube through the liquid jet." We believe that our alternative explanation in terms of current conduction through the fluid stream is a more plausible interpretation of this phenomenon, and is particularly relevant to the low conductivity experimental results discussed in this section.

CONCLUSIONS

Gavis and Wagner's proposed empirical correlation is not well supported by their own charging data. The following conclusions, reached by G&W, are not supported by the data:

(1) $I \propto \sigma_0^{\frac{1}{4}}$

(2) $I \propto (Pd)^{-3/4}$

The following conclusions reached by G&W (tacitly or explicitly) are neither supported nor contradicted by the data:

(1) I independent of h ;

(2) I independent of kinetic parameters;

(3) I independent of physico-chemical parameters;

(4) I independent of filter conductivity.

Charge relaxation played a very significant part in G&W's tests. Only those data for which $\lambda_r \gtrsim 0.2$ m correspond to experimental conditions in which most of the charge in the fluid was convected out of the metal filter holder. As the relaxation length approached the thickness of the metal support screen currents decreased very rapidly. No currents were measurable when the relaxation length was less than the support screen thickness.

Considering only the high relaxation length data obtained by G&W ($\lambda_r \geq 0.2$ m), we conclude:

(1) Currents depend, approximately, on flow rate, according to $I \propto Q^2$.

(2) Currents are independent of σ_0 .

(3) No dependence on Pd was demonstrated.

(4) No dependence on h was demonstrated.

Our model and theory, as applied to the high relaxation length flow regime, agree with conclusions (1) and (2) and are tacitly supported by (3) and (4). There is reasonably close agreement between our theory and G&W's high relaxation length experiments if we assume that the effective volume of fluid through which current conduction occurred was about $130 \times 10^{-6} m^3$.

APPENDIX

SOME COMMENTS ON WAGNER'S THEORY FOR THE CHARGING PROCESS IN FUEL FILTRATION

In several publications Wagner has presented a dimensional analysis[1,3,4] and tentative theory[1,3] for charge generation in filters.

(1) A dimensional analysis must include all variables that could influence the process under consideration, whether or not the variables are held constant in a given set of experiments. Wagner omits two variables - temperature and ionic diffusivity (or mobility) from his dimensional analysis, apparently because they were invariant in his experiments (Ref. 3, p. 208). It is entirely possible that temperature will affect charging only indirectly by its effect on a primary variable such as conductivity. It seems unlikely, however, that charging does not depend on the ionic mobilities - there is certainly no a priori rationale for omitting this variable from the dimensional analyses.

(2) In view of G&W's model for the charging process,[2,3] we would also expect the filter matrix conductivity to appear as a variable in the dimensional analysis. According to G&W's model a perfectly insulating filter would give rise to no charging at all - a conclusion not contained in their predictions.

(3) We have some fundamental reservations about the "Tentative Theory of Charge Generation in Filters" (in the Appendix of Ref. 3, p. 217);

(a) This theory postulates <u>continuous</u> migration of charge[†] to the filter surfaces and current conduction through the filter matrix. This assumption seems physically surprising for cases in which the conductivity of the solid filter matrix is much less than that of the permeant fluid - as was the case in most of G&W's charging experiments.

(b) The dimensional analysis for the "charge transfer coefficient" (Ref. 3, p. 220) contains some important, tacit assumptions. The Π theorem does <u>not</u> state that the dimensionless variables (Π groups) of a system can be related by a product of power in the form:

$$\Pi_1 = \phi \Pi_2^{\alpha} \Pi_3^{\beta} \Pi_4^{\sigma} \ldots$$

with ϕ a constant. In fact, the dimensionless variables may be any type of function of each other - sums, exponentials, logarithms, etc. An empirically determined, dimensionally self-consistent correlation can be neither confirmed nor refuted by dimensional analysis.

[†]Ref. 3, p. 219, Eq. (7A) - the relevant term is $\left. \frac{P\tau_0}{d_p^2} \frac{dq_r}{dr_r} \right|$ c.t.l.

PWH:cp

REFERENCES

1. Wagner, J.P., Ph.D. thesis, The Johns Hopkins University, 1966.
2. Gavis, J., and Wagner, J.P., Chem. Eng. Sci., 23, 381 (1968).
3. Wagner, J.P., Fire Res. Abs. and Rev. 15, 3 (1974).
4. Wagner, J.P., Loss Prevention, Vol. 9, CEP Technical Manual, AIChE, New York, 1975.
5. Lauer, J.L., and Antal, P.G., J. Coll. Int. Sci. 32, 407 (1970).
6. "1974 Millipore Catalogue and Purchasing Guide," Catalogue No. LMC 0174/P, Millipore Company, Bedford, Massachusetts, 1974.
7. Bikales, N.M. (Ed.), "Encyclopedia of Polymer Science and Technology," Vol. 5, p. 524, Wiley-Interscience, New York, 1964.
8. Klinkenberg, A. and Poulston, B.U., J. Inst. Petrol. 44, 379 (1958); Chem. Week, p. 45, December 26, 1964.
9. Koszman, I. and Gavis, J., Chem. Eng. Sci. 17, 1023 (1962).

Peter W. Huber

BIOGRAPHICAL SKETCH

Birthdate: 3 November 1952

Birthplace: Toronto, Canada

Citizenship: Canadian

Education

MASSACHUSETTS INSTITUTE OF TECHNOLOGY

1974 S.B.-S.M. in Mechanical Engineering (Honors Program).

1974-1976 Doctoral Program, Department of Mechanical Engineering. Minor in Law (Harvard Law School).

Professional Experience

MASSACHUSETTS INSTITUTE OF TECHNOLOGY

September 1975 to present: Teaching Assistant, Fluid Mechanics, Department of Mechanical Engineering.

June 1972 to present: Research Assistant, Department of Mechanical Engineering.

Awards and Honors

Selected for Honors Program in Mechanical Engineering, MIT.

Joseph Warren Barker Fellowship in Engineering, 1973-1974.

Pi Tau Sigma

Languages

Completely fluent in French (raised in Geneva, Switzerland); some Russian.

Publications

Huber, P.W. and Sonin, A.A., "A Model for the Electric Charging Process in Fuel Filtration," J. Coll. Inter. Sci. 52, 415 (1975).

(This paper was presented at the 79th National Meeting, AIChE, in Houston (March 1975). Reprinted in capsule form in Chemical Engineering Progress, Technical Manual #9, Loss Prevention.)

Peter W. Huber

Publications (continued)

"Theory for the Electric Charging Process in Liquid Hydrocarbon Filtration," to be submitted to J. Coll. Inter. Sci.

"Electric Charging in Filtration: a Comparison of Theory and Experiments," to be submitted to J. Coll. Inter. Sci.

"A New Look at Some Old Data on Electric Charging in Fuel Filtration," to be submitted to Chem. Eng. Sci.